Synthesis of dynamic squat movements by quadratic optimization and study of the influence of the parameters of the musculoskeletal model

Bach Quoc Hoa

THÈSE DE DOCTORAT

présentée à

Sorbonne Université

par

Bach Quoc HOA

pour obtenir le diplôme de

Doctorat de Sorbonne Université

Spécialité : Robotique

Synthèse de mouvements dynamiques de squat par optimisation quadratique et étude de l'influence des paramètres du modèle musculo-squelettique

---

soutenance prévue le 17 Décembre 2021

JURY

M. Olivier Bruneau	Professeur des Universités à ENS Paris Saclay	Rapporteur
M. Mohammed Samer	Professeur des Universités à l'UPEC	Rapporteur
Mme. Agnes Roby-Brami	Directrice de recherche à Sorbonne Université	Examinatrice
Mme. Pauline Maurice	Chargée de Recherche CNRS	Examinatrice
M. Eric Desailly	Directeur Recherche Fondation Ellen Poidatz	Examinateur
M. Faïz Ben Amar	Professeur des Universités à Sorbonne Université	Directeur de thèse
M. Vincent Padois	Directeur de recherche INRIA Bordeaux	Co-directeur de thèse

Abstract

The project lies within the context of improving the outcome of lower limb orthopaedic surgery in children with cerebral palsy. Cerebral palsy (CP) is the most common physical disability of childhood which affects the developing fetal or infant brain. Children usually suffer deficiencies related to lower limbs such as increased deep tendon reflexes, tremors, muscular hypertonicity and weakness resulting to altered movements like scissors gait with toe-walking. The assessment and treatment of abnormalities of motor function in children with CP are challenging. Many different types of interventions are proposed to restore and promote anatomical structures and musculoskeletal conditions, to prevent secondary impairments and, above all, to increase a child's developmental capabilities. To manage musculoskeletal impairments, single-event multilevel orthopedic surgery (SEMLS) is proven to be the most effective treatment method for children with CP, allowing short hospitalisation and rehabilitation periods.

Due to the invasiveness and complexity of this intervention and the varying degrees of impairment among different patients, planning is essential to optimize the outcome and maximize patient function. Currently, the clinical assessment of the patient is conducted via integrated 3D gait analysis, medical imaging and the personal experience of surgeons. Despite providing quantitative description of the physiology of the patient body through the kinematics and dynamics of the movements, these approaches cannot measure some important quantities such as joint and muscle forces and cannot monitor the effect of isolated changes in the neuro-musculoskeletal system. Researchers have attempted to use statistical and machine learning approaches to produce more complete qualitative prediction of both the kinematics and the dynamics of movements for a combination of surgical procedures. Nonetheless, they are black box methods and cannot provide insight on the scientific basis behind motor function and hence the effect of a specific intervention on the musculoskeletal system.

Computational physics-based simulations with musculoskeletal models are often suggested to have the potential to identify the causal relation between individual impairments, their interactions and the treatment outcome. This thesis explores this solution by developing a physics-based simulation method as a prediction tool of the effects of surgical interventions of lower limbs on human movements. At present, the most common approach is using experimental captured data as input of simulations of 3D gait analysis and human movement generation. Although the results allow clinicians to identify the potential principals of a movement, the dependency on the capture data limits the prediction capacity of this approach.

In this work, we develop an optimization-based dynamic task controller capable of synthesizing movement without using any specific experimental capture data. The controller architecture is inspired from whole-body control in robotics which has shown interesting results with humanoids as well as in the other domains of robotics. We test our method by synthesizing squat motions with different skeletal and musculoskeletal models representing healthy and cerebral palsy individuals. The physical simulations are built and run with OpenSim, a biomechanical open-source software providing tools to model musculoskeletal systems and physical environments. The controller is programmed with the OpenSim C++ API. In parallel, experiments are carried out to collect data related to body kinematics, force-ground contact forces and electromyographic signals. The numerical models are also scaled to reflect the morphology of the subject so experimental data can be used to compare with simulated data. Results show that the proposed controller is able to generate different strategies of squat. It produces major features of the movement under different performance conditions and with different types of human models. Based on this ability, squat synthesis as a planning tool of lower limb musculoskeletal surgical interventions is also studied. For this purpose, simulations of tendon transfer procedures are carried out to investigate different options of attachment points. Several physically relevant criteria are established to assess the outcomes. Results are encouraging and suggest that further developments could be extended to other types of movement, notably walking, to demonstrate potential distinguished utilities of the approach.

Acknowledgements

First and foremost, I would like to thank my advisors, Vincent Padois and Faiz Ben Amar, who were extremely patient, insightful and understanding. Without them, I would be completely lost, both in terms of my research and my mental health. They were always complementary to each other, and try to bring positive impacts and new orientations to my work, and to my reasoning in general.

Next, I want to thank M. Eric Desailly. Without him, for sure, I would never been able to finish my PhD and obtain the diploma. He helped me far more than he should, with his kindness, initiatives and knowledge of biomechanics.

I'm also grateful to have Guillaume Matheron as my colleague during the first two years of my PhD. Without him, I wonder how much more time I would have wasted to figure out what to do with Linux and CMake. I will also never forget the stories and the chess games with Valentine Marcel, who just happens to have the same birthday as mine, just one year prior.

Of course, I am hugely indebted to my family and close friends, who were supporting me, through the difficult times and until the end, and to Ylenia Urbino, a wonderful person who accompanied me when I was at my limits during the most stressful period of the PhD.

Finally, I would like to thank my PhD committee members for having accepted to evaluate my work, and for the enriching discussion during and after the defense.

Contents

List of Figures

List of Tables

List of Symbols

The next list describes several symbols that will be later used within the body of the document

$\boldsymbol{\chi}$	Optimization variable vector
$\boldsymbol{\nu}$	Generalized acceleration
$\boldsymbol{q}$	Generalized coordinate
CNS	Central Nervous System
CoM	Center of Mass
DoF	Degree(s) of Freedom
QP	Quadratic Programming
RF	Rectus femoris
s.t.	subject to
SEMLS	single-event multilevel orthopedic surgery
w.r.t	with respect to

Chapter 1

Introduction

Our work lies within the context of improving the outcome of lower limb orthopaedic surgery in children with cerebral palsy. Cerebral palsy (CP) is a prevalent group of neuromotor disorders that affect the developing fetal or infant brain and persist through the life span [Rosenbaum et al., 2007, Oskoui et al., 2013]. It is the most common physical disability of childhood, with a worldwide prevalence of 2.1 per 1000 live births [Oskoui et al., 2013]. The clinical features in affected limbs are increased deep tendon reflexes, tremors, muscular hypertonicity, weakness, and a characteristic scissors gait with toe-walking. Impairments can also be observed related to balance, coordination, vision and hearing [Krigger, 2006]. *Although the neurological injury associated with cerebral palsy is non-progressive, adults with the disorder often develop musculoskeletal and neuro-logical symptoms, such as severe pain, chronic fatigue, and a premature decline in mobility and function, as they age [Tosi et al., 2009].*

The assessment and treatment of abnormalities of motor function in children with CP are challenging due to the wide variety of impairments of the developing central nervous system and their clinical manifestations [Rosenbaum, 2003, Lynn et al., 2009]. Many different procedures exist, ranging from physical and occupational therapy, neurosurgical and pharmacological interventions to reduce hypertonia and orthopedic surgeries. They aim to restore and promote anatomical structures and musculoskeletal conditions, to prevent secondary impairments and, above all, to increase a child's developmental capabilities [Lamberts et al., 2016, Rosenbaum, 2003]. For example, to temporarily relieve spasticity, a muscle control disorder "manifested by increased stretch reflex which is intensified with movement velocity" [Bar-On et al., 2015], injection of botulinum toxin, commonly known as Botox, in the affected muscles is a common solution. To achieve a more permanent effect, clinicians perform dorsal rhizotomy, a spinal surgical procedure relaxing the muscles by identifying and cutting abnormal nerve fibers contributing to spasticity. Patients then take progressive physical strength training programs to improve muscle strength and walking velocity [Krigger, 2006].

To manage musculoskeletal impairments, orthopedic surgery is the preferred approach, especially when less invasive treatments are not sufficient. Generally, orthopedic interventions are categorized into four categories: musculotendinous or tendinous lengthenings, tendon transfers, osteotomies (cutting the bone) and arthrodeses (artificial induction of joint ossification between two bones by surgery) [Lynn et al., 2009]. Amongst current available treatments, there are two approaches: single-level orthopedic surgery and single-event multilevel orthopedic surgery (SEMLS). For single-level orthopedic surgeries, patients undergo a succession of interventions, leading to considerably long hospitalisation and rehabilitation periods. This can negatively impact the outcome of the treatment as well as the quality of life of the patients and their families. [Lynn et al., 2009]. On the contrary, in a SEMLS, corrections are performed at a minimum of two anatomical levels during a single operative event, hence only one hospital admission and recovery period are required [Lamberts et al., 2016]. Currently, this approach is proven to be the most effective treatment method to treat musculoskeletal deformities in children with CP [Lamberts et al., 2016, McGinley et al., 2012].

Given the invasiveness of orthopaedic surgery and the varying degrees of neurologic impairment exhibited

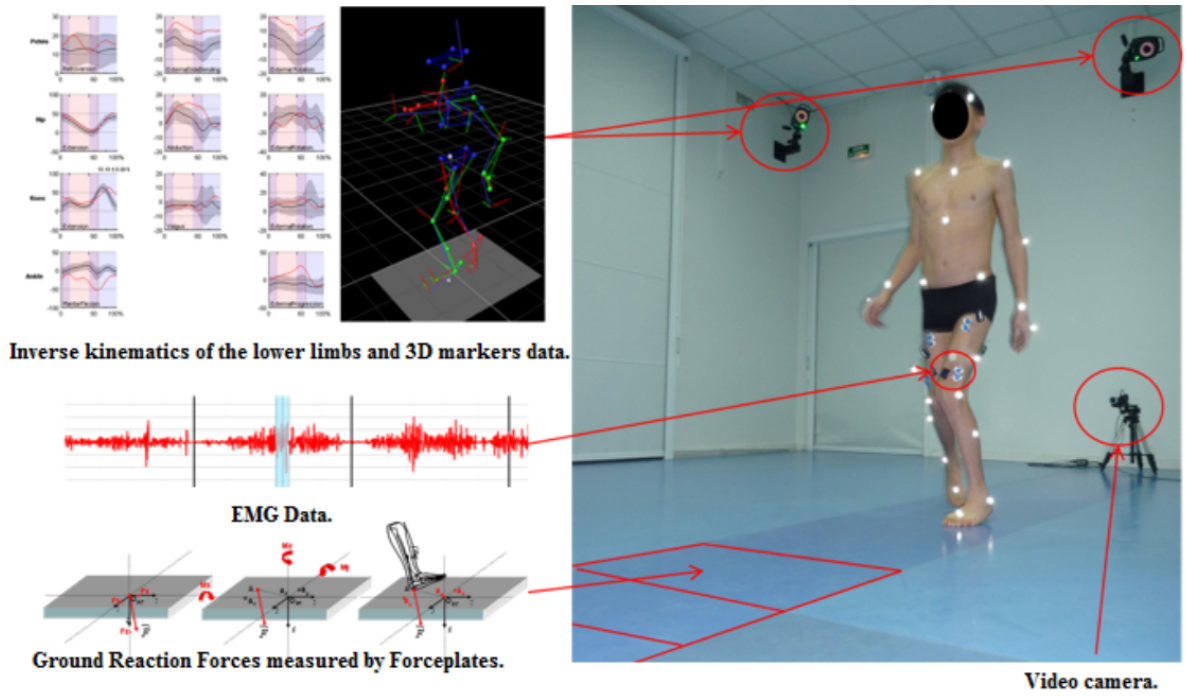

Figure 1.1: Clinical Gait Analysis set-up at Ellen Poidatz Foundation. Image courtesy of E. Desailly [Desailly, 2008]

among different patients, SEMLS must be planned ahead to optimize the outcome and maximize patient function. Currently, this is conducted based on the clinical assessment of the patient, integrated 3D gait analysis (Fig. 1.1), medical imaging and the personal experience of surgeons. However, treatment planning is still challenging because there is currently no clear scientific basis for determining how patients' neuromusculoskeletal impairments contribute to abnormal movements [Arnold* and Delp, 2005]. Data providing a quantitative description of the kinematics and dynamics of movements can be obtained thanks to modern equipment. They include high-speed camera systems tracking the changing positions and orientations of body segments, strain-gauge or piezoelectric transducers measuring the magnitudes and directions of ground reaction forces, and surface or in-dwelling electromyography (EMG) electrodes recording muscle activity [Pandy, 2001]. However, experiments alone cannot provide certain important quantities such as muscle and joint forces and are unable to explain the coordination of musculoskeletal systems to produce a movement. Additionally, monitoring the function and the effect of isolated changes in the neuro-musculoskeletal system is complicated due to the limits of current measurements techniques [De Groote and Falisse, 2021].

The identification of the parameters influencing an SEMLS has been attempted by several research studies through statistical and machine learning approaches. These works include qualitative prediction of a few selected outcome indicators in treating stiff knee gait by linear discriminant analysis [Reinbolt et al., 2009] and in psoas[1] lengthening by random forests [Schwartz et al., 2013]. Quantitative gait parameters were also predicted, such as post-treatment knee flexion during stance for patients presenting crouch gait [Hicks et al., 2011], knee flexion during gait after rectus femoris[2] transfer [Hersh et al., 1997] and pelvic tilt[3] after hamstring[4] lengthening [Galarraga et al., 2016]. To produce a more complete qualitative prediction of lower limb kinematics for a combination of surgical procedures, [Vigneron et al., 2017] developed a statistical machine learning method based on dimension reduction and multiple linear regression. "All these methods, however, have the drawback that they are black box methods and therefore do not allow investigating the mechanisms relating outcomes in motor function to the specific interventions" [Halilaj et al., 2018]. Assessing surgical outcome is also complicated as improvement of motor function

[1] A hip flexor muscle locating in the lower lumbar region of the spine and extending through the pelvis to the femur.
[2] One of the four quadriceps muscles of the human body.
[3] One of the orientations of the pelvis w.r.t the thighbones.
[4] Posterior thigh muscles in between the hip and the knee.

may be related to natural acquisition of motor skills rather than attributable only to surgical interventions, especially in the case of children under the age of six [McGinley et al., 2012].

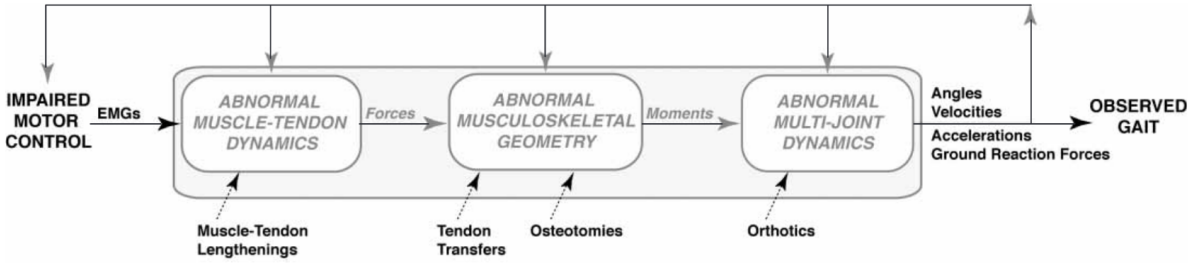

Figure 1.2: Many factors contribute to movement abnormalities in persons with cerebral palsy. Gait analysis is used routinely to record electromyographic (EMG) patterns, joint angles, and ground reaction forces during walking, but the transformation between EMG patterns and coordinated multijoint movement (shaded region) is complicated. Furthermore, to make treatment decisions clinicians must try to predict how the motions induced by muscles might change after treatment. Computational models that characterize patients' muscle–tendon dynamics, musculoskeletal geometry, and multijoint dynamics during walking may enhance interpretation of motion analysis studies and improve the planning of treatments. Image and captions taken from [Arnold and Delp, 2005]*

On the other hand, computational musculoskeletal models and physics-based simulations have shown potential to establish the causality between individual impairments, their interactions and the treatment outcome [Morrison et al., 2018, Pitto et al., 2019]. For several decades, physics-based modeling and simulation has gained traction as the principal method of uncovering the neuromechanics of movement [Pandy, 2001]. Explicit computational models can describe laws of physics and represent abnormalities in musculoskeletal geometry and multi-joint dynamics (Fig. 1.2). Combining these models with experimental data as input to computation process is the most common approach to perform objective functional analyses.

Globally, a physics-based simulation is built based on two aspects:

- representation of the musculoskeletal system with sufficient complexity to describe patient-specific features and surgical procedures
- movement generation predicting body kinematics, kinetics, energy consumption, and neuromuscular activity.

Since these are topics that have drawn a lot of attention and interest, especially from researchers in the bio-mechanics and robotics communities, it is helpful to look at the current state-of-the-art.

1.1 Human Body Modeling

Human body is often considered as a simplified biped system and can be modeled as such. A model can be planar (2D) [Bessonnet et al., 2002, Chevallereau and Aoustin, 2001, Ren et al., 2007] or spatial (3D) [Bessonnet et al., 2010, Kim et al., 2008], skeletal [Mombaur, 2009] or musculoskeletal [Xu et al., 2015]. Generally, the system is constructed from rigid segments connected by mechanical joints. These joints are actuated by joint actuators or by line actuators representing muscle tendon units (MTU), whose model can be linear or non-linear (Fig. 1.3). Joint actuators such as torque generators are commonly used in complex movement simulation such as walking thanks to their simplicity and computational efficiency [Xiang et al., 2010]. On the other hand, some particularities of the motor system strongly influencing the way we move cannot be accounted for using such models: the unilateral nature of muscular actuation (a muscle can only pull), the actuation redundancy and the state dependant nature of muscles internal dynamics and their impact on the overall system's dynamics [Anderson and Pandy, 2001a] as well as phenomenon such as fatigue [Xia and Law, 2008]. These aspects are represented more directly and intuitively on musculoskeletal models. *These musculoskeletal models can then be used in combination with*

3D experimental gait data (i.e., marker positions, and ground reaction forces) to estimate biomechanical parameters during dynamic function—for example, joint angles—but also muscle activations and forces ultimately allowing calculation of joint contact forces [Killen et al., 2020].

In the application of CP treatments, one of the major challenges perspective is to determine a reasonable level of complexity of the musculoskeletal models to represent the neuromusculoskeletal dysfunctions of the patients (i.e., the altered musculoskeletal geometry, musculoskeletal parameters, and altered neural control). These models are also subject-specific, meaning they are able to describe distinguish features of different individuals.

In parallel with the description of patient-specific features, surgical interventions are also needed to be represented in the musculoskeletal model. For tendon transferring procedures, it's obligatory to use line actuators as they allow the demonstration of the modification of muscle attachment points and actuation path. With more complex muscle models, such Hill-type muscles [Haeufle et al., 2014], muscle tendon unit lengthening can be represented by tuning the physiological parameters of the muscle model.

Finally, the solvability of control problems to compute actuator activations depends partly on the intricacy of muscle model and the number of muscles incorporated in the human model. This is particularly problematic, as complex muscle and joint models are usually non-linear, as well as the number of degrees of freedom (DOF) and actuators can be important. This aspect is discussed more in detail in the following section.

1.2 Optimization - The Backbone of Human Movement Generation

Due to the redundancy of the multibody system of human body, human movement is believed to follow a certain "principal of optimality", thanks to evolution and learning [Kulić et al., 2016]. It is, therefore, a straightforward idea to use mathematical optimization as a tool for motion analysis or motion synthesis in humans [Kulić et al., 2016]. For the sake of clarity, we use the term "motion synthesis" to indicate the generation of movement without relying on motion or force tracking.

The problem formulation of an optimization for movement synthesis consists of defining meaningful objective functions representing human performance measures and constraints. A general framework for a optimization problem can be defined as follow.

$$\begin{aligned} \min_{\boldsymbol{\chi}} \quad & f(\boldsymbol{\chi}) \\ \text{s.t} \quad & \boldsymbol{h}_i = 0; \quad i = 1..m \\ \text{s.t} \quad & \boldsymbol{g}_j \leq 0; \quad j = 1..k \end{aligned} \tag{1.1}$$

where $\boldsymbol{\chi}$ is the optimization variables (joint angle profiles, joint torque profiles, muscle forces, etc.), f is a cost function to be minimized, h_i represents the m-equality constraints, and g_j represents the k-inequality constraints.

The cost function varies depending on human subjects, movements and applications. In tracking data application, the cost function is usually the squared distance between estimated values and measurements. Hypotheses about the functional control during movement can be formulated as performance measures such as dynamic effort (sum of muscle forces squared) [Schultz and Mombaur, 2009, Ozsoy, 2014], mechanical energy [Ren et al., 2007] and metabolic energy [Wang et al., 2012, Anderson and Pandy, 2001a], and be included in the cost function with assigned priorities. Equality constraints comprise the system dynamic equations, geometry constraints, movement phase transitions. Inequality constraints contain boundary conditions of actuators and generalized coordinates, foot-ground contact behavior, foot clearance, self-collision and so on.

Based on the form of the cost function, the methods of optimization-based approach can be divided into two categories: static and dynamic optimization. Static optimization evaluates the performance

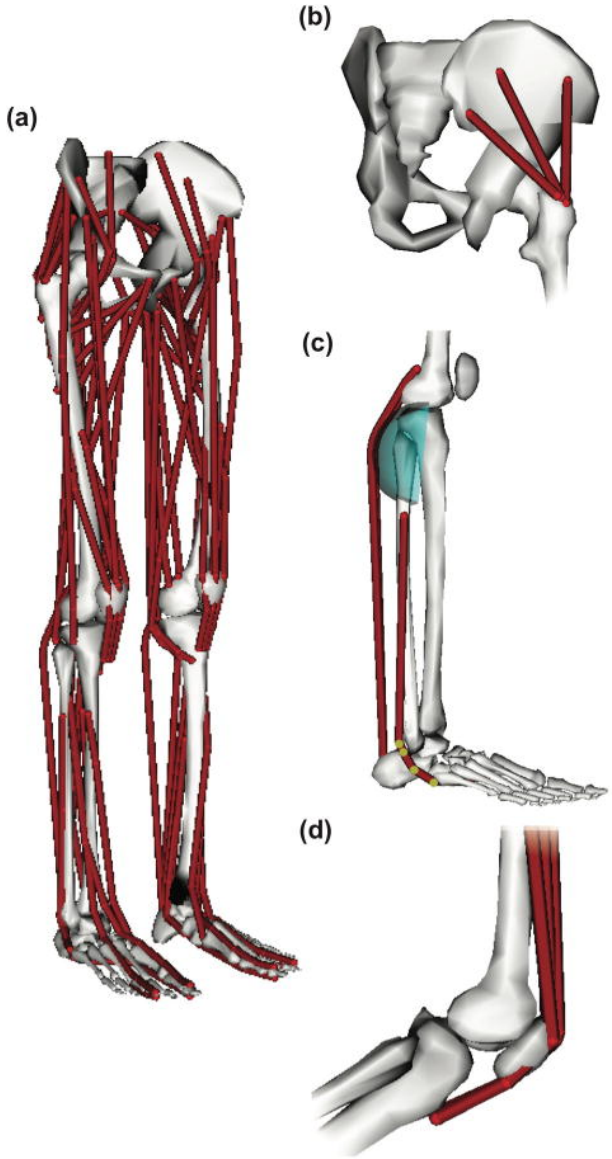

Figure 1.3: Muscles were modeled as massless linear actuators. (a) The model included 80 muscle-tendon units (40 per leg) actuating the lower limbs. (b) Muscles with broad attachment areas (e.g., gluteus medius) were modeled using multiple independent muscle-tendon units. (c) Muscle geometry was modeled using a set of body-fixed points (highlighted) and wrapping surfaces. (d) The force transmission mechanism between the quadriceps and patellar ligament was modeled implicitly by wrapping the quadriceps muscles over the patella and inserting the muscles directly to the tibia. Image and caption taken from [Rajagopal et al., 2016]

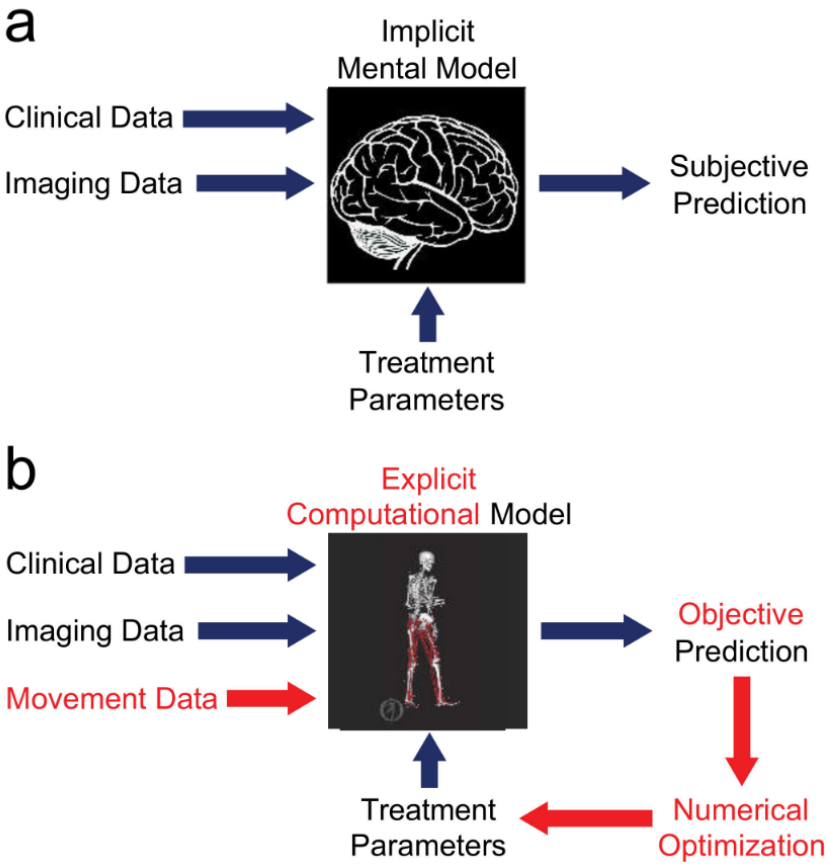

Figure 1.4: Comparison of (a) current and (b) future treatment design paradigms. The current paradigm relies on an implicit mental model in the mind of the clinician. Given clinical and imaging data and proposed treatment parameters as inputs, the implicit mental model produces a subjective prediction of post-treatment function, so different clinicians may propose extremely different treatment designs. The future paradigm replaces the implicit mental model with an explicit computational model that obeys laws of physics and principles of physiology. With this approach, movement data are added to the inputs, the explicit computational model produces an objective prediction of post-treatment function, and the entire process is wrapped in numerical optimization to identify the treatment design that will maximize the patient's functional outcome. Image and caption taken from [Fregly, 2021]

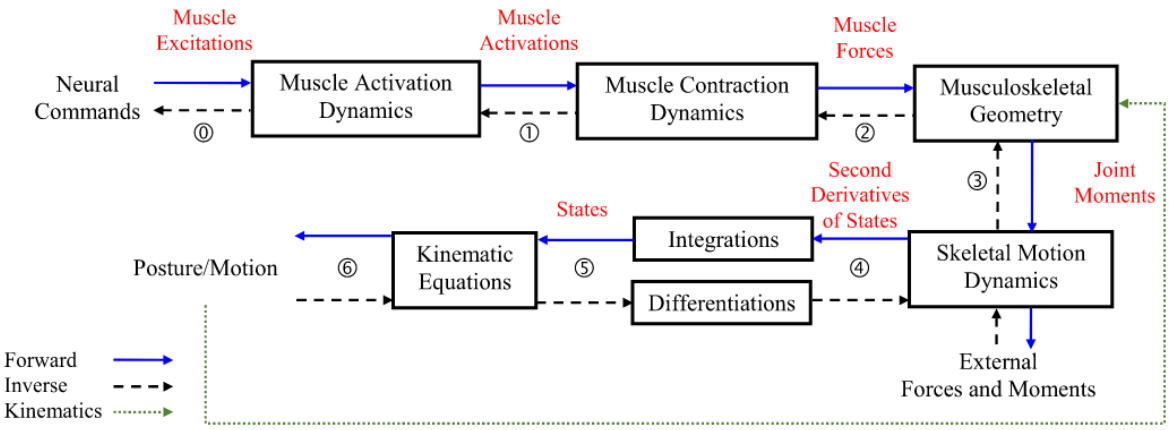

Figure 1.5: Dynamic formulation workflow. Forward dynamic formulation follows the path from 0 to 6 for a neuromusculoskeletal model, taking neural controls as input to compute motion. Inverse dynamic formulation follows the path from 6 to 0, solves neural controls from motion . Image taken from [Ezati et al., 2019]

criterion limited to quantities that can be computed at any instant in time during a simulation such as total actuator forces or stability margin. On the contrary, dynamic optimization can be constructed from quantities evaluated over a period of time such as total metabolic energy over a period of time.

Optimization-based methods can also be characterized by the formulation of the dynamic: inverse or forward, as shown in Fig. 1.5. For inverse dynamics optimization, muscle and joint forces are solved from kinematic data, and eventually ground reaction forces acquired via force plates. In forward dynamics problem, muscle forces/activations are optimization variables for the optimization process to estimate model kinematics. One of the most valuable aspects of this approach is movement synthesis as it offers the potential to validate hypotheses and predict functional outcomes without requiring experimental data. However, as the dynamic of the system is integrated over time, forward dynamics optimization methods are much less computationally efficient than inverse dynamics ones.

1.3 Related Work

The combination of musculoskeletal modeling with experimental data as input of an optimization process is a prevailing method to simulate movement. There are several measurements that can be used: electromyography (EMG) signals, 3D kinematics of body segments, especially lower limbs, foot-ground reaction forces, joint torques and energy consumption [Sutherland, 1978].

Tracking captured motion data is a common optimization task that allows to produce human-like movement. If the tracking motion task is dominant in the cost function of the optimization problem formulation, meaning it is associated to a high weight relative to other tasks, the results are independent from the task conditions [Ezati et al., 2019]. These optimisation methods can be supplemented with experimentally acquired electromyography (EMG) data to constrain estimated muscle activations [Pizzolato et al., 2015, Lloyd and Besier, 2003]. Calculated muscle activation and force patterns allow researchers and clinicians to imply any changes in muscle function due to different pathologies, or locomotion strategies [Killen et al., 2020].

Static Optimization [Rosenberg and Steele, 2017] *simulated impacts of ankle foot orthoses on muscle demand and recruitment in typically-developing children and children with cerebral palsy and crouch gait* by using static optimization. The optimization process estimates muscle forces by minimizing the sum of squared muscle activations required to generate experimental kinematics and ground reaction forces at each instance. Static optimization is also used in [Steele et al., 2012] to estimate muscle forces and compressive tibiofemoral forces during crouch gait. First, the generalized coordinates of the model

during the movement were computed by a static optimization process to minimize the errors between computed and experimental marker positions. Then, the known motion is used as input for another static optimization to compute the joint moments and muscle forces. The cost function is a weighted sum of muscle activations to be minimized where weighting values are imposed to be between 0 and 1 while the constraint is the dynamic equation. In the same manner, [Vandekerckhove et al., 2021] also used static optimization to "explore the effect of hip muscle weakness and femoral deformities on the gait performance of CP and typical developing subjects". The results suggested that "surgical correction of femoral deformities was more likely to be effective than strength training of hip muscles in enhancing CP gait performance". [Thelen et al., 2003, Thelen and Anderson, 2006] designed a method called *Computed Muscle Control* that requires only one integration of the state equations. The method couples static optimisation with feedforward and feedback controls to estimate both muscle activations and forces allowing the tracking of experimental kinematics data.

Dynamic Optimization In the study of the interplay between the elements of the neuromusculoskeletal system during a movement, it is desired to alter some of model parameters to determine the subsequent consequences. This method is generally unavailable in experiments but can be easily performed with forward dynamic simulation [Thelen et al., 2003]. For example, vertical jumping was simulated in [Zajac, 1993] with forward dynamics formulation and optimal control and showed that "jump height was more sensitive to muscle strength than to muscle speed, and insensitive to musculotendon compliance" and "uniarticular muscles generate the propulsive energy and biarticular muscles fine-tune the coordination". [Allen and Neptune, 2012] built a 3D modular human walking control based on simulated annealing algorithm [Goffe et al., 1994], an optimization algorithm to find global optimum. Muscle excitation patterns and initial joint velocities were computed through optimization to minimize muscle stress and the difference between the simulated and experimentally measured walking data including pelvis translations, trunk, pelvis, hip, knee and ankle joint angles and GRFs, and muscle stress. Forward dynamic optimization (Fig. 1.5) is time consuming, as demonstrated in [Anderson and Pandy, 2001a] where it took a CPU time of 10,000 hours (the wall-clock time was lower as 32 processors were running in parallel) to compute muscle activations of a half-cycle human gait. In later work, [Anderson and Pandy, 2001b] found that muscle forces computed by static and dynamic optimization were "remarkably similar".

Null space projection This technique consists of the decomposition of the total torque into two dynamically decoupled torque vectors: the torque corresponding to the commanded task behavior and the torque that only affects posture behaviors in the null space provided by the kinematic redundancy of the musculoskeletal system, as demonstrated in [Khatib et al., 2009] to synthesize human motion. However, this method presents several drawbacks, such as the difficulty in implementing time-dependant constraints, unnatural movement and unrealistic joint torque profiles.

Optimal control Optimal control drives the model from an initial state to a final state by solving for the histories of control and parameters to minimize a cost function, as defined in [Xiang et al., 2010] The problem of quantifying muscular activity of the human body can be formulated as an optimal control problem [Kaplan and Heegaard, 2001]. [Pandy et al., 1995] developed an optimal control model to simulate rising from a chair and introduce the time derivation of force as a new performance criterion. This approach was found to minimize the peak forces developed by the muscles. In [Kaplan and Heegaard, 2001], neural excitation for steady pedaling is solved using optimal control with second-order direct collocation. For large scale systems, direct collocation can reduce considerably the amount of computation time by discretizing the differential equations. However, implementation is laborious since first and second derivatives of the state equations with respect to the control variables are formulated analytically [Thelen et al., 2003].

Predictive Control Accurately tracking trajectories of some extremities is not how humans naturally move. Unlike robots, most people are not skilled enough to follow perfectly both kinematic and force trajectories. It is suggested in [Azevedo et al., 2004] that during walking, "humans perform global progression of the whole body, without trying to track a specific trajectory, while minimizing the overall energy consumption and correcting any trend to fall". To validate these hypotheses, model predictive

control were used to synthesize walking gaits for biped robots. The method is basically a constrained nonlinear optimization problem with a moving horizon. A set of coherent physical constraints was established related to standing posture, locomotion rhythm, static and dynamic equilibrium. However, integrating the dynamics equation of a musculoskeletal model is computationally expensive, even with reduced number of muscles [Yamaguchi and Zajac, 1990] or simplified muscle model [Neptune and Hull, 1998].

[Chung et al., 2015] predicts 3D human running (joint kinematics and torques) along curved paths without data-tracking. The cost function of the optimization problem consists of multiple tasks including minimizing dynamic effort and upper-body yawing moment to avoid slipping on the ground. Simulation results from this methodology show good correlation with experimental data obtained from human subjects.

[Falisse et al., 2019] Rapid predictive simulations with complex musculoskeletal models suggest that diverse healthy and pathological human gaits can emerge from similar control strategies

Disadvantages of optimal control approach Optimal control and dynamic optimization approaches can be used to draw insights into the principles behind human movements and muscle functions [Hamner et al., 2010]. However, defining the initial states and guesses to facilitate the convergence of optimal solutions is usually challenging, especially with models of high complexity like human bodies.

1.4 Contributions

Our motivation behind this work is to design a tool based inspired from robotics to study how neuromuscular impairments contribute to abnormal movement, and to predict the functional consequences of a modification of the musculoskeletal system. At present, the most common approach is using experimental captured data as input of simulations of 3D gait analysis and human movement generation. Although the results allow clinicians to identify the potential principals of a movement, the dependency on the capture data limits the prediction capacity of this approach. It is proposed in this work to address physics-based motion synthesis using a reactive optimization-based dynamic task controller. The controller architecture is inspired from whole-body controller in robotics which has shown interesting results with humanoids as well as in the other domains of robotics. Without requiring experimental data related to kinematics or contact forces, the method consists in computing joint kinematics and muscle activities by solving optimization problems describing the strategy of producing a target movement. The formulation of the optimization problems can also be modified to reflect strategy adaptation to different conditions and musculoskeletal modifications. We believe that this method has the capacity of predicting the implication of musculoskeletal modifications on movement and muscle behavior. As a result, it can be incorporated in the development of physics-based simulation tools that provide clinicians valuable information to be considered in orthopaedic treatment planning.

In chapter 2, a detailed description of the human body modeling is presented, with emphasis on actuator modeling. Linear actuators are our choice of modeling muscle actuation and their advantages are specified. Then, the review of whole-body controller is presented based on the work of [Lober, 2017], consisting of the task and constraint definitions as well as prioritization schemes.

The first contribution of this work is the development of a reactive optimization-based dynamic task controller, presented in chapter 3. We demonstrate how the robotic whole-body controller is adapted as a two-step optimization-based scheme for simulating movements with musculoskeletal models. The principal idea is to decouple to torque actuation space and the muscle actuation space by leveraging the linearity of actuator models. In this way, the controller takes advantage of both the low complexity of joint-actuated models and the characters of muscle-actuated models and demonstration through synthesis of two different strategies of squat under different conditions. Demonstrations of squat synthesis via the controller are performed with fixed-base and floating-base human models. The physical simulations are built and run with OpenSim, a biomechanical open-source software providing tools to model musculoskeletal systems and physical environments. The controller is programmed with the OpenSim C++ API. In parallel, experiments are carried out to collect data related to body kinematics, force-ground con-

tact forces and electromyographic signals. The numerical models are also scaled to reflect the morphology of the subject so experimental data can be used to compare with simulated data. The proposed controller is able to generate major features of the movement strategies under different performance conditions and with different types of human models.

The second contribution is the application of our physics-based simulation method as a prediction tool of the effects of surgical interventions of lower limbs on human movements. As mentioned previously, the need of testing different surgical scenarios and their respective outcomes, on a specific patient, in order to personalize the surgical plan is of great demand. We investigate the performance of our method in two orthopaedic interventions. In the first one (Chapter 5), we assess the influence of tendon attachment points on the outcome of rectus femoris transfer surgery, a stiff-knee gait treatment. Based on the simulation results, we confirm the clinicians' choice of attachment point in terms of related to muscle moment arms and forces. In the second one Chapter 6), we investigate the implication of the combination of patellar tendon advancement (PTA) and distal femoral extension osteotomy (DFEO), which are crouch gait treatments, on knee extensors' activities. The outcomes give rise to a perspective of a more complete tool with the goal of optimizing this treatment method. Finally, conclusions and perspectives of our approach are discussed in chapter 7. Overall, the results are encouraging and suggest that further developments could be extended to other types of movement, notably walking, to demonstrate potential distinguished utilities of the approach.

Chapter 2

Human Modeling and Whole-Body Control

Human movement synthesis is a predictive simulation. The approach has the potential of identifying the causal relationship between musculoskeletal elements and movement strategies without relying on experimental data. The methods based on this approach can offer clinicians the possibility of studying the influence of isolated neuro-musculoskeletal features by adjusting model parameters [De Groote and Falisse, 2021].

To synthesize human-like movement, there are two aspects to be considered: biomechanical human modeling and movement synthesis method. Human modeling takes into account how skeletal and actuation structures are represented, connected and interacting with each other in accordance with the laws of physics. To model the musculoskeletal profile of a particular individual, each body segment, actuation element and joint are characterized by different personalized parameters related to mechanical and physiological properties. In the context of modeling patients suffering musculoskeletal deficiencies, these elements are modified to reflect not only impairments but also modifications as the outcomes of surgical interventions. For example, impaired muscles can be reflected by changing the physiological parameters of fibers and tendons; changing tendon attachment points represents tendon release and reattachment in tendon transfer procedures. With a personalized model, a synthesis method is established representing the motor strategies of the central nervous system (CNS). The common approach is to assume that the performance of a movement is optimized in terms of one or multiple criteria, e.g. the metabolic cost, while taking into account the properties of the musculoskeletal system. In this work, we develop our method based the whole-body control theory in robotics and Quadratic Program (QP). The movement is synthesized as an optimized process where multiple objectives and constraints are involved. Control objectives are corresponded to high-level physical-relevant intentions, such as lifting a body part, reaching targets or saving energy. Constraints are related to the dynamic feasibility and system intrinsic limits. This chapter presents the detailed descriptions of biomechanical human modeling and the structure of the controller. They allow us to develop our controller schemes for movement synthesis.

2.1 Musculoskeletal Modeling

Once the topology of the model is defined, the actuation system is designed in terms of complexity, alongside with the contact modeling contributing an important role of representing the interaction between the human body and the environment. In the end, the forces applied by actuators and contact wrenches produce body accelerations in accordance with the equation of motion. These aspects will be detailed in the following sections.

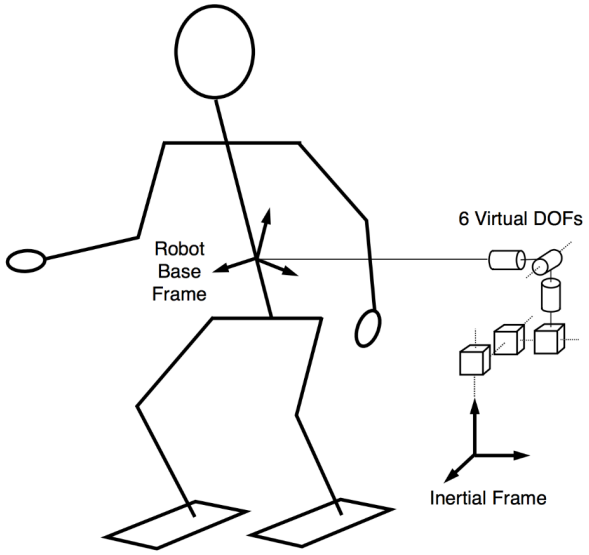

Figure 2.1: Kinematic representation of floating-base systems. The floating-base is connected to the inertial frame through a 6-DoF joint. Image taken from [Mistry et al., 2010]

2.1.1 Multibody Dynamics

The skeletal model follows the human body map, consisting generally of two legs and two arms joined by a torso [Kulić et al., 2016]. From the robotic modeling point of view, the model is a tree structure with a base body as its root which can float freely in Cartesian space. To capture the configuration of the system, it is common to use the generalized coordinates $\boldsymbol{q} \in \mathbb{R}^n$, n the number of generalized coordinates consisting of the floating-base pose $\boldsymbol{q}_b \in \mathbb{R}^6$ and the joint space coordinates $\boldsymbol{q}_j \in \mathbb{R}^{n-6}$. The generalized coordinates is expressed as

$$\boldsymbol{q} = \begin{bmatrix} \boldsymbol{q}_b \\ \boldsymbol{q}_j \end{bmatrix} \tag{2.1}$$

The generalized velocities and accelerations are then expressed as $\boldsymbol{\nu} = \begin{bmatrix} \boldsymbol{\nu}_b \\ \dot{\boldsymbol{q}}_j \end{bmatrix}$ and $\dot{\boldsymbol{\nu}} = \begin{bmatrix} \dot{\boldsymbol{\nu}}_b \\ \ddot{\boldsymbol{q}}_j \end{bmatrix}$ where indices $\bullet_b$ and $\bullet_j$ denote definitions with respect to (w.r.t) the base and the joints respectively.

Supposing that the joint models are perfect and the body segments are rigid, the dynamics of musculoskeletal systems can be defined as the mapping between the forces acting on the system and the accelerations they produce [Stanev, 2018], and expressed as the equation of motion (EoM)

$$M(\boldsymbol{q})\,\dot{\boldsymbol{\nu}} + \boldsymbol{c}(\boldsymbol{q}, \boldsymbol{\nu}) + \boldsymbol{g}(\boldsymbol{q}) = \begin{bmatrix} \mathbf{0}_6 \\ \boldsymbol{\tau} \end{bmatrix} + \sum_j J_{cj}^T(\boldsymbol{q})\,\boldsymbol{\omega}_{cj} \tag{2.2}$$

with M the inertia matrix, $\boldsymbol{c}$ the centrifugal and Coriolis effects vector, $\boldsymbol{g}$ the gravity force vector, $\boldsymbol{\tau}$ the joint torques generated by actuators. $\boldsymbol{\omega}_{cj}$ captures the i_{th} external contact wrench applied to the system and $J_{cj}(\boldsymbol{q})$ the associated Jacobian.

$$M(\boldsymbol{q})\,\dot{\boldsymbol{\nu}} + \boldsymbol{c}(\boldsymbol{q}, \boldsymbol{\nu}) + \boldsymbol{g}(\boldsymbol{q}) = \boldsymbol{\tau} \tag{2.3}$$

From this equation, we can see that the floating base is not actuated, hence the human body is an underactuated system.

The intrinsic physical constraints have to be also considered to represent thoroughly the model behavior. They are expressed as the following inequalities:

- joint position limits

$$\boldsymbol{q}_{min} \leq \boldsymbol{q} \leq \boldsymbol{q}_{max} \tag{2.4}$$

- joint velocity limits

$$\boldsymbol{\nu}_{min} \leq \boldsymbol{\nu} \leq \boldsymbol{\nu}_{max} \tag{2.5}$$

- joint torque limits

$$\boldsymbol{\tau}_{min} \leq \boldsymbol{\tau} \leq \boldsymbol{\tau}_{max} \tag{2.6}$$

Special Case : Actuators Following Linear Control-Force Model

In equation 2.3, the expression of the joint torques $\boldsymbol{\tau}$ depends on the topology of the actuator chain and the characteristics of the actuators themselves. In case of actuators following linear control-force model, the joint torque produced at a joint can be formulated as

$$\boldsymbol{\tau} = T(\boldsymbol{q})\,\boldsymbol{u} \tag{2.7}$$

with $\boldsymbol{u}$ the control input vector and $T(\boldsymbol{q})$ a matrix representing the actuation characteristics. This matrix accounts for the arrangements of the actuators w.r.t the joints and depends on the configuration of the body.

The dynamic equation 2.3 can be rewritten as

$$M(\boldsymbol{q})\,\dot{\boldsymbol{\nu}} + \boldsymbol{c}(\boldsymbol{q},\boldsymbol{\nu}) + \boldsymbol{g}(\boldsymbol{q}) = \begin{bmatrix} \mathbf{0}_6 \\ T(\boldsymbol{q}) \end{bmatrix} \boldsymbol{u} + \sum_j J_{cj}^T(\boldsymbol{q})\,\boldsymbol{\omega}_{cj} \tag{2.8}$$

Thanks to their simplicity and computational efficiency, this type of actuators can used in human movement simulation with linear optimization processes.

2.1.2 Actuator Modeling

There are various types of actuators that can be implemented in the human modeling. Here, we present three common types of actuators: joint actuators, path actuators and muscles. While joint actuators apply torques directly at the joints, path actuators and muscles cooperate to drive the passive joints and carry out motion.

Joint Actuators

The most basic joint actuator is the linear torque generator. The torque amplitude is proportional to control input

$$\tau = \tau_{max}\,u \tag{2.9}$$

where τ_{max} is the maximum force and u is the control input. As the model is linear, equation 2.7 can be applied and the corresponding transmission matrix T is a diagonal matrix whose elements are

$$T_{i,i} = \tau_{max,i} \tag{2.10}$$

with $\tau_{max,i}$ the maximum available torque of the i^{th} torque generator. It is worth noting that the range of the control inputs is $[-1, 1]$, meaning the torque actuators can generate both extension and flexion torques. This type of actuator can be useful to study the joint torque profiles during a movement.

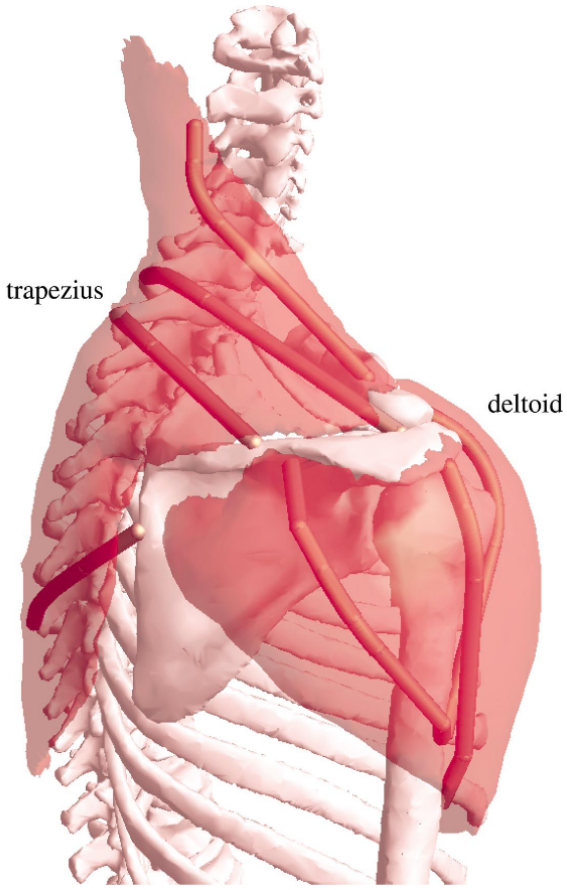

Figure 2.2: Multiple paths were used to model the action of each muscle group. In this model, the trapezius was separated into four bundles and the deltoid into three. Image taken from [Pandy, 2001]

Path Actuators

This type of actuators emulates the muscle path in the body, meaning they are defined from anatomical landmarks, such as muscle origins and insertion points which are fixed on the bones [Pandy, 2001]. They can wrap around body segments or other path actuators, depending on the configuration of the skeletal system, and span over multiple joints and produce acceleration directly or indirectly at multiple levels in the kinematic tree [Stanev, 2018].

The most common method to model realistically muscle routing is the centroid-line method. In this method, the muscle path, represented as a line passing through the locus of cross-sectional centroids of the muscle [Jensen and Davy, 1975]. Comparing to the straight-line method, where the muscle's line of action is a straight line joining the attachment sites, the results produced with the centroid-line method is considered more "meaningful" biomechanically (Fig. 2.2).

The dynamic model of path actuator is a simple linear model

$$f = F_{max}\, u \tag{2.11}$$

where F_{max} is the maximum force and u is the excitation, which is also referred to as control input. During a movement, multiple path actuators work together to actuate the passive joints. Their function reflects the redundancy of the muscular system, therefore they are useful to study muscle recruitment at a basic level and also offer cheap computation and easy formulation of control problems. On the other hand, dynamic behaviors related to length, length variation and control variation as well as fatigue are omitted, leading to unnatural actuator forces. As path actuators are linear actuator, equation 2.3 can be applied. The selection matrix takes into account the moment arms of the muscles and its elements are

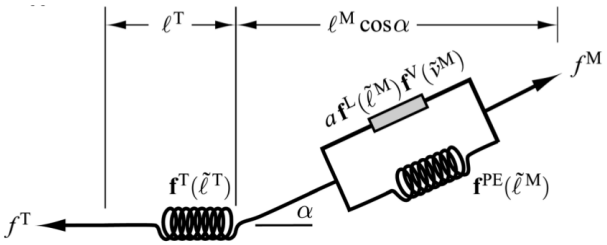

Figure 2.3: Hill-type musculotendon actuators consist of an active contractile element, a passive elastic element, and an elastic tendon. Image from [Millard et al., 2013]

expressed as

$$T_{i,j} = F_{max,j}\, d_{i,j}(\boldsymbol{q}) \tag{2.12}$$

with $F_{max,j}$ the maximum force of the j^{th} actuator and $d_{i,j}(\boldsymbol{q})$ the moment arm with respect to (w.r.t) the i^{th} joint. Due to the spatial attachment configuration of muscles, their moment arm is configuration dependent.

Muscle actuators

Muscle actuators can be considered as a subset of path actuators, whose dynamic model is non-linear and takes into account multiple physiological and kinematic parameters. There are two major classes of muscle models that have been used in biomechanics and motor control, namely Hill-type and Huxley-type [Stanev, 2018]. The Huxley-type model [Huxley, 1974] focusing on cross-bridge, the molecular mechanism behind the sliding filament theory of muscle contraction [Huxley, 2004], lends the physiological plausibility to results. Nonetheless, this model is computationally demanding and model parameters are not easily obtained or scaled across different muscles as is the case for the Hill-type model [Stanev, 2018]. The Hill-type model (Fig. 2.3) is designed to produce some of the most physiological factors influencing force production: muscle excitation, muscle contraction and muscle stiffness. The model consists mainly of three elements. The contractile element is in parallel with a passive element, and they are in series with the tendon.

Hill-type muscle force The muscle force f^M produced is computed as

$$f^M(a, \tilde{l}^M, \tilde{v}^M) = f_0^M(af^L(\tilde{l}^M)f^V(\tilde{v}^M) + f^{PE}(\tilde{l}^M)) \tag{2.13}$$

where

- a is the muscle activation ranging between 0 and 1.
- $\tilde{l}^M$ and $\tilde{v}^M$ are respectively the muscle length and muscle intrinsic shortening velocity normalized by the optimal fiber length l_0^M and muscle maximum intrinsic shortening velocity v_{max}^M.
- f_0^M is the peak isometric force.
- $f^L(\tilde{l}^M)$ is the active Force-Length (F-L) curve, peaking at f_0^M and l_0^M, describing how the muscle maximum active force varies non-linearly with its length.
- $f^V(\tilde{v}^M)$ is the Force-Velocity (F-V) curve, describing how the muscle force varies nonlinearly with its rate of lengthening during non-isometric contractions. This curve is associated with the contractile element.
- $f^{PE}(\tilde{l}^M)$ is the Passive-Force-Length (F-PE) curve, describing how the muscle force produced when the muscle is stretched beyond a threshold length. This curve is associated with the passive element representing the muscle stiffness.

Hill-type activation dynamics Muscles cannot generate force or relax instantaneously due to the underlying chemical reaction, meaning there is a delay between muscle excitation u and activation a. This is represented by a first-order ordinary differential equation (ODE)

$$\dot{a} = \frac{u - a}{\Omega(a, u)} \tag{2.14}$$

where Ω is a coefficient computed from u, a and activation or deactivation time constant, depending on whether the muscle is contracting or relaxing.

Hill-type musculotendon equilibrium Muscles are attached to bones through tendons and can stretch them beyond their slack length. In this case, tendons are modeled as an elastic element developing force following the Tendon Force-Length (F-T) curve $f^T(\tilde{l}^T)$. The equilibrium between muscle and tendon forces is expressed as

$$f^M(a, \tilde{l}^M, \tilde{v}^M)\, cos(\alpha) = f_0^M f^T(\tilde{l}^T) \tag{2.15}$$

with α the pennation angle at which muscle fibers are attached to tendon.

The three equations 2.13, 2.14 and 2.15 are assembled into a set of first-order differential equations and solved for the musculotendon force f^{MT}. By using normalized parameters, Hill-type can be easily scaled across different muscles [Zajac, 1993].

2.1.3 Contact Modeling

Contact modeling is crucial for biomechanical simulation, especially in case of free-floating system where the wrench of foot-ground contact influences strongly the dynamic behavior of the system. Common approaches for contact modeling can be divided into two categories: discrete contact dynamics and continuous contact dynamics

Discrete Contact Dynamics Models

The discrete model, also referred to as the non-smooth model or the rigid model, is used mainly if the impact involves rigid or very hard and compact bodies. In this model, the process is assumed to happen in an instant, provoking the discontinuous changes in kinetic quantities without displacement [Gilardi and Sharf, 2002]. Penetration between the bodies in contact is not allowed, meaning contact forces are unilateral. The classical formulation describes contact unilateral forces by separating them into the normal and tangential components.

With $\boldsymbol{f}_c$ the contact force and $\boldsymbol{n}$ the normal to the contact surface, the normal component is expressed as

$$f_c^n = \boldsymbol{f}_c \cdot \boldsymbol{n} \tag{2.16}$$

The value of the normal component depends on the contact state. If there is contact, $f_c^n \geq 0$, otherwise $f_c^n = 0$.

The tangential component is closely related to friction. A standard friction model is the Coulomb dry friction model, which describes two regimes of friction: *kinetic friction*, where relative motion occurs between the bodies in contact, and *static friction*, where frictional force still keeps the bodies stick together. The tangential component is expressed as following

$$\begin{cases} \boldsymbol{f}_c^t = \mu_c f_c^n \frac{\dot{\boldsymbol{x}}^t}{\|\dot{\boldsymbol{x}}^t\|} \Leftarrow \| \dot{\boldsymbol{x}}^t \| > 0 \\ \| \boldsymbol{f}_c^t \| \leq \mu_c f_c^n \Leftarrow \| \dot{\boldsymbol{x}}^t \| = 0 \end{cases} \tag{2.17}$$

with $\dot{\boldsymbol{x}}$ the relative velocity of the bodies and μ_c is the Coulomb friction coefficient.

Continuous Contact Dynamics Models

The continuous model, also referred to as compliant contact model, explicitly accounts for the deformation of the bodies during impact or contact by defining the normal contact force f_c^n as an explicit function of local indentation δ Two common models are Hertz model and Hunt-Crossley model.

Hertz Model Hertz is usually used in situations where contacts occur between spherical objects. Multiple assumptions are adopted in a Hertz problem: static applied load, smooth contact surfaces, small deformation, linearly elastic material and so on. The impact force is defined as

$$f_c^n = k\delta^n \tag{2.18}$$

where k and n are constants related to material and geometric properties. Since Hertzian model does not account for energy dissipation, this model can be used only for low impact speeds and hard materials[Gilardi and Sharf, 2002].

Hunt-Crossley Model This model accounts for energy dissipation by including a non-linear damping term

$$f_c^n = b\delta^p\dot{\delta}^q + k\delta^n \tag{2.19}$$

where b is the damping parameter related to the coefficient of restitution, p is usually set equal to n and $q = 1$ [Hunt and Crossley, 1975]. The biggest advantage is this model is that the contact force has no discontinuities at initial contact and separation, but it begins and finishes with the correct value of zero [Gilardi and Sharf, 2002].

In practice, the foot-ground contact can be modeled with a continuous contact model, taking account parameters related to their geometry and material. The contact forces are computed based on the current state of the system that gives the deformation between the elements, and the chosen contact dynamics model.

2.2 Whole-Body Control

In robotics, whole-body control (WBC) is a closed-loop control method that takes advantage of the full mobility of the entire body of redundant, floating-base robots to performs multiple tasks in compliant multi-contact interactions with the environment [Moro and Sentis, 2019]. The tasks vary from walking, running, reaching, climbing stairs to manipulating objects. "While humans may occasionally be outperformed by robots in a single task, they are vastly more capable of adapting and combining behaviors to solve multiple different tasks" [**?**]

In the optimization-based WBC framework, the control problem can be formulated as a quadratic multi-objective optimisation problem under linear constraints [Padois, 2016]. The objectives are expressed as linear cost functions and associated with coefficients related to their priorities. In a forward dynamic simulation, at each time step, the resulting optimisation problem is solved to find local optimal actuation inputs which minimize the cost functions while respecting the constraints. The general form can be expressed as

$$\begin{aligned} \underset{\boldsymbol{\chi}}{\text{argmin}} \quad & f(\boldsymbol{\chi}) \\ \text{s.t} \quad & G\boldsymbol{\chi} \leq \boldsymbol{h} \\ & A\boldsymbol{\chi} = \boldsymbol{b} \end{aligned} \tag{2.20}$$

f is the cost function in terms of $\boldsymbol{\chi}$, the optimization variables. The smaller its value is, the better the task is performed. G and $\boldsymbol{h}$ represent to the equality constraint while A and $\boldsymbol{b}$ define the inequality constraints.

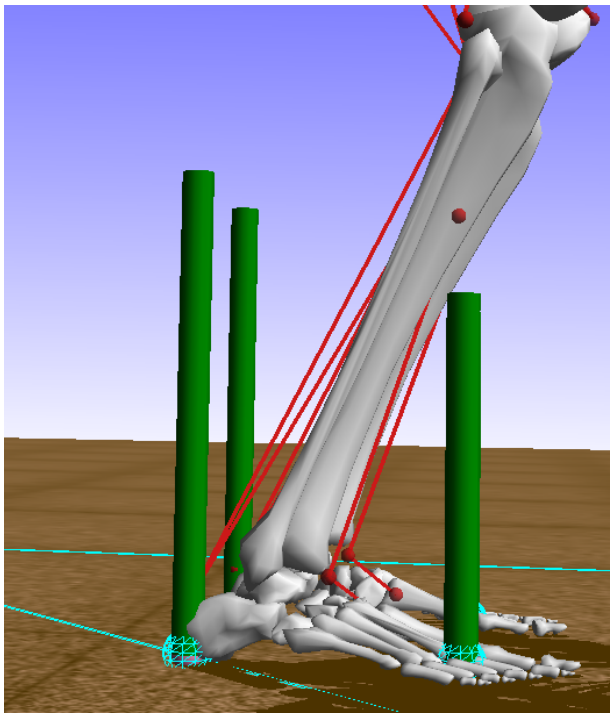

Figure 2.4: Feet with three spherical volumetric contact elements. The green bars represent the amplitudes of the contact forces.

2.2.1 Constraint Formulation

Multiple constraints are imposed on a biomechanical system as showed in 2.1.1. In this section, these constraints are transformed to adapt to the QP formulation by introducing an optimization variable vector into their expressions. In our work, the optimization variables are chosen as

$$\boldsymbol{\chi} = \begin{bmatrix} \dot{\boldsymbol{\nu}} \\ \boldsymbol{u} \\ \boldsymbol{\omega}_c \end{bmatrix} \tag{2.21}$$

with $\boldsymbol{\omega}_c$ the concatenation of external contact wrenches $\boldsymbol{\omega}_{cj}$. $\boldsymbol{u}$ appearing in the vector implies that the actuators follow a linear dynamic model.

Dynamics

The equation of dynamics describes how the actuators and other applied forces influence the evolution of the state of the robot. We rewrite the dynamic equation in terms of chosen optimization variables

$$M(\boldsymbol{q})\,\dot{\boldsymbol{\nu}} + \boldsymbol{c}(\boldsymbol{q},\boldsymbol{\nu}) + \boldsymbol{g}(\boldsymbol{q}) = S(\boldsymbol{q})\boldsymbol{u} + J_c^T(\boldsymbol{q})\,\boldsymbol{\omega}_c \tag{2.22}$$

where $J_c(\boldsymbol{q})$ the concatenation of $J_{cj}(\boldsymbol{q})$ and $S(\boldsymbol{q}) = \begin{bmatrix} \mathbf{0}_6 \\ T(\boldsymbol{q}) \end{bmatrix}$. Replacing 2.21 into the above equation yields

$$\begin{bmatrix} -M(\boldsymbol{q}) & S(\boldsymbol{q}) & J^T(\boldsymbol{q}) \end{bmatrix} \boldsymbol{\chi} = \boldsymbol{c}(\boldsymbol{q},\boldsymbol{\nu}) + \boldsymbol{g}(\boldsymbol{q}) \tag{2.23}$$

The equality constraint 2.23 ensures that the obtained controls produce a physically feasible movement.

Joint Limits

The angular joint limits can be expressed as an inequality on $\boldsymbol{q}$

$$\boldsymbol{q}_{min} \leq \boldsymbol{q} \leq \boldsymbol{q}_{max} \tag{2.24}$$

To formulate this constraint, $\boldsymbol{q}$ needs to be calculated by second-order approximation

$$\boldsymbol{q}(t+h) = \boldsymbol{q}(t) + h\boldsymbol{\nu}(t) + \frac{h^2}{2}\dot{\boldsymbol{\nu}}(t) \tag{2.25}$$

where h is the prediction period, which is generally some multiple of the control period. Replacing 2.25 in 2.24 yields the expression of the inequality in terms of $\boldsymbol{\chi}$

$$\begin{bmatrix} I & 0 \\ -I & 0 \end{bmatrix} \boldsymbol{\chi} \leq \frac{2}{h^2} \begin{bmatrix} \boldsymbol{q}_{min} - \boldsymbol{q} - h\boldsymbol{\nu} \\ \boldsymbol{q}_{max} - \boldsymbol{q} - h\boldsymbol{\nu} \end{bmatrix} \tag{2.26}$$

Joint Speed Limits

The angular joint speed limits can be expressed as an inequality on $\boldsymbol{q}$

$$\boldsymbol{\nu}_{min} \leq \boldsymbol{\nu} \leq \boldsymbol{\nu}_{max} \tag{2.27}$$

To formulate this constraint, $\boldsymbol{\nu}$ needs to be calculated by first-order approximation

$$\boldsymbol{\nu}(t+h) = \boldsymbol{\nu}(t) + h\dot{\boldsymbol{\nu}}(t) \tag{2.28}$$

Replacing 2.28 in 2.27 yields

$$\begin{bmatrix} I & 0 \\ -I & 0 \end{bmatrix} \boldsymbol{\chi} \leq \begin{bmatrix} \boldsymbol{\nu}_{max} - \boldsymbol{\nu} \\ -\boldsymbol{\nu}_{min} - \boldsymbol{\nu} \end{bmatrix} \tag{2.29}$$

Control Input Limits

Similar to the joint limits, the control input constraint can be written as

$$\boldsymbol{u}_{min} \leq \boldsymbol{u} \leq \boldsymbol{u}_{max} \tag{2.30}$$

Using $\boldsymbol{\chi}$, 2.30 can be rewritten as

$$\begin{bmatrix} \boldsymbol{0} & S(\boldsymbol{q}) & 0 \\ \boldsymbol{0} & -S(\boldsymbol{q}) & 0 \end{bmatrix} \boldsymbol{\chi} \leq \begin{bmatrix} \boldsymbol{u}_{max} \\ -\boldsymbol{u}_{min} \end{bmatrix} \tag{2.31}$$

As the model of linear actuators does not represent the dynamics of muscle contraction, the actuators can adopt any value of control input and can provoke sudden change of acceleration and potentially instability. This problem can be partially dealt with by changing the boundaries of the control inputs dynamically following these rules

$$\boldsymbol{u}_{max} = min(\boldsymbol{u} + \delta\boldsymbol{u}_{ou}; \boldsymbol{U}_{max}) \tag{2.32}$$

$$\boldsymbol{u}_{min} = max(\boldsymbol{u} + \delta\boldsymbol{u}_{ol}; \boldsymbol{U}_{min}) \tag{2.33}$$

where $\delta\boldsymbol{u}_{ol}$ and $\delta\boldsymbol{u}_{ou}$ are respectively the predefined lower and upper offsets from the current control inputs $\boldsymbol{u}$, and $\boldsymbol{U}_{min}$ and $\boldsymbol{U}_{max}$ are respectively the minimum and maximum control inputs allowed by the actuators. In terms of numerical value, $\boldsymbol{U}_{max}$ are usually set to $\boldsymbol{1}$; for a torque generator, $\boldsymbol{U}_{min} = \boldsymbol{-1}$ as it can drive a joint in both directions and for a path actuator, $\boldsymbol{U}_{min} = \boldsymbol{0}$ as the actuator can only pull the bodies to which they attached. Attention should be paid on choosing the offsets to maintain $\boldsymbol{u}_{max}$ higher than $\boldsymbol{u}_{min}$.

Contact Constraint

A system interacts with the environment through contacts. To maintain a contact, the relative movement between the two considered bodies at the contact point is zero, thereby the linear velocity at a given contact point i is zero.

$$J_{ci}(\boldsymbol{q})\dot{\boldsymbol{\nu}} + \dot{J}_{ci}(\boldsymbol{q})\boldsymbol{\nu} = 0 \tag{2.34}$$

Expressing this constraint in terms of $\boldsymbol{\chi}$ yields

$$\begin{bmatrix} J_{ci}(\boldsymbol{q}) & \mathbf{0} \end{bmatrix} \boldsymbol{\chi} = -\dot{J}_{ci}(\boldsymbol{q})\boldsymbol{\nu} \tag{2.35}$$

Center of Mass Boundaries

To avoid the model losing balance (falling backward or forward), the projection of center of mass (CoM) on the ground is imposed to be inside the convex hull of the foot-support area. For a sagittal model, considering x_m the coordinate of the CoM on the horizontal axis, the boundary constraint imposed on the projection of the CoM on the ground can be expressed as

$$x_{m,min} \leq x_m \leq x_{m,max} \tag{2.36}$$

with $x_{m,min}$ the lower boundary close to the heel and $x_{m,max}$ the boundary close to the toe. The projection of CoM x_m is calculated by second-order approximation

$$x_m(t+h) = x_m(t) + h\dot{x}_m(t) + \frac{h^2}{2}\ddot{x}_m(t) \tag{2.37}$$

where h is the prediction period. Replacing 2.37 in 2.38 yields

$$\ddot{x}_{m,min} \leq \ddot{x}_m \leq \ddot{x}_{m,max} \tag{2.38}$$

with

$$\ddot{x}_{m,min} = \frac{2}{h^2}(x_{m,min} - x_m - h\dot{x}_m)$$

$$\ddot{x}_{m,max} = \frac{2}{h^2}(x_{m,max} - x_m - h\dot{x}_m)$$

The CoM acceleration can be computed in terms of generalized accelerations $\dot{\boldsymbol{\nu}}$

$$\ddot{x}_m = \frac{\boldsymbol{S}_m}{M}\sum_i m_i(J_{m,i}\,\dot{\boldsymbol{\nu}} + \dot{J}_{m,i}\,\boldsymbol{\nu}) \tag{2.39}$$

with $J_{m,i}$ the Jacobian w.r.t the CoM of the body i^{th} and m_i its mass, $M = \sum_i m_i$ the total mass of the system and $\boldsymbol{S}_m = [1\ 0\ 0]$ the row vector to select the component x of the whole body CoM position vector.

2.2.2 Task Formulation

Tasks can be defined as the control of one or more DoF of the system toward objectives [Salini et al., 2011], The objectives include desired accelerations, wrenches, or torques, and in operational-space or joint-space. The mathematical expressions of tasks are the functions the errors between the desired and current values of the task [Lober, 2017].

Acceleration Task

One of the most common tasks are to move a controlled frame from one pose (position + orientation) to another. These position or orientation tasks are converted to acceleration tasks via task servoing [Lober, 2017]. The acceleration task consists of tracking desired accelerations references by minimizing the errors between actual accelerations and desired ones. From the generalized accelerations, one can express an acceleration of a point in the operational space as

$$\ddot{\boldsymbol{x}}_i = J_i(\boldsymbol{q})\dot{\boldsymbol{\nu}} + \dot{J}_i(\boldsymbol{q}, \boldsymbol{\nu})\boldsymbol{\nu} \tag{2.40}$$

where $J_i(\boldsymbol{q})$ and $\dot{J}_i(\boldsymbol{q}, \boldsymbol{\nu}$ are the Jacobian and its derivative at the point. Given the desired acceleration $\ddot{\boldsymbol{x}}_i^{des}$, the tracking problem can be written as

$$f_i^{\ddot{\boldsymbol{x}}} = \left\| \ddot{\boldsymbol{x}}_i - \ddot{\boldsymbol{x}}_i^{des} \right\|_2^2 \tag{2.41}$$

with $f_i^{\ddot{\boldsymbol{x}}}$ the objective function to be minimized. This term is then rewritten in terms of $\boldsymbol{\chi}$, the optimization variable

$$f_i^{\ddot{\boldsymbol{x}}} = \left\| [J_i(\boldsymbol{q}) \quad \boldsymbol{0}]\, \boldsymbol{\chi} - \left(\ddot{\boldsymbol{x}}_i^{des} - \dot{J}_i(\boldsymbol{q}, \boldsymbol{\nu}) \right) \right\|_2^2 \tag{2.42}$$

Acceleration tasks can also be expressed in joint space

$$f_i^{\dot{\boldsymbol{\nu}}} = \left\| \dot{\boldsymbol{\nu}}_i - \dot{\boldsymbol{\nu}}_i^{des} \right\|_2^2 \tag{2.43}$$

and then rewritten in terms of χ

$$f_i^{\dot{\boldsymbol{\nu}}} = \left\| [I \quad \boldsymbol{0}]\, \boldsymbol{\chi} - \dot{\boldsymbol{\nu}}_i^{des} \right\|_2^2 \tag{2.44}$$

Wrench Task

For underactuated systems like humanoid and human body, external wrenches have a great influence on the interaction with the environment. The task is expressed as the squared norm of task errors

$$f_i^{\boldsymbol{\omega}} = \left\| \boldsymbol{\omega}_i - \boldsymbol{\omega}_i^{des} \right\|_2^2 \tag{2.45}$$

We can select wrench components to be controlled by using a selection matrix S_i^{ω} and rewrite 2.45 in terms of $\boldsymbol{\chi}$

$$f_i^{\boldsymbol{\omega}} = \left\| [\boldsymbol{0} \quad S_i^{\omega}]\, \boldsymbol{\chi} - \boldsymbol{\omega}_i^{des} \right\| \tag{2.46}$$

Torque Task

$$f_i^{\boldsymbol{\tau}} = \left\| \boldsymbol{\tau} - \boldsymbol{\tau}^{des} \right\|_2^2 \tag{2.47}$$

In the special case of linear actuators, Eq. 2.7 allows 2.47 to be written in terms of $\boldsymbol{\chi}$

$$f_i^{\boldsymbol{\tau}} = \left\| [\boldsymbol{0} \quad S(\boldsymbol{q}) \quad \boldsymbol{0}]\, \boldsymbol{\chi} - \boldsymbol{\tau}^{des} \right\| \tag{2.48}$$

2.2.3 Prioritization strategies

Thanks to the redundancy nature of human body, multiple tasks are to be performed simultaneously. In these cases, their cost functions are combined together before being solved. However, more often than not, conflicts exist between certain tasks, and they need to be addressed by modulating their associated priorities. The common approaches of task prioritization can be categorized into strict task priorities and non strict task priorities.

Strict Task Priorities

The goal of strict task priorities, handled by hierarchical strategies is that the higher tasks are achieved without any disturbance from the lower tasks [Salini et al., 2011]. In a hierarchical strategy, the tasks are organized in discrete levels of priority and optimized in descending order. The solution to the optimization of a task is used in the equality constraints of the optimization of next lower-priority task.

Algorithm 1 Hierarchical Multi-Objective Optimization

1: **for** $i \leftarrow 1$ to n_{task} **do**

$$\begin{aligned} \boldsymbol{\chi}_i^* = \underset{\boldsymbol{\chi}}{\text{argmin}} \quad & f_i(\boldsymbol{\chi}) + w_0 f_0(\boldsymbol{\chi}) \\ \text{s.t} \quad & G\boldsymbol{\chi} \leq \boldsymbol{h} \\ & A_i \boldsymbol{\chi} = \boldsymbol{b}_i \end{aligned} \tag{2.49}$$

2: $A_{i+1} \leftarrow \begin{bmatrix} A_i \\ E_i \end{bmatrix}$ ▷ with E_i in the general task formulation $f_i = \| E_i \boldsymbol{\chi} - \boldsymbol{f}_i \|_2^2$

3: $\boldsymbol{b}_{i+1} \leftarrow \begin{bmatrix} \boldsymbol{b_i} \\ \boldsymbol{\chi}_i^* \end{bmatrix}$

4: $\boldsymbol{\chi} \leftarrow \boldsymbol{\chi}_i^*$

5: **end for**

6: **return** $\boldsymbol{\chi}$

Algorithm 1 is a sequence of null-space projection in the dynamic domain. The regularization term, $w_0 f_0(\boldsymbol{\chi})$ remove solution redundancy while the operation $A_{i+1} \leftarrow \begin{bmatrix} A_i \\ E_i \end{bmatrix}$ the null space of the objective function, which has just been solved, to the objective function of the next lower-priority task through the equality constraint [Lober, 2017]. However, this formulation is not compatible with inequality constraints, such as those restricting contact forces in-side friction cones to avoid foot slippage [Liu et al., 2016]. Furthermore, while critical tasks with higher priorities are fulfilled, it's not always possible to find a control set for to achieve tasks with lower priority performed only in the null space of higher priority tasks.

Non Strict Task Priorities

Weighted prioritization, on the other hand, allows lower priority tasks to be achieved outside of the null space of higher priority tasks. Compromise between the tasks is found based on their respective weights [Salini et al., 2011]. The optimal solution favors the minimization of the tasks assigned to higher weights while lower weighted tasks are still partially achieved. However, interference between tasks is not definitively excluded, hence there is no guarantee of tasks being perfectly fulfilled.

Algorithm 2 Weighted Optimization

$$\begin{aligned} \boldsymbol{\chi}^* = \underset{\boldsymbol{\chi}}{\text{argmin}} \quad & \sum_{i=1}^{n_{task}} w_i f_i(\boldsymbol{\chi}) + w_0 f_0(\boldsymbol{\chi}) \\ \text{s.t} \quad & G\boldsymbol{\chi} \leq \boldsymbol{h} \\ & A\boldsymbol{\chi} = \boldsymbol{b} \end{aligned} \tag{2.50}$$

return $\boldsymbol{\chi}^*$

Chapter 3

The two-step optimization based synthesis approach of squat movement

As stated in [Dan et al., 1999], "the emergence of motor strategies can be regarded as a manifestation of priority management by the subject's nervous system faced with the redundancy problem. Such priorities depend on intrinsic and extrinsic constraints as well as on optimization factors for the task". It is therefore natural to describe the synthesis of a human movement as an optimization problem, in which a person is considered to be performing a number of tasks with different priorities to achieve physically-relevant goals while respecting certain constraints. The goals can be minimizing the consumed energy, reaching a target by a member of the body or moving at a desired speed. The constraints are related to the physical limits of the musculoskeletal system, the characteristics of the movement as well as the boundaries and obstacles from the environment. Mathematically, these elements can be expressed by simple objective functions, equalities and inequalities, then solved by optimization algorithms to find an optimal solution. Thanks to this approach, the redundancy nature of the muscular system is overcome. This approach is appealing as it allows both to generate many types of human movement from high-level specification and to define them in a simple way. [Al Borno et al., 2012].

In robotics, as detailed in Section 2.2, optimization is implemented in whole-body controllers to generate human-like movements for humanoids. As robots usually follow predefined trajectories (reference), generated offline or through online trajectory planification, one of the main tasks is to reduce the errors between the reference and the actual positions of the controlled organs. However, humans do not follow a predefined trajectory during movements, and do not develop this skill of trajectory tracking throughout their lives. In consequence, synthesizing human-like movement without using established trajectories is one of the main challenges that we face. To this end, we develop a two-step optimization control scheme based on the theory of the whole-body control, and also inspired from the idea of decoupling the dynamics of the skeletal system with the one of the muscular system. Indeed, the skeletal system allows to formulate optimization problems with low dimensions, therefore increasing their solvability, while the muscular system takes into account the properties specifically related to the muscle actuation. We synthesize human-like movements with skeletal joint-actuated models. Once the history of joint torques and model states are obtained, they are used to compute muscle controls.

In this section, we study the synthesis of squat movements with our controller. Squat is involved in many daily movements and tasks, such as lifting objects and sit-to-stand and it requires multiple muscle groups coordinating simultaneously [Fry et al., 2003]. For this reason, it has been used for therapeutic treatment to strengthen lower-body muscles and connective tissue after surgeries such as joint replacement [Dahlkvist et al., 1982]. In the context of cerebral palsy, squat can be adopted as a means to measure functional strength of the lower extremities in children with CP [Magiera and Heathcock, 2020]. The section begins with the general introduction of basic notions of squat. Next, we detail the mathematical foundation of the two-step optimization controller. Examples of squat synthesis are presented and the results are analyzed to gain insight into the prediction capacity of the controller.

3.1 Overview of The Squat Movement

3.1.1 Squat Execution

Squat is a basic movement taking part in numerous functional activities in daily life, exercise training, or working environment [Lu et al.,]. It involves moderate to high range of motion of hip, knee and ankle joints and can be divided into three phases in the following chronological order: descent, maintenance and ascent [Verdini et al., 2017].

The movement begins from an upright configuration with knees and hips fully extended. Next, the descent phase is initiated with the simultaneous execution of ankle dorsiflexion, knee flexion, and hip flexion to lower the centre of gravity of the body. When the squat depth is achieved, the maintenance phase commences with all movements suspended to hold the squat posture. This phase is optional and the squat can continue right away with the ascent phase. In this final phase, the person reverses direction and lifts back to the upright posture, performing synchronized plantar flexion, knee extension and hip extension. During the entire movement, a stable support base is required by positioning the feet generally shoulder-width apart and flat on the floor. The toes are oriented straight ahead or at a small angle towards the outside. Meanwhile, the back is typically kept straight.

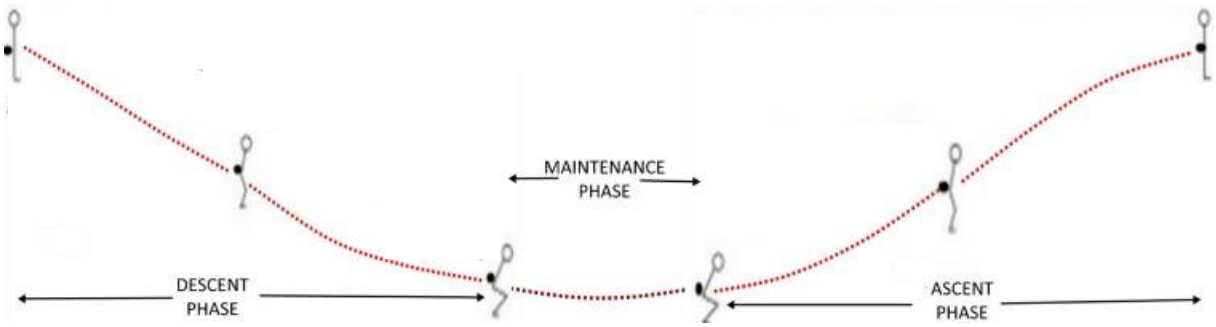

Figure 3.1: The three phases of a squat cycle. Image courtesy [Verdini et al., 2017]

3.1.2 Joint Kinetics and Kinematics During The Squat

Squat can be categorized based on squat depth, typically measured by the degree of flexion at the knee, since it affects considerably joint kinetics, kinematics and muscle activities [Hartmann et al., 2013]. There are three types of squat: partial squats (40°knee angle), half squats (70 to 100°), and deep squats (greater than 100°) [Schoenfeld, 2010]. It is estimated that over 200 muscles contribute to execute a squat [Solomonow et al., 1987]. Most of the lower extremities muscles are recruited, including the quadriceps femoris, hip extensors, hip adductors, hip abductors, and triceps surae [Nisell, 1986]. In parallel, other upper-body musculature such as the abdominals and erector spinae also support in maintaining the stability of the torso [Schoenfeld, 2010]. In this section, we review in detail findings in the literature on the kinetics and kinematics in the sagittal plane of each joint as well as the muscle activities during squat performance. To help clarify the details related to muscles (position, attachment, function, etc.) in the following sections, Fig. 3.2 is presented to illustrate the muscular anatomy of the lower limbs.

Ankle

In this work, the ankle is associated to the talocrural joint, the articulation of the tibia and fibula with the talus. It is a hinge joint, allowing for dorsiflexion and plantarflexion movements in the sagittal plane, with the ranges of rotations are 20°and 50°respectively [Clarkson, 2000]. The ankle joint plays an essential role of supporting in power generation during squat performance [Hung and Gross, 1999]. It is reported

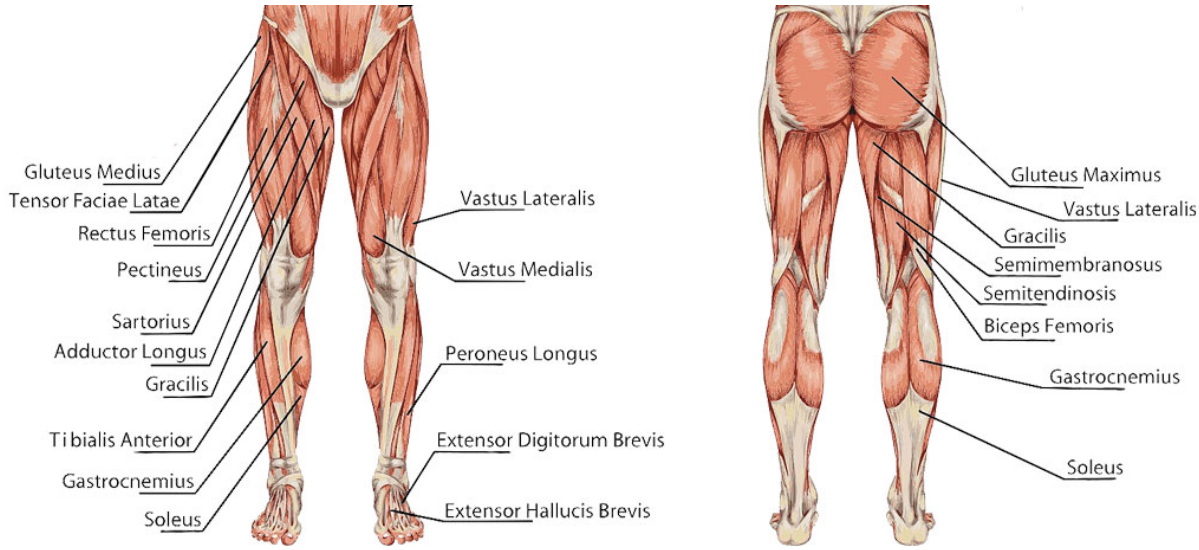

Figure 3.2: Major lower body muscles. Image taken from [OSMIFW, 2021]

.

that ankle moments are considerably lower than those at the knee and hip, varying between 50 and 300 Nm [Escamilla et al., 2001a].

The major muscles responsible for these two movements are gastrocnemius and soleus. They contract concentrically during plantar flexion and eccentrically during dorsiflexion [Signorile et al., 1995]. The soleus is observed to exhibit higher activity of the gastrocnemius when squatting at high degrees of flexion [Toutoungi et al., 2000]. This is due to the fact that the gastrocnemius is a bi-articular muscle and functions mostly isometrically during a squat [Schoenfeld, 2010]. This means that tension is produced while muscle length evolves insignificantly. Another important ankle muscle is the tibialis anterior, responsible for dorsiflexion. Co-contraction of the gastrocnemius and the tibialis anterior during the mid-descent phase of high speed squat is assumed to provide stability to the ankle [Dionisio et al., 2008].

Knee

The knee joint consists of the tibiofemoral and the patellofemoral joint. The tibiofemoral is the articulation of the tibia and the femur. It can be represented in the sagittal plane as a hinge joint, with a range of flexion of -5°to approximately 160°[Signorile et al., 1995]. The patellofemoral joint, on the other hand, has a special structure. It is a "a gliding joint in which the patella slides over the trochlear surfaces of the femur during flexion and extension of the knee. This provides additional mechanical leverage in extension because of a greater force arm, as well as reducing wear on the quadriceps and patellar tendons from friction against the intercondylar groove" [Schoenfeld, 2010].

One of the primary musculature of the knee joint is the quadriceps muscle group. It is the largest and strongest extensor muscles, consisting of rectus femoris and vastus group (vastus lateralis, vastus intermedius and vastus medialis) [Physiopedia, 2021]. During the squat, they execute concentric knee extension, as well as eccentrically resisting knee flexion [Schoenfeld, 2010]. Their activities achieve the maximum level at approximately 80°to 90°of flexion [Escamilla et al., 2001b]. The vastus lateralis and vastus medialis are reported to produce similar activities and forces during the squat [Markolf et al., 1990]. On the other hand, the vasti muscles contribute significantly more than the rectus femoris, with "approximately 50% greater muscular force output" [Escamilla et al., 2001b]. This can be explained similarly as in the case of the gastrocnemius w.r.t the ankle. Indeed, the rectus femoris is also a bi-articular muscle, carrying out hip flexion and knee extension at the same time. This leads naturally to the negligible variation in muscle length as it shortens on one end and while lengthening on the other end, thus the smaller produced force compared to those produced by the uni-articular vasti muscles. Finally, these muscles are assisted by the tendons for optimal force exertion on the tibia [Schoenfeld, 2010].

The antagonists of the quadriceps are the hamstrings, consisting mainly of the biceps femoris, the semitendinosus and the semimembranosus. They are bi-articular muscles, acting upon hip and knee joints. With respect to the knee joint, they carry out knee flexion and decelerate knee extension. It is reported that co-contraction of the quadriceps and the hamstrings happens during squat performance to "neutralize the anterior tibiofemoral shear imparted by the quadriceps and thus alleviating stress on the ACL (anterior cruciate ligament)" [Escamilla, 2001].

Hip

The hip joint is the articulation between the head of the femur and the acetabulum of the oscoxae [Schoenfeld, 2010]. It is typically modeled as a ball-and-socket joint with three degrees of freedom: flexion and extension in the sagittal plane, abduction and adduction in the frontal plane, and internal/external rotation and horizontal abduction/adduction in the transverse plane [Signorile et al., 1995]. During the squat, hip flexion is reported to reach a peak angle approximately of $95 \pm 27°$[Hemmerich et al., 2006].

The major muscles contributing to the squat performance are the gluteus maximus (GLU), the hamstrings and the rectus femoris. GLU is a powerful hip extensor that has three functions: contracting eccentrically to control squat descent, contracting concentrically to overcome external resistance on the ascent and stabilizing the knee and pelvis [Schoenfeld, 2010]. Both its average and peak muscle activities are in close relation with squat depths. Specifically, they are reported to be higher in deep squats compared to partial and half squats [Caterisano et al., 2002]. On the other hand, squat depths don't influence greatly the activity of the hamstrings. They demonstrate fairly consistent muscle force between partial squats and full squats [Escamilla et al., 2001b], as their muscle lengths vary insignificantly during the squat, hence the moderate EMG activity reported in [Escamilla et al., 2001b]. In general, "lateral hamstrings produce greater activity than the medial hamstrings" [Escamilla et al., 2001b]. Rectus femoris (RF), a knee extensor, is observed by [Robertson et al., 2008] to exhibit increasing EMG activity at the end of the descent phase before reaching the maximal depth. They also suspect that RF may act "more as a hip flexor or as a stabilizer at both hip and knee" [Robertson et al., 2008].

3.2 The two-step optimization scheme

Based on the physiological description of the squat movement in the previous section, we develop our two-step optimization scheme to synthesize this movement on computational simplified human models. The two-step synthesis scheme (Fig. 3.10) starts by synthesizing the desired squat motion on the joint-actuated model thanks to the reactive optimization-based dynamic task controller, or step I (detailed in Subsection 3.2.1). At the end of step I, the trajectories of joint torques $\boldsymbol{u}$ and state (generalized angles $\boldsymbol{q}_d$ and velocities $\boldsymbol{\nu}_d$) are obtained and input into step II, where the static optimization is carried out on the muscle-actuated model to estimate the muscle activations best achieving the trajectories computed in step I.

3.2.1 Step I - Reactive Optimization-based Dynamic Task Control

Step I consists mainly of four stages, as shown in Fig. 3.3. The first one includes four feedback control loops, each one corresponding to a physically-relevant high-level task. The inputs and outputs of the controllers are listed in the table 3.1.

Based on the hypothesis established in the previous section, the identified physically-relevant high-level objectives (tasks) are lifting the head, maintaining balance, reducing joint torques and minimizing angular momentum (AM) variation. The duration of a squat phase (the ascent phase or the descent phase as we consider them having the same duration) is a fixed parameter. The desired values of the parameters related to the physically-relevant high-level tasks of the feedback loop are input into the module responsible for formulating optimization problems. In parallel, the Task Switch (Subsection 3.2.2) provide it with

computed task weight values according to the current state of the human model. The essential elements of the QP problems are then delivered to the solver. After the resolution, the control inputs for the torque generators of the joint-actuated model are obtained and fed into the simulator. OpenSim carries out the forward dynamic to obtain the resulting states and joint torques. The values of state elements are returned back to the controllers.

At each time step, the controller solves a multi-objective optimization formulated similarly to equation 2.20

$$\begin{aligned} \underset{\boldsymbol{\chi}}{\text{argmin}} \quad & \sum_{i=1}^{n_{task}} w_i f_i(\boldsymbol{\chi}) + w_0 f_0(\boldsymbol{\chi}) \\ \text{s.t} \quad & G\boldsymbol{\chi} \leq \boldsymbol{h} \\ & A\boldsymbol{\chi} = \boldsymbol{b} \end{aligned} \tag{3.1}$$

Here, a cost function is constructed as the weighted sum of all individual cost functions f_i of the i_{th} task expressed in terms of $\boldsymbol{\chi}$, the optimization variables. $w_0 f_0(\boldsymbol{\chi})$ is the regularization term removing the solution redundancy. The chosen optimization variable vector is

$$\boldsymbol{\chi} = \begin{bmatrix} \dot{\boldsymbol{\nu}} \\ \boldsymbol{u} \end{bmatrix}$$

Solving this optimization problem yields a control set of torque generators and the resulting generalized accelerations. Below are the details of the formulations of the high-level tasks as well as the controllers.

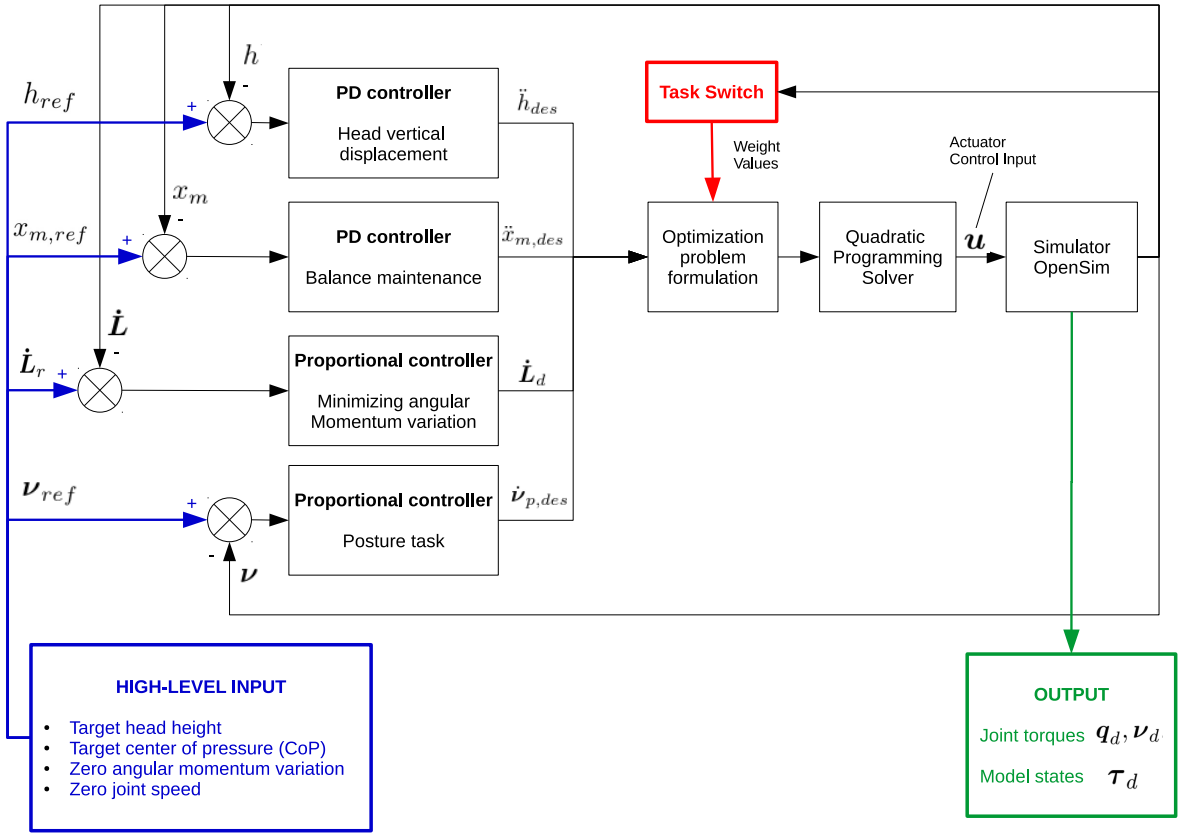

Figure 3.3: The closed-loop control of Step I.

Head vertical displacement

We consider that a squat cycle consists of two phases starting by the descent phase and finishing with the ascent phase, as shown in Fig. 3.4. The purpose of the task is approaching the controlled point located at

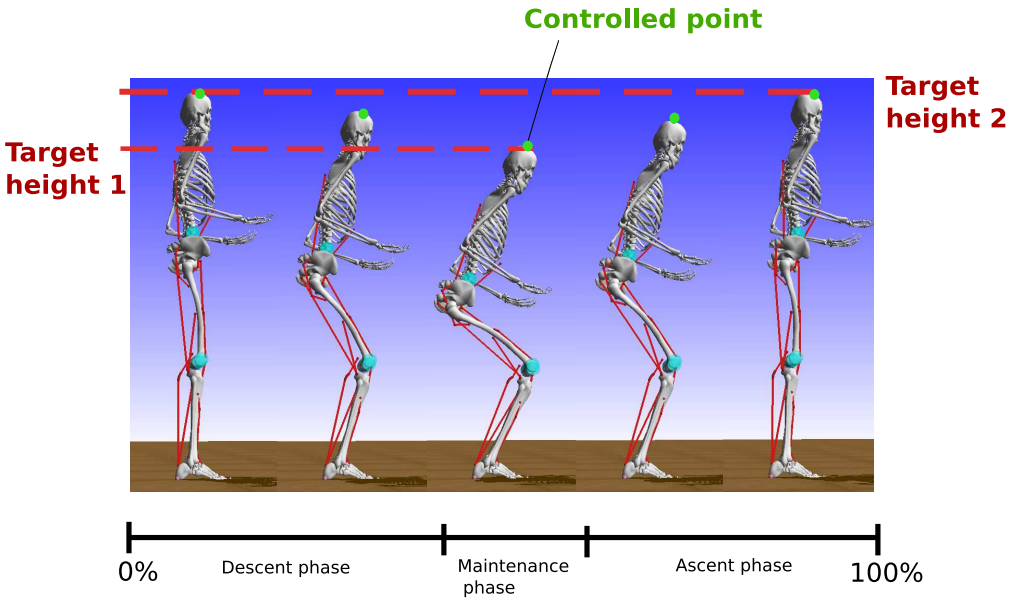

Figure 3.4: The squat cycle starts with the descent phase and finishes with the ascent phase. Each phase has a target height for the controlled point of the head.

the top of the head towards the two target heights. For the ascent phase, the target height 2 is achieved when the body stands up straight. For the descent phase, the target height 1 is considered as the body lowers to the minimum height. This position task is converted to an acceleration task by means of task servoing [Lober, 2017]. The task performance indicator is formulated as

$$f_1(\boldsymbol{\chi}) = \| \ddot{h} - \ddot{h}_{des} \|_2^2 \tag{3.2}$$

with $\ddot{h}$ the acceleration of the controlled point. The desired acceleration is expressed in Cartesian space through a PD controller

$$\ddot{h}_{des} = \ddot{h}_{ref} + K_p(h_{ref} - h) + K_v(\dot{h}_{ref} - \dot{h}) \tag{3.3}$$

with K_p and K_v the position and the velocity gains, h_{ref}, $\dot{h}_{ref}$ and $\ddot{h}_{ref}$ the target height, vertical velocity and vertical acceleration respectively. In case of squat movements, we set $\dot{h}_{ref} = 0$, $\ddot{h}_{ref} = 0$ and h_{ref} to either target head 1 or target head 2. To drive these errors to zero in a critically damped fashion, the velocity gains can be chosen such as $K_v = 2\sqrt{K_p}$. The vertical acceleration of the controlled point is computed as $\ddot{h} = \begin{bmatrix} 0 & 1 & 0 \end{bmatrix} (J_{sp}\,\dot{\boldsymbol{\nu}} + \dot{J}_{sp}\,\boldsymbol{\nu})$ with $J_{sp}(\boldsymbol{q})$ the Jacobian w.r.t the controlled point.

Maintaining balance

To ensure the equilibrium of the system, we aim to maintain the projection of the center of mass (CoM) close to a set-point $x_{m,ref}$ inside the convex hull of the foot-support area. As the model is planar, only the coordinate x_m represented along the sagittal axis of the body of the CoM ground projection is considered. The task performance indicator is formulated as an acceleration task:

$$f_2(\boldsymbol{\chi}) = \| \ddot{x}_m - \ddot{x}_{m,des} \|_2^2 \tag{3.4}$$

with $\ddot{x}_m$ can be computed using Eq. 2.39. The desired CoM acceleration is expressed in Cartesian space through a PD controller

$$\ddot{x}_{m,des} = \ddot{x}_{m,ref} + K_p^m(x_{m,ref} - x_m) + K_v^m(\dot{x}_{m,ref} - \dot{x}_m) \tag{3.5}$$

The reference acceleration $\ddot{x}_{m,ref}$ and velocity $\dot{x}_{m,ref}$ are set as null. It is worth noting that this task is not redundant even with the integration of the CoM boundary constraints (cf. 2.2.1), as they play different roles in the control of CoM. This task aims to centralize the CoM projection towards a reference point $x_{m,ref}$ in the middle of the range between the boundaries. However, this task cannot be fulfilled due to conflict with other tasks, resulting the CoM drifting away towards a boundary. In this case, the CoM boundary constraint prevents the CoM from breaching the limit and therefore maintain the balance of the model.

Minimizing angular momentum variation

It has been shown by many works [Macchietto et al., 2009, Goswami and Kallem, 2004, Kajita et al., 2003, De Lasa et al., 2010] that minimizing angular momentum is a strategy to improve balance stability and robustness. In our work, The formulation of the task is based on the work in [De Lasa et al., 2010] and [Herr and Popovic, 2008]. Angular momentum, L, is calculated as the sum of individual segment angular momenta about the body's CoM and is written as

$$L = PJ\dot{\boldsymbol{q}} \tag{3.6}$$

with $J = [J_1^T \cdots J_{n_b}^T]^T$ the concatenation of Jacobian matrices mapping generalized velocities to angular velocities of the bodies, $P = [I_1 \cdots I_{n_b}]$ the concatenation of inertia matrices about the CoM of the bodies and n_b is the number of bodies in the model. The variation of angular momentum (AM) about the CoM of the whole body $\dot{\boldsymbol{L}}$ is controlled linearly

$$f_3(\boldsymbol{\chi}) = \| \dot{\boldsymbol{L}}_d - \dot{\boldsymbol{L}} \|_2^2 \tag{3.7}$$

The desired AM variation is computed as

$$\dot{\boldsymbol{L}}_d = k_p(\boldsymbol{L}_r - \boldsymbol{L}) \tag{3.8}$$

and the current AM variation is expressed as

$$\dot{\boldsymbol{L}} = PJ\dot{\boldsymbol{\nu}} + (\dot{P}J + P\dot{J})\boldsymbol{\nu} \tag{3.9}$$

We set the reference AM variation $\boldsymbol{L}_r = 0$.

Regularization task

The regularization term is a weighted sum of squared optimization variables

$$f_0(\boldsymbol{\chi}) = \sum_{i=1}^{n_{opt}} \alpha_i \chi_i^2 \tag{3.10}$$

with n_{opt} the number of optimization variables. Apart from narrowing down the solution space, this term also allows to smooth out the obtained activation and acceleration profiles as well as minimize indirectly the energy produced by the actuators.

Posture task

The purposes of the posture task is two fold. The first objective is to reduce the movement in a damping manner at the end of each phase and achieve a fixed configuration (squat or stand up). The second objective is to overcome the singularity problem at the stand up configuration. Specifically, when reaching the standing posture, the kinematic chain is approaching a singular configuration and locally loses the ability to generate vertical motions.

The priority of the posture task is completely opposite to the ones of the aforementioned main tasks. When the model approaches the target squat depth, the stand up configuration or cannot descent further

down (deep / Asian squat), the priority is put on the posture task while the other high-level tasks are inhibited. On the other hand, when the model performs movement during the ascent and descent phase, the posture task is inactive.

The posture task is activated or deactivated according to the task switch process detailed in Subsection 3.2.2. The details of the task switch process are presented in 3.2.2 The task performance indicator is formulated as

$$f_p(\boldsymbol{\chi}) = \| \dot{\boldsymbol{\nu}} - \dot{\boldsymbol{\nu}}_{p,des} \|_2^2 \tag{3.11}$$

where the desired acceleration is expressed through a proportional controller

$$\dot{\boldsymbol{\nu}}_{p,des} = K_p^p(\boldsymbol{\nu}_{ref} - \boldsymbol{\nu}) \tag{3.12}$$

with $\boldsymbol{\nu}_{ref} = \mathbf{0}$.

3.2.2 Task Switch

The transitions between dynamic movement and static posture are key moments during a squat cycle (Fig. 3.5). They occur at three stages

- the end of the descent phase / the beginning of the maintenance phase
- the end of the maintenance phase / the beginning of the ascent phase
- the end of the ascent phase

We hypothesized that during the transitions, the goals that the person performing squat wishes to accomplish change substantially, hence the modifications of the priorities of the high-level tasks implemented in the controller. To carry these modification, we develop "Task Switch", the process of varying weight values of the high-level tasks [Liu et al., 2016]. In its implementation of the controller, the conditions triggering these transitions depends on the type of squat performed and the characteristics of the human model. For example, in half squat simulations, a tolerance interval is specified preceding the target squat depth. If the knee angle enters this interval, the transition is activated. We provide the details related to these elements for all the synthesized squat types in this work.

As mentioned earlier in Subsection 3.11, to achieve static configurations, the posture task is privileged while the main tasks of moving head vertically, maintaining balance and minimizing angular momentum variation are inhibited. Since during dynamic movement, the posture task is completely inactive and the three above-mentioned are active, significant variations happen their associated weight values during the transitions to static posture. The event also happens in the opposite direction when the body starts to move after the maintenance phase. This leads inevitably to abrupt fluctuations of great amplitude in the control inputs of the actuators, producing hence unnatural joint torques compared to those estimated experimentally and also destabilizing the control scheme. It is, therefore, necessary for us to smooth out the weight variations of the tasks.

There are two elements that we use in the task switch process: exponential decay and human reaction time. The first element is a rapid decrease at a rate proportional to the current value of the considered quantity. We use this model to describe the weight value evolution during the transitions. We can express the weight value as

$$\frac{dw}{dT} = -\lambda w \tag{3.13}$$

The solution to the above equation is

$$w(T) = w_0 e^{-\lambda T} \tag{3.14}$$

with w the current weight value, w_0 the initial weight value, λ the decay constant and T the current active period of task switch. In our application, w and w_0 are already known parameters (task weights chosen for each phase), while λ is to be chosen. Here is where the second element comes into play. We hypothesize

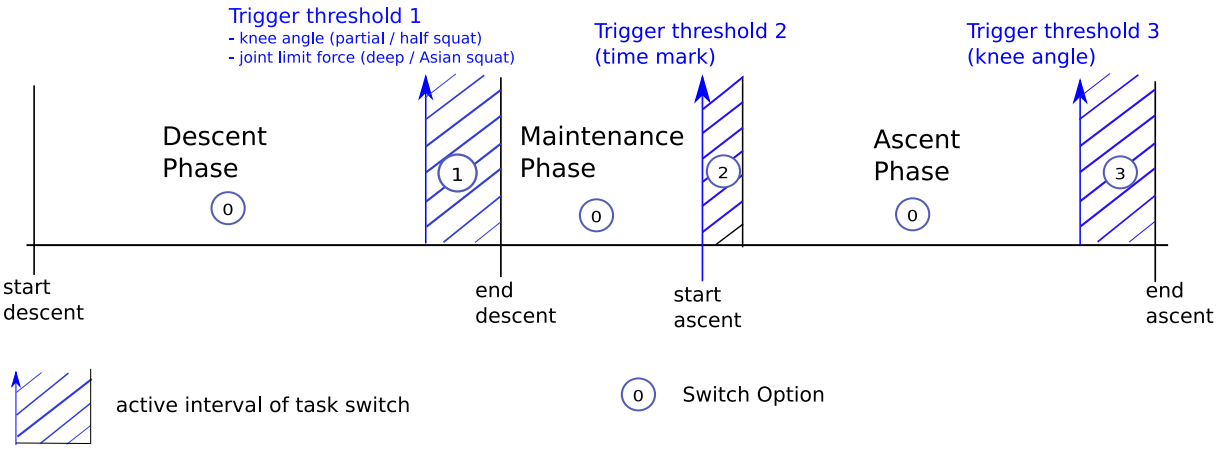

Figure 3.5: ***The timeline of task switches during a squat cycle.*** *Task switch occurs at three different stages of a squat cycle, corresponding to three Switch Option in the implementation: (1) at the end of descent phase, (2) at the beginning and (3) at the end of the ascent phase. During the dynamic movement, the Switch Option is reset to 0. The trigger thresholds are different depending on the stage, hence Switch Option. If task switch is active at the end of the descent phase and the ascent phase, the trigger threshold is predefined knee angles (trigger threshold 1 and 3). Otherwise, the trigger threshold is the start time of the ascent phase (trigger threshold 2). In the special case of Asian squat (Subsection 4.1), the trigger threshold 1 is the joint limit force, as the target squat depth is unknown in advance.*

that the execution of the transitions between dynamic movement and static posture is carried out during the human reaction time. Considering the transition from dynamic movement to static posture, at $T = 0$, the three tasks responsible of the movements are privileged. At $T = T_{reac}$, with T_{reac} the human reaction time, the weight values become really close to zero, after following the evolution depicted by the exponential decay. It is important to note that the time T is the duration from the beginning of the task switch (the moment when it's triggered) to the current time. To clarify the notation, we introduced the parameter t_{switch} capturing the initiation time of task switch. In consequence, the expression of T is expressed as

$$T = t - t_{switch} \tag{3.15}$$

with t the period in which a squat has been being performed. We can visualize the weight variations at Fig. 3.6.

Implementation of Task Switch

Every squat has three stages where task switch is active, as shown in Fig. 3.5. Its implementation varies slightly depending on the stage on which it takes place, as shown in Fig. 3.5. We introduce the variables Switch Option indicating the stage of transition, and Switch Time, which is t_{switch} mentioned earlier. The algorithm of the task switch process is shown in Fig. 3.8

Switch Option 1: Task switch at the transition from the descent phase to the maintenance phase In the current case of half squat (squat depth between 70°and 100°), the implementation of task switch is inspired from our experimental protocol of squat trials (more details of the protocol in the Subsection 4.2.1). The subject, while performing squat, cannot know the current squat depth is. To assure that the subject reaches the target squat depth, a supervisor follows the execution and tells the subject to stop at his estimation of the target squat depth. Once the subject hears the signal, he reacts by stopping the movement, then holding the current position for a short period of time before lifting up back to the stand up posture. We assume that the subject needs a short period of time to stop his movement, which is his reaction time. During this small period, he changes his intention from lowering the body to stop moving and commands his lower limbs' muscles to contract.

From the control point of view, the intention of the subject is represented by the physically-relevant high-

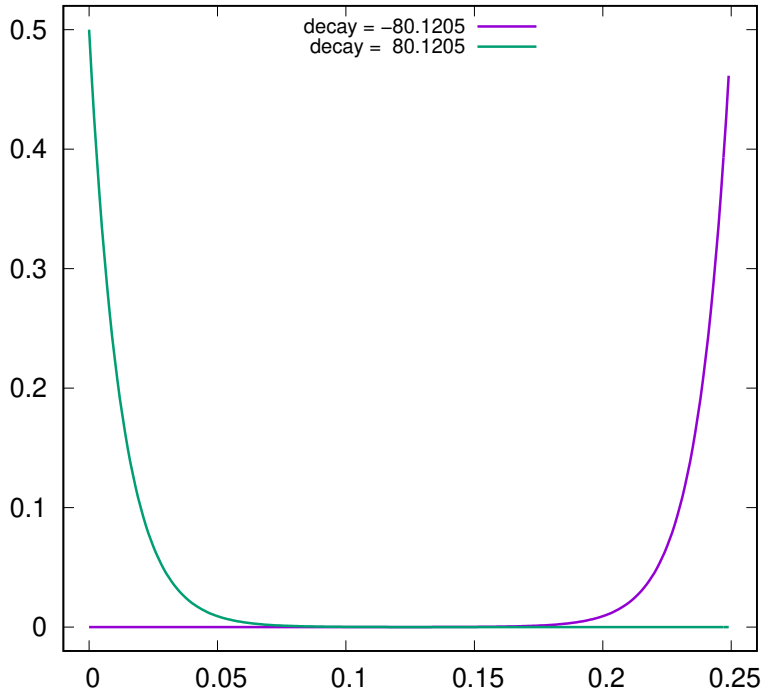

Figure 3.6: Examples of exponential decay variation during a human reaction time of $T_{reac} = 250ms$. The tendency of the variation can be inverse by changing the sign of the decay constant λ.

level tasks implemented in our controller. Changing the intention corresponds to altering the priorities of the high-level tasks. Consequently, the weight values associated to them are modified. We introduce a parameter representing the human reaction time and adopt the exponential decay to depict the evolution of weight values during the task switch.

During the squat trials, the trigger factor of the task switch is the signal from the supervisor. In our control scheme, the "signal" is simply represented by a value that the knee angle has to pass before reaching the target depth, as shown in Fig. 3.7.

Switch Option 2: Task switch at the transition from the maintenance phase to the transition phase In reality, the subject decides to lift up his body on his own will without receiving external signal nor instruction. In our control scheme, the moment of this transition is initiated by a chosen time mark indicating the beginning of the ascent phase (or the end of the maintenance phase). After a period of human reaction time, the priorities of the high-level tasks are adjusted to the values allowing the synthesis of the ascent phase.

Switch Option 3: Task switch at the end of the ascent phase When approaching the stand up configuration, we assume that the subject slows down his joint movement. This event is represented in our controller scheme by this task switch. It is executed in the same manner as the one occurring at the end of the descent phase, triggered when the knee angle reaches a predefined knee angle (trigger threshold 3 in Fig. 3.5). The posture task is the main task, allowing the achievement of the stand up configuration and avoiding the singularity configuration.

Switch Option 0 During the dynamic movement of the descent and ascent phase, Switch Option is reset to 0 and Task Switch is inhibited.

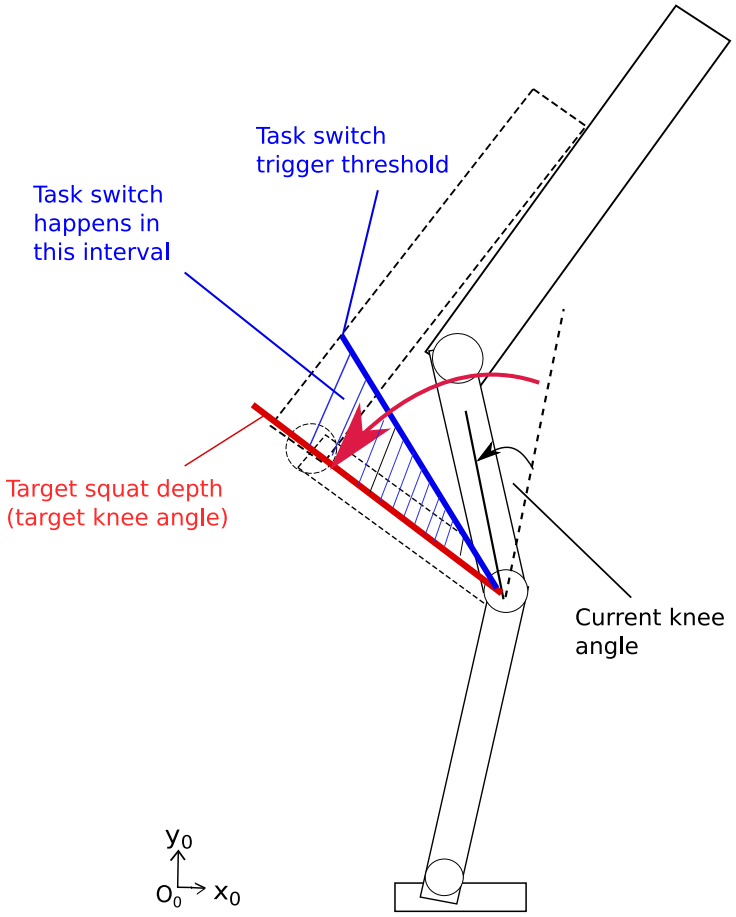

Figure 3.7: The knee angle continues to increase (anti-clockwise rotation) during the descent phase. Once its value reaches the threshold squat depth, the task switch is triggered and carried out during the human reaction time. It is accomplished before or at the moment when the knee angle achieves the target squat depth. In parallel, the knee angle interval where the task switch is executed is equal or greater than the angle traveled during the human reaction time.

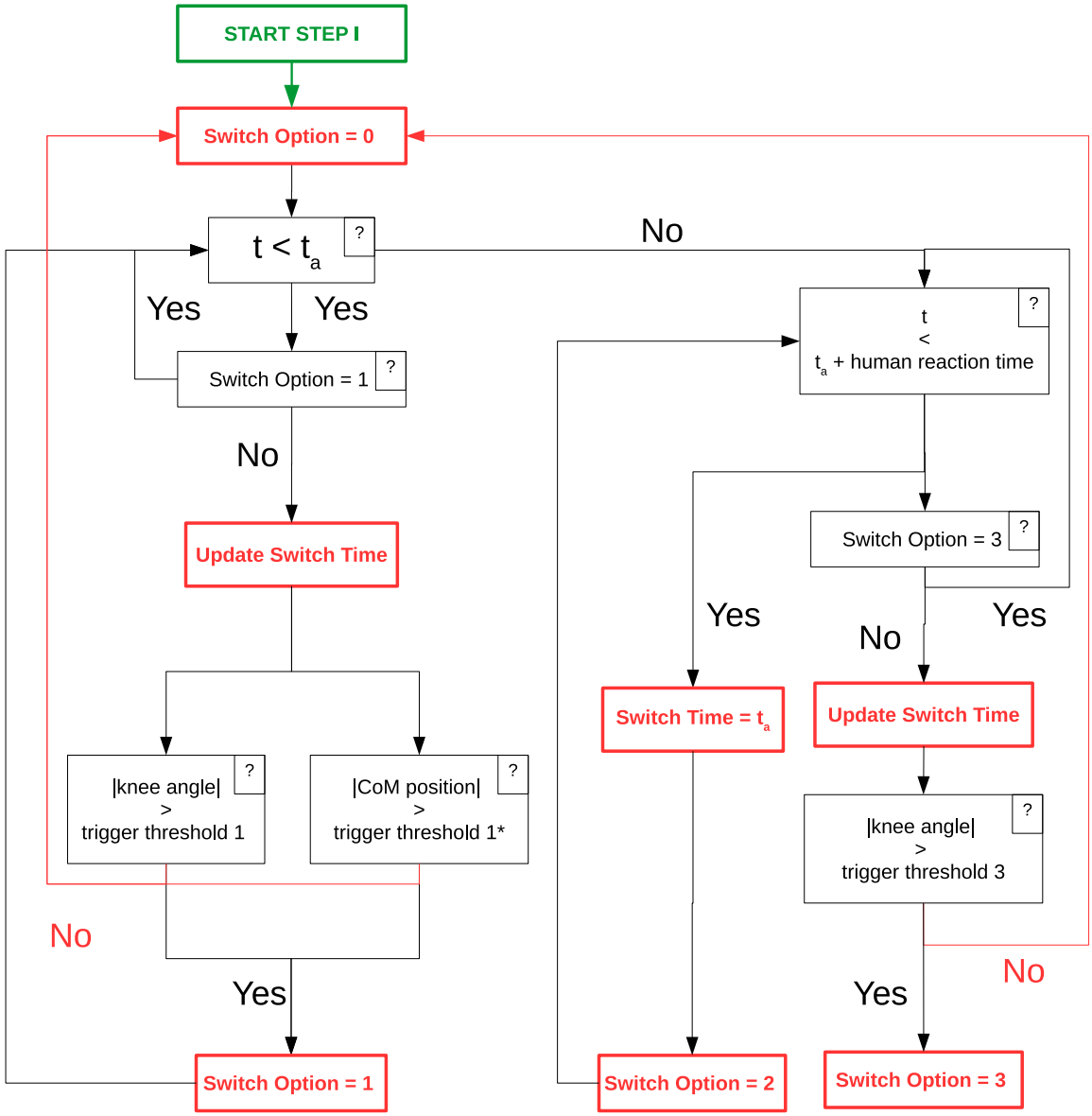

Figure 3.8: The algorithm to supervise and update task switch option and task switch time. The red box represents the action. The box containing the "?" sign is represents a verification of the indicated condition. Every time switch time is updated, it takes the value of the current simulation time. In case of half squat synthesis, only the knee angle is verified against "trigger threshold 1" (an angle value) before assigning the switch option to 1. However, for Asian squat (Subsection 4.1), the CoM position is also examined. In this case, "trigger threshold 1" is a position value.*

Table 3.1: Parameters of the feedback control loops in Step I

Task	Input	Output
Head vertical displacement	h_{ref}	$\ddot{h}_{des}$
Maintaining balance	$x_{m,ref}$	$\ddot{x}_{m,des}$
Minimizing angular momentum variation	$\boldsymbol{L}_r$	$\dot{\boldsymbol{L}}_d$
Posture	$\boldsymbol{\nu}_{ref}$	$\dot{\boldsymbol{\nu}}_{p,des}$

3.2.3 Step II - Muscle Activation Synthesis

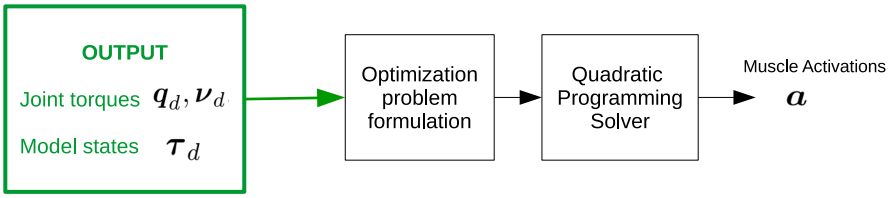

Figure 3.9: The open loop optimization control of Step II.

The structure of Step II is basically an open loop control, receiving the states and joint torques computed from Step I tom compute the muscle activations. The joint torques obtained in step I are reproduced on the muscle-actuated model by finding the optimal control inputs $\boldsymbol{a}^*$ of the path actuators. For this purpose, the optimization problem is formulated as

$$\begin{aligned} \boldsymbol{a}^* = \underset{\boldsymbol{a}}{\text{argmin}} \quad & w_{\boldsymbol{\tau}} f_{\boldsymbol{\tau}}(\boldsymbol{q}_d, \boldsymbol{\nu}_d, \boldsymbol{\tau}_d, \boldsymbol{a}) + w_0 f_0(\boldsymbol{a}) \\ \text{s.t} \quad & \boldsymbol{a}_{min} \leq \boldsymbol{a} \leq \boldsymbol{a}_{max} \\ & \dot{\boldsymbol{a}}_{min} \leq \dot{\boldsymbol{a}} \leq \dot{\boldsymbol{a}}_{max} \end{aligned} \tag{3.16}$$

with $\boldsymbol{a}$ the muscle activations, $\boldsymbol{\tau}_d$ the desired torques and $(\boldsymbol{q}_d, \boldsymbol{\nu}_d)$ the desired state obtained in step I. The two tasks implicated are tracking joint torques and minimizing total control inputs.

Tracking joint torque

Since the path actuator model does not take into account the dynamics of muscle contraction, the torques produced by the path actuators are only configuration dependent. The task can be expressed as

$$f_{\boldsymbol{\tau}}(\boldsymbol{q}_d, \boldsymbol{\nu}_d, \boldsymbol{\tau}_d, \boldsymbol{a}) = \| \, S^a(\boldsymbol{q}_d)\boldsymbol{a} - \boldsymbol{\tau}_d \, \|_2^2 \tag{3.17}$$

Minimizing total muscle activations

The task is defined as minimizing the weighted sum of squared muscle activations

$$f_0(\boldsymbol{a}) = \| \, \boldsymbol{a} \, \|_2^2 \tag{3.18}$$

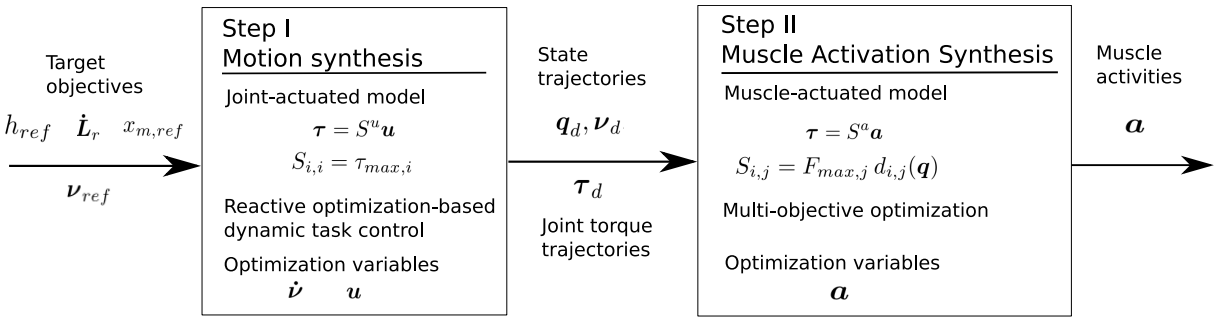

Figure 3.10: The two-step squat movement synthesis method. Step I relies on the reactive optimization-based dynamic task control to produce the desired squat movement ($\boldsymbol{q}_d$ and $\boldsymbol{\nu}_d$) and the joint torques $\boldsymbol{u}$ with the joint-actuated model. The task objectives are reaching head target heights h_{ref}, maintaining reference variation of angular momentum $\dot{\boldsymbol{L}}_r$, maintaining center of mass set-point $x_{m,ref}$ as well as respecting the duration of a squat phase. Step II is a sequence of optimizations computing the muscle activity patterns $\boldsymbol{a}$ on the muscle-actuated model.

3.3 Simulation Example: Half Squat Synthesis with A Low Number of Muscles

We demonstrate how the controller synthesizing squat motion without requiring any experimental data related to the kinematics of human body. The type of squat to be generated is a half squat with the target squat depth of 90°. For this purpose, we build a fixed-base human model via OpenSim [Delp et al., 2007], a physiologically-based simulator. OpenSim also provide an API in C++, allowing us to implement our controller and analyse its performance through the behavior of the created model. The details related to modeling and the results are presented in details in the following subsections.

3.3.1 OpenSim

Before going further into the descriptions of the human model used in this example, we begin with a small introduction of OpenSim. OpenSim is a free software package for musculoskeletal modeling and simulation. It consists mainly of an end-user application with a graphical user interface (GUI) (Fig. 3.11 and a software development kit (SDK), providing musculoskeletal modeling elements, and tools for fitting generic models to subject-specific data, performing inverse kinematics and forward dynamic simulations 3.12 [Seth et al., 2011]. Physics-based analyses of the behavior of musculoskeletal models performed by Simbody, the dynamics engine behind OpenSim and also "a popular biomechanics simulation application" [Sherman et al., 2011].

An OpenSim model is built using the elements (components) that have computational counterparts in the underlying Simbody multibody system. These include: bones (rigid bodies), joints (mobilizers, constraints and forces), contact elements (rigid constraints and compliant forces), as well as ligaments and muscle actuators (forces). A controller element consisting of user-defined functions is provided to represent neural commands originating in the central nervous system that control muscle activity [Seth et al., 2011]. **In our work, despite this provided controller element, we choose to input the actuator controls directly via the forces elements.**

In addition to the features for the construction of musculoskeletal models and the visualization of their motion, OpenSim also provides a set of tools for synthesizing, reporting and analyzing simulation outcomes related to the kinematics and dynamics of the model. The information that these tools can produce includes internal coordinates from available spatial marker positions corresponding to known landmarks on rigid segments, joint reaction forces and individual muscle contributions to joint or center-of-mass accelerations. For more details about OpenSim and Simbody, the reader is directed to the works of [Seth et al., 2011, Seth et al., 2018, Sherman et al., 2011, Sherman et al., 2013].

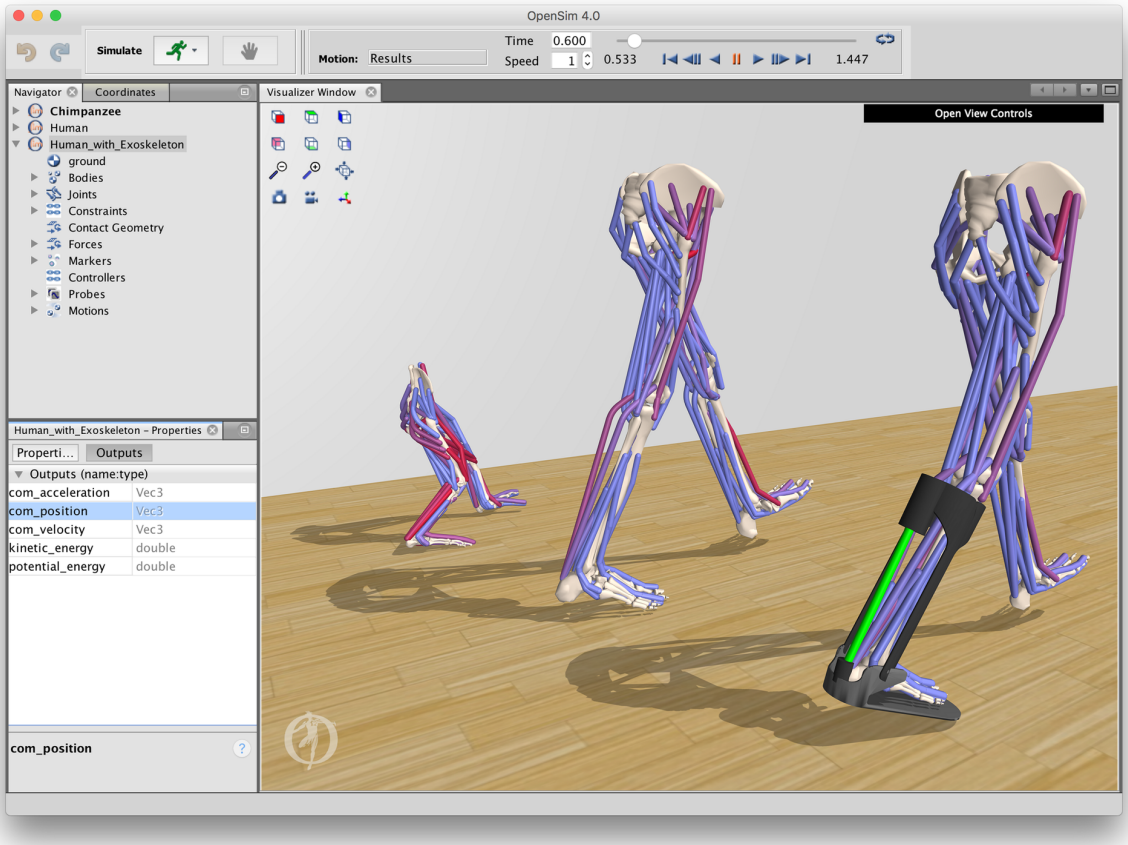

Figure 3.11: A graphical user interface provides access to tools for inspecting, modifying, and simulating musculoskeletal models. Shown here are the results of muscle-driven simulations of human and chimpanzee walking that were generated by tracking experimental motion capture data. Image and caption taken from [Seth et al., 2018]

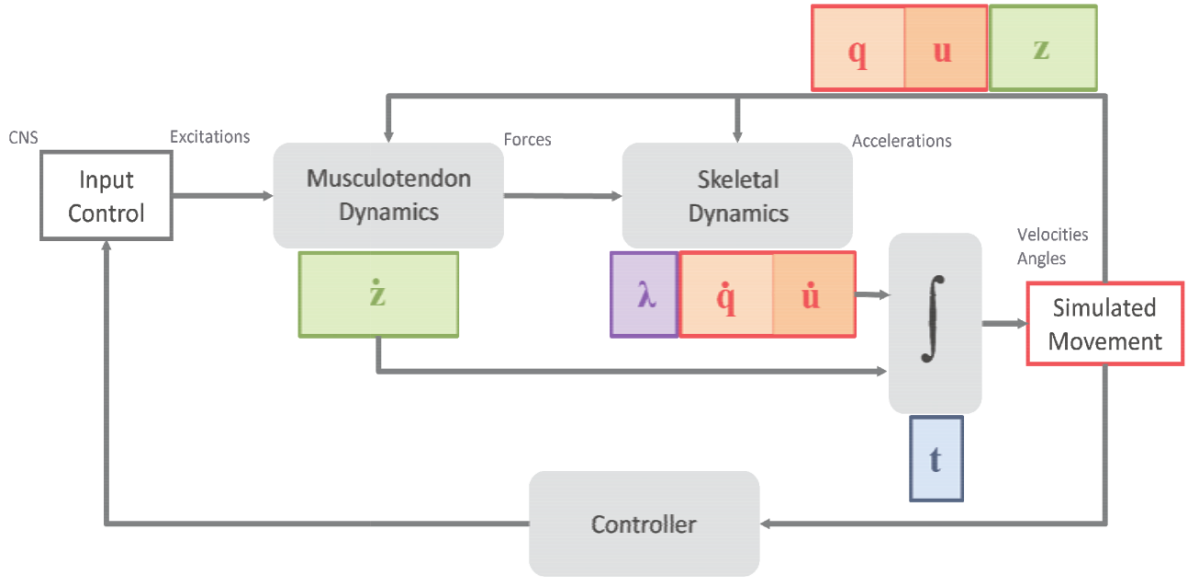

Figure 3.12: A canonical block-diagram of the dynamical musculoskeletal system. Inputs are muscle excitation or more generally actuator controls, and the outputs are trajectories for generalized coordinates, $\boldsymbol{q}$, and speeds, $\boldsymbol{u}$, as well as muscle states, $\boldsymbol{z}$, as a function of controllers time, t. The primary sources of system dynamics are musculotendinous actuators and the skeletal multibody dynamics. Controllers may also introduce dynamics to simulate signal transmission delay and other physiological behaviours. Image and caption taken from [Seth et al., 2011].

3.3.2 Human Model

The model, constructed with OpenSim, is a simplified model of the whole-body skeletal model proposed by [Catelli et al., 2019] and [Rajagopal et al., 2016]. The musculotendon parameters are derived from anatomical measurements of cadaver specimens and magnetic resonance images of young healthy subjects [Rajagopal et al., 2016]. The muscle paths are guided with wrapping surfaces (Fig. 3.13), allowing great ranges of motion at the knee and hip joints and thus make the model suitable for squat simulation [Catelli et al., 2019]. Our model contains 4 DoFs and consists of the torso, two arms, the pelvis, the right leg and the right foot fixed to the ground (Fig. 3.14). Since all the four joints are revolute joints, the model is planar and the movement is performed only in the sagittal plane. In addition, as only one leg is implemented, the mass of the torso is reduced by half of the original one to achieve more reasonable muscle activities. Nine primary muscles among lower-limb muscle are implemented, among which six are

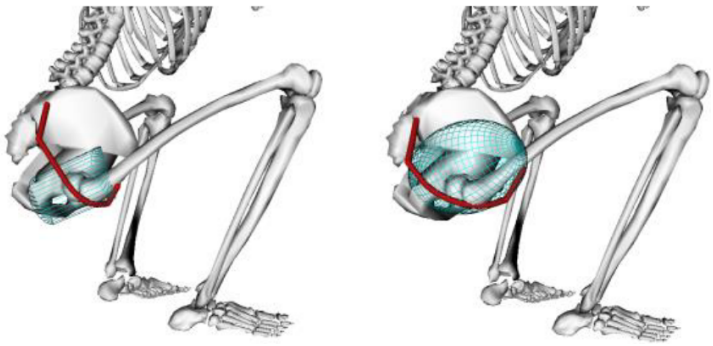

Figure 3.13: Wrapping surfaces (cyan) are implemented to prevent the muscles crossing into the bones during extreme hip flexion and provide more realistic muscle moment arms. Image taken from [Catelli et al., 2019]

uni-articular and three are bi-articular. Specifically, the hip joint is flexed by the iliopsoas (ILIO) and the rectus femoris (RF) and extended by the gluteus maximus (GLU) and the hamstring (HAM). The knee joint is extended by the vasti (VAS) and the RF, whereas its flexion is produced by the gastrocnemius

Table 3.2: Muscle parameters for the 4-DoFs planar model used in the simulation example

Muscle	**Abbreviation**	**Maximal Force (N)**
Biceps femoris short head	BIFEMSH	557.1
Hamstring	HAM	2201.0
Gastrocnemius	GAS	3115.5
Gluteus maximus	GLU	3337.6
Iliopsoas	ILIO	2447.9
Rectus femoris	RF	2191.7
Soleus	SOL	6194.8
Tibialis anterior	TA	1227.4
Vastus	VAS	6142.5

(GAS), the bicep femoris short head (BIFEMSH) and the HAM. At the ankle, dorsiflexion is produced by the tibialis anterior (TA) and plantar-flexion by the soleus (SOL) and the GAS respectively. At the lumbar joint (blue), two muscles are added to carry out extension and flexion of the torso w.r.t the pelvis. All the muscles are modeled with the element "Path Actuator" of OpenSim, following the model described by the equation 2.11.

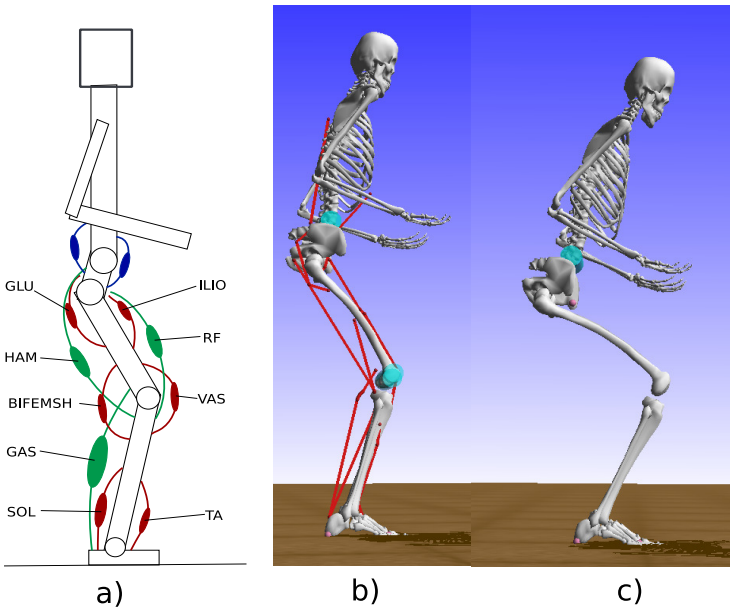

Figure 3.14: The muscle layout a) of the planar 4-DOFs models b) and the joint-actuated model c). The muscle-actuated model has 9 muscles (OpenSim Path Actuators): 6 uni-articular (red) and 3 bi-articular (green). The blue path actuators in the layout actuating the lumbar joint are not studied. The right foot is fixed to the ground. The joint-actuated model shares the same skeletal structure with the muscle-actuated model. Please note that the torque actuators are not represented visually.

3.3.3 Results

We analyze the resulst in terms of joint kinematics and muscle forces and discuss the relation between the model complexity of the feasibility of the muscle activation synthesis process.

Joint Kinematics

In general, the major characteristics of joint kinematics during squat performance are exhibited in Fig. 3.17. At the middle of the squat cycle is the maintenance phase, when the knee joint reaches the predefined squat depth. At this moment, all joint angles stay unchanged and joint speeds are zero. The lower the squat depth, the greater the ranges of motion of all the other joints. The hip joint demonstrates the greatest range of motion and joint speed, while little movement is observed at the lumbar joint. The limit of rotational speeds imposed on the hip joint can be noticed by the plateau situated at $100°/s$.

Muscle Forces

In terms of muscle activity, the simulation outcome predicts that the most active muscles are GLU, HAM, SOL and especially VAS. They are mainly uni-articular strong muscles, exerting forces to create joint torques countering the one generated by inertial forces. On the other hand, except the HAM, the other two bi-articular muscles are not highly active. These results concur with the findings in the works of [Schoenfeld, 2010, Toutoungi et al., 2000, Escamilla et al., 2001b]. It is noticeable that force spikes presented at almost every force graphs, except for the BIFEMSH that is absolutely inactive during squat performance. These spikes are the direct consequence of activating the posture task which also deactivates completely the three tasks of moving the head, maintaining balance and minimizing the angular momentum variation. Co-contraction between TA and SOL at the maintenance phase, between VAS and HAM throughout most of the cycle (indicated in [Escamilla, 2001]), and between GAS and SOL when the model configuration is close to stand up position, are observed, presumably providing more stability and control to the model, especially when the squat depth increases.

Controller Performance

Task Switch We can observe how the values of the two parameters influencing the high-level tasks' weight values evolve during a squat cycle. "Switch Option" indicates the stage at which a task switch takes place. We can notice Option 1, the transition from the descent phase to the maintenance phase, lasts until the end of the maintenance phase, then is followed by Option 2, the transition from the maintenance phase to the ascent phase. Option 3 takes place towards the end of the squat cycle, when the human model approaches the stand up configuration. Finally, Option 0 corresponds to period without task switch.

Is The Human Model Too Simple? To perform lower squat depth, the bigger force amplitudes are required, especially for highly active muscles. An important detail revealed by the results is that it's impossible to synthesize a squat of 90°squat depth. This can be seen through the saturation of forces of HAM and GLU muscle (Fig. 3.18 and the errors of torque tracking of the second step (Fig. 3.23). Specifically, the hip desired torque differs from the one generated by synthesized muscle forces up to 50 Nm during the maintenance phase. This phase is indeed not stable during simulations, and the model rotates forward instead of being fixed in a configuration. This unsuccessful simulation of the 90°squat depth raises questions about the complexity of the human model. Indeed, the model used in this example is highly simplified, with many muscles are lumped together to created a unique muscle unit, as the case of GLU, VAS and HAM. Even the maximal force produced by these muscles takes into account the ones of their "sub-muscles" by summing them altogether, their muscle attachment points and therefore their moment arms w.r.t the joints upon which they act are excluded. In addition, the linear optimization process is influenced by the size of the muscle parameter set. We expect that with a greater number of implemented muscles, the controller can find a feasible solution of deeper squats.

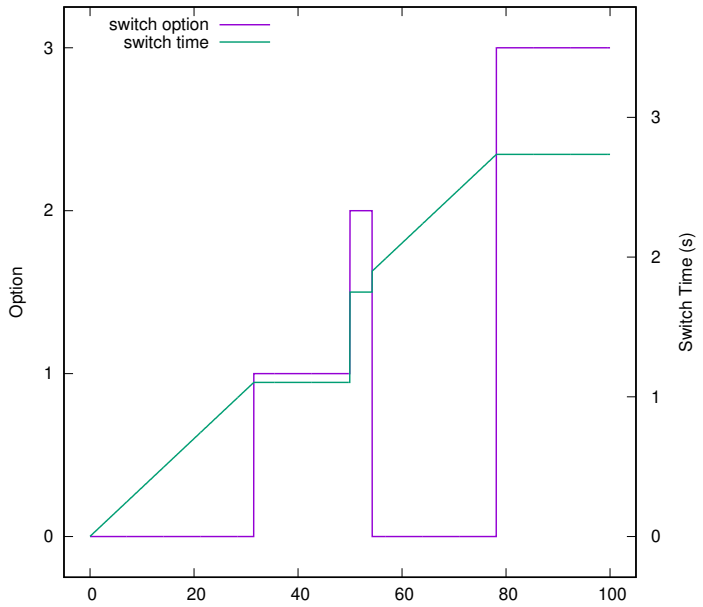

Figure 3.15: The evolution of task switch option and the start time of task switch.

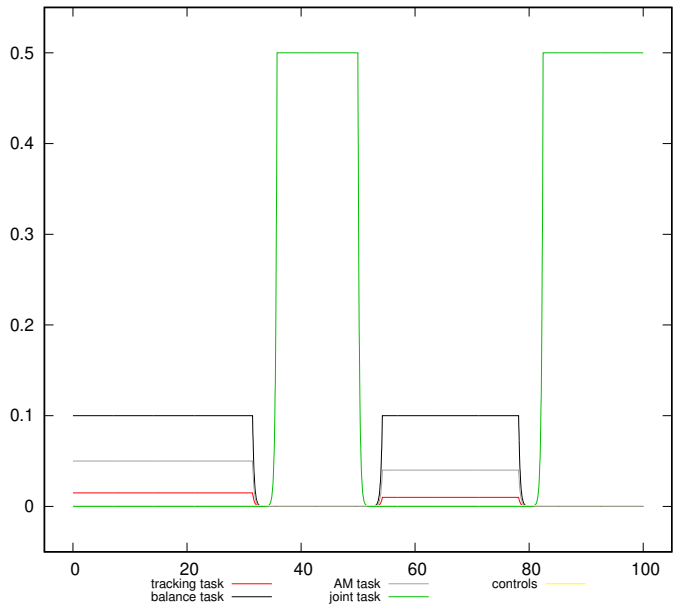

Figure 3.16: The evolution of task weights during a squat cycle. The posture is the dominant task during task switches of Option 1 and 3, with a weight of 0.5*, while the other high-level tasks are inhibited. On the other hand, for Option 2, its value decreases exponentially to zero.*

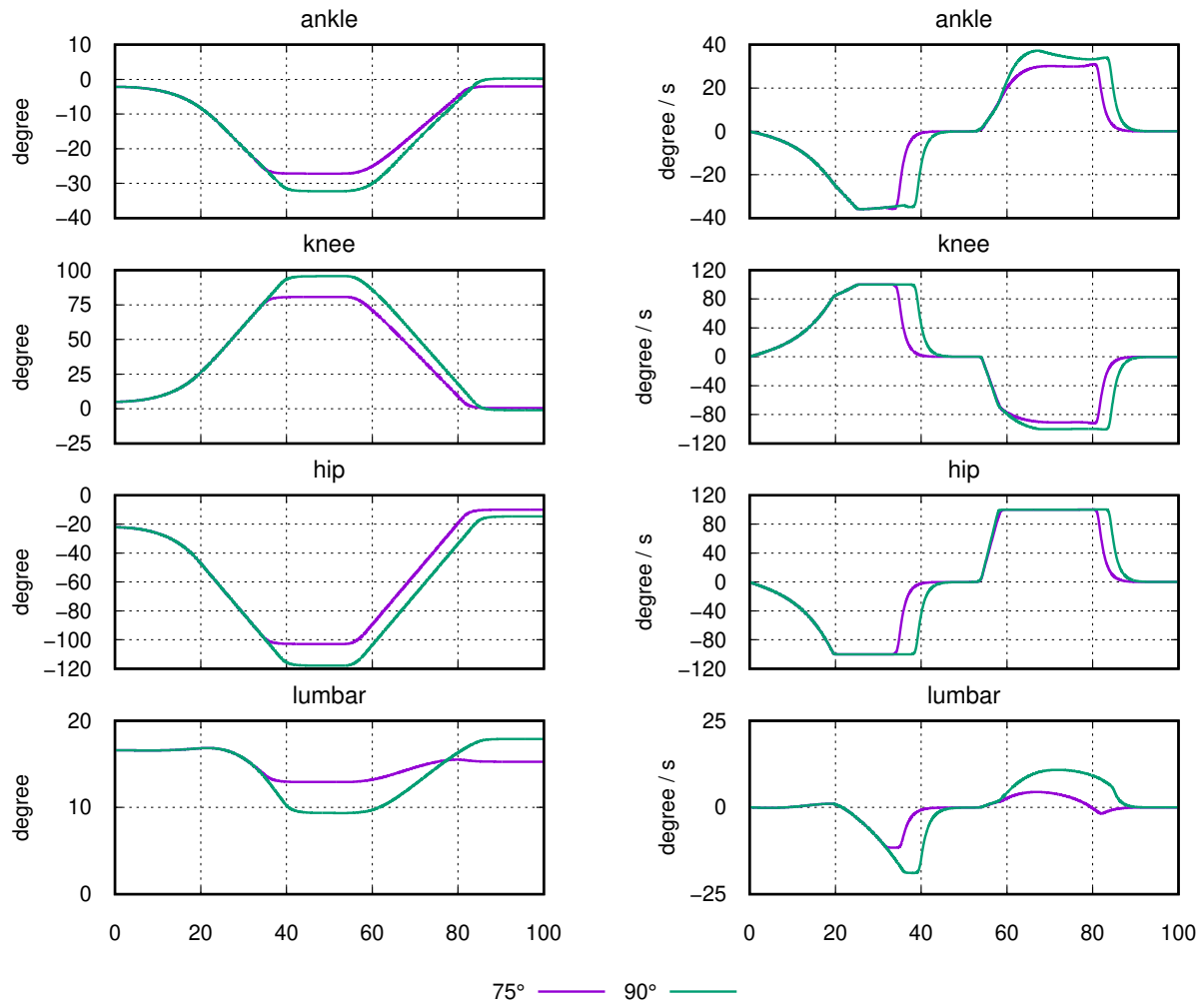

Figure 3.17: Joint kinematics produced by the controller for two different squat depths.

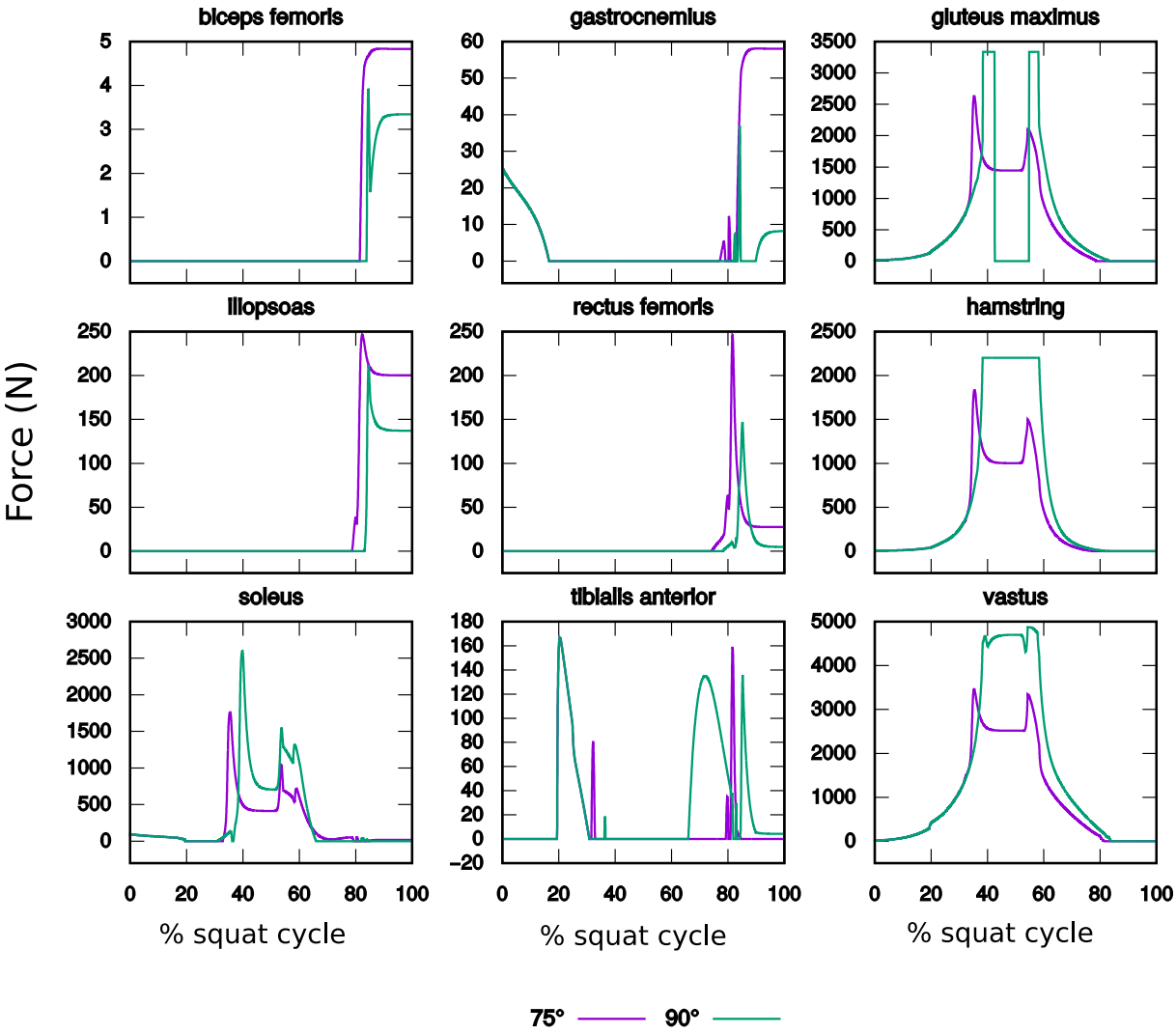

Figure 3.18: Muscle forces produced by the controller for two different squat depths.

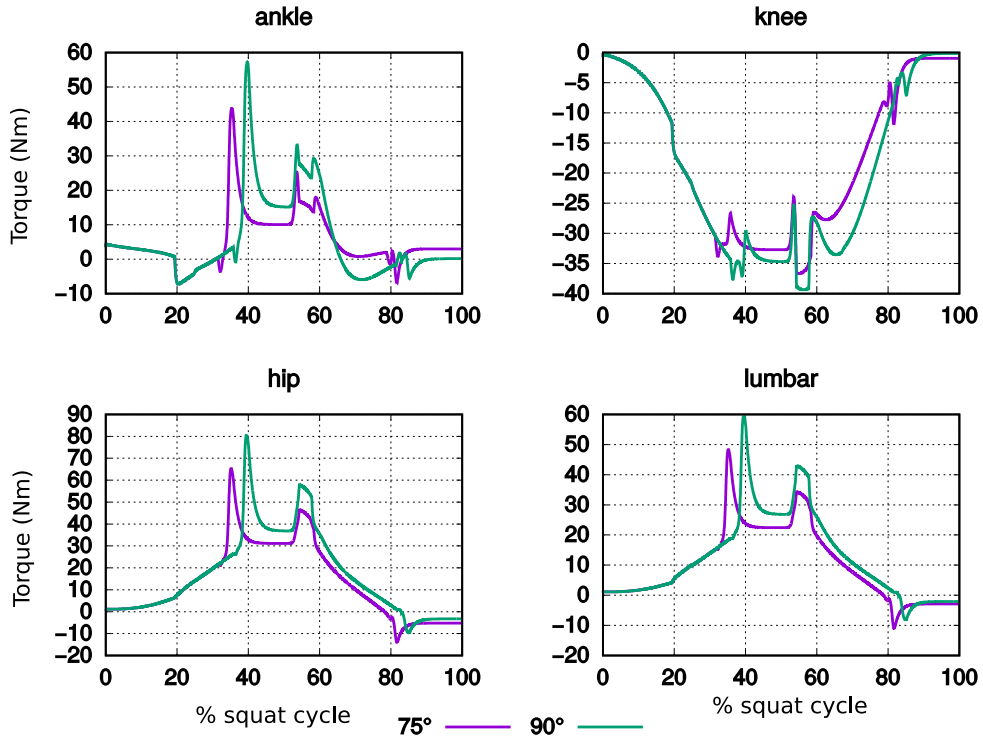

Figure 3.19: Synthesized joint torques for two different squat depths.

3.4 Simulation Example: Half Squat Synthesis with A Great Number of Muscles

In the previous section, we observe that the half squat with a squat depth of 90°is not feasible to synthesize. The potential cause is the insufficient number of muscles not allowing to track the desired hip joint torques. In this section, we want to verify our assumption by synthesizing this squat with a model consisting of a higher number of muscles. We do not perform Step I again as the musculoskeletal models are not used in this step. Only Step II is performed with the new model.

3.4.1 Human Model

We create a new model by keeping the skeletal structure but implementing 38 muscles. They are shown Fig. 3.20, Fig. 3.21 and Fig. 3.22. As in the simplified model, the muscles are modeled with OpenSim Path Actuator (Eq. 2.11). The lists of muscles, with their names, abbreviations and maximal forces are detailed in the appendix A.

3.4.2 Results

A part from SOL, GAS and TA, the muscle forces are altered significantly by increasing the number of muscles. The three GLU muscles of the "full" model contribute in the maintenance phases, and their total muscle forces are lower than the GLU muscle force of the simplified model. On the other hand, the hamstring muscle, which is divided into semimembranosus and semitendinosus, sees its muscle forces plummet. This is more coherent to its function of bi-articular muscle. The same phenomenon takes place for vastus muscles, which is represented by three muscles in the "full" model. In terms of tracking performance of Step II, the hip joint is fully reproduced by the new muscular system.

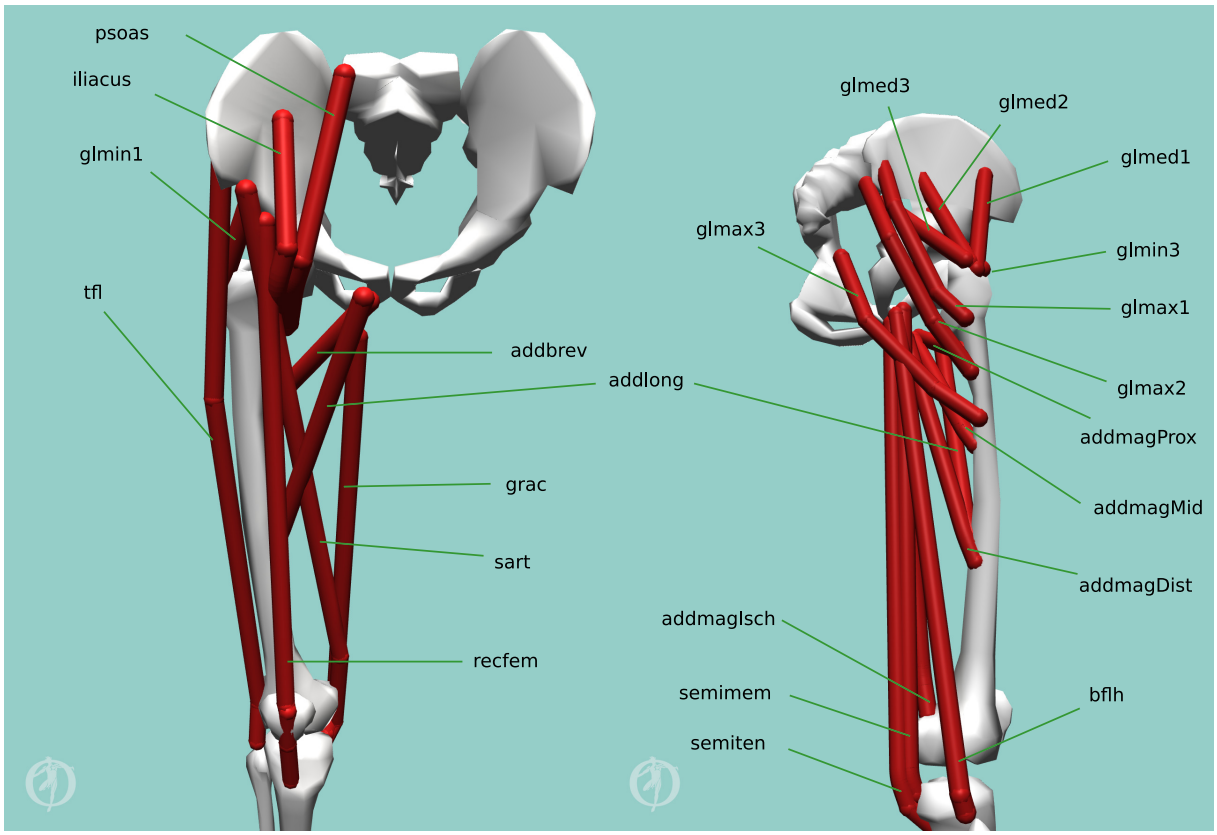

Figure 3.20: Hip flexors (left) and hip extensors (right)

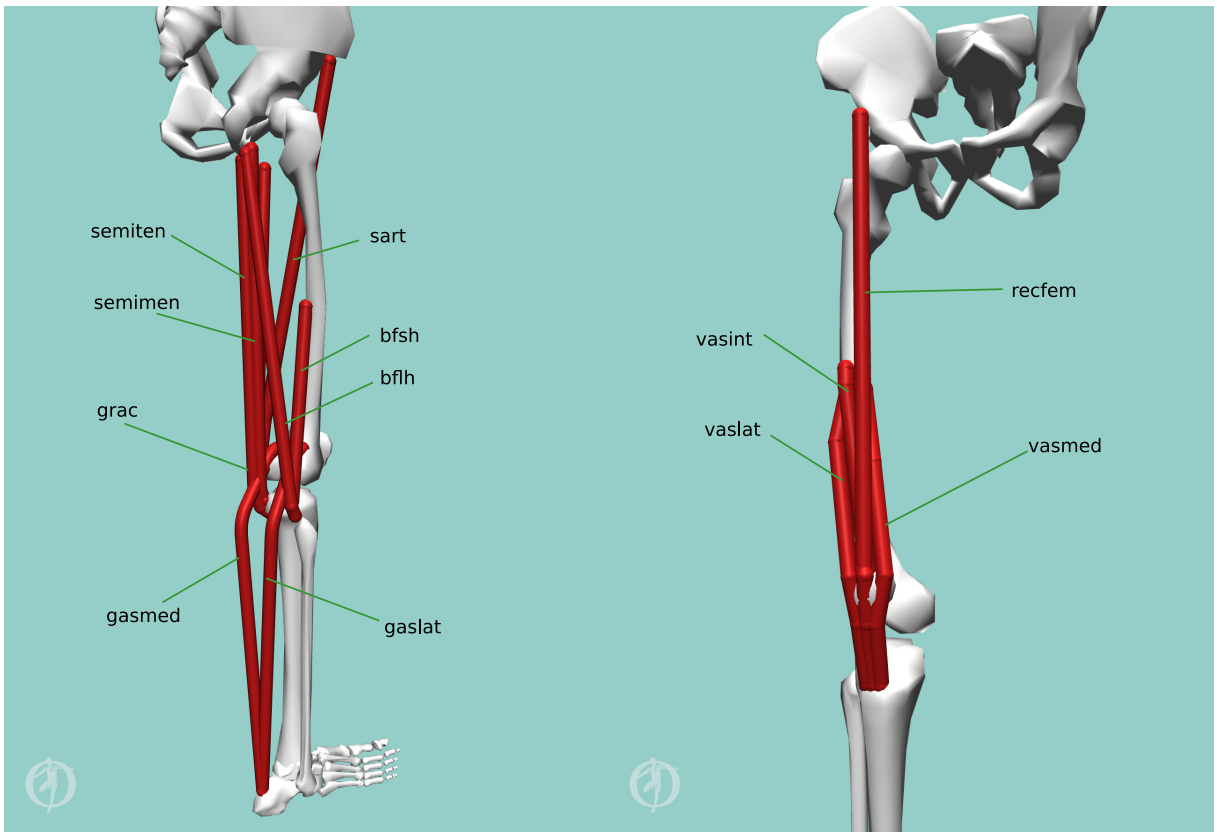

Figure 3.21: Knee flexors (left) and knee extensors (right)

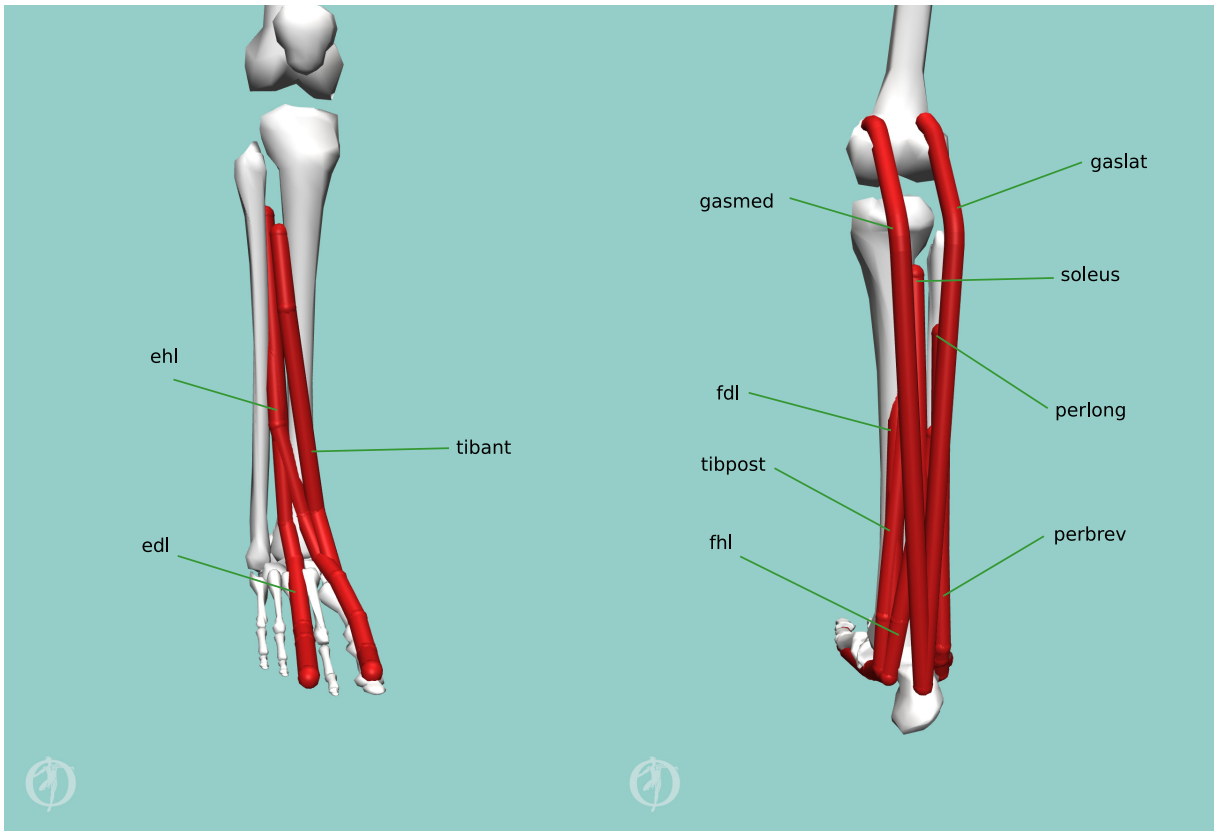

Figure 3.22: Ankle dorsiflexor (left) and ankle plantar flexors (right)

3.5 Conclusions

In this chapter, we detail the development of the two-step optimization based controller for squat movement synthesis. The equations and relationships presented in this chapter is based on the work on reactive whole-body control as well as our observation and assumptions on squat performance. The core element of the controller is the optimization problem in Step I that is formulated in such a manner that its resolution produces squat movement without using motion capture date. It consists basically of two parts. The physically-relevant high-level tasks constituting the first part are expressed as cost functions designed to produce the desired overall behavior. They represent the goals the the person performing squat seeks to accomplish with varying degrees of importance. The second part are the control constraints related to the limits of the human body, as well as the physics laws that must be respected.

The main functions of the controller are twofold. The first one is to carry out the dynamic movements during the ascent phase and descent phase. The second one is to achieve the static postures at the maintenance phase and at the end of the end of the squat cycle. Through the examples of half squat synthesis, we learn that it's feasible to produce squat with different depths with major features concurring with the literature. On the other hand, the effect of model complexity on the performance of the controller is noticeable. In the next chapters, we continue to study the performance of the controller and explore its capacity of synthesizing other types of squats and under different performance conditions.

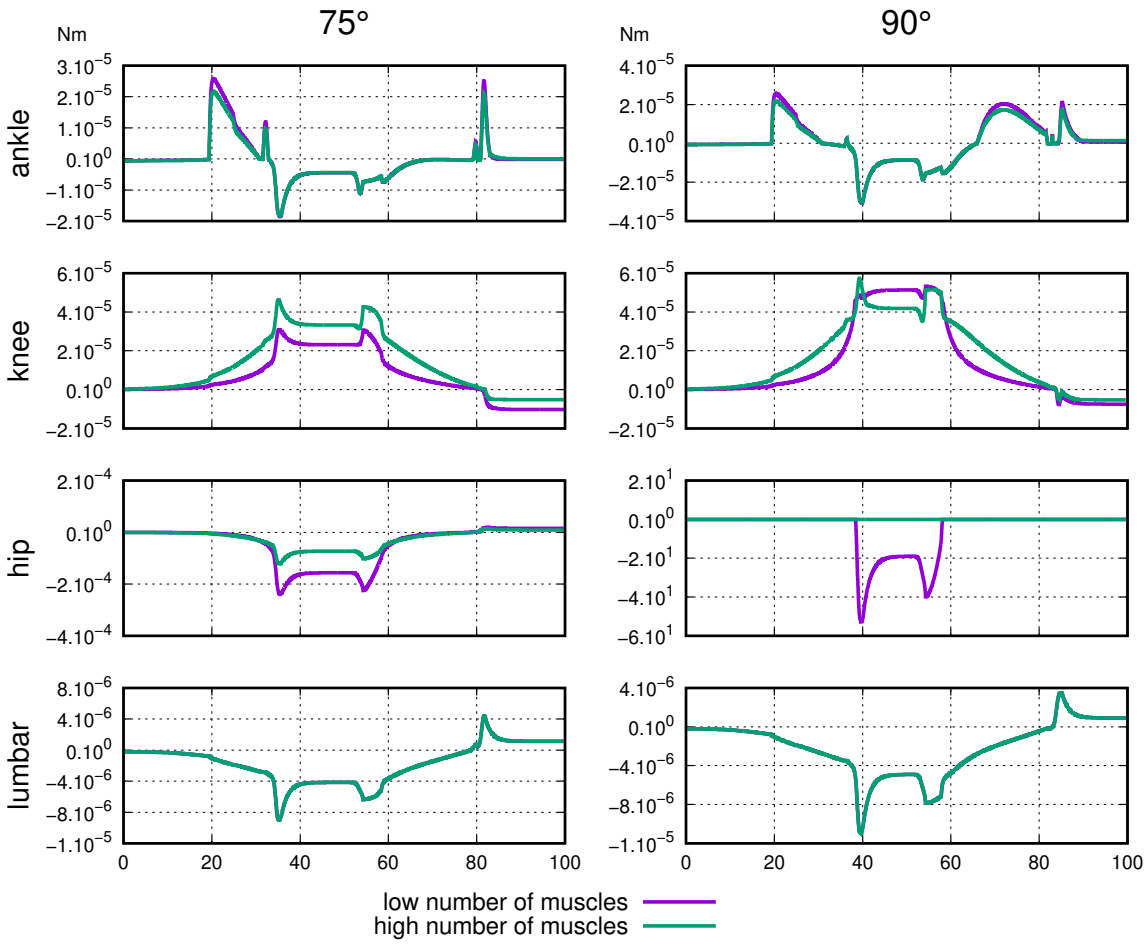

Figure 3.23: Tracking errors of Step II (Muscle Activation Synthesis) for two different squat depths. With the lower target squat depth of 90°, Step II cannot track the desired hip joint torques computed from Step I as they surpass the capacity of the muscles in the simplified human model. Noted that the desired torques to be tracked by both models are the same.

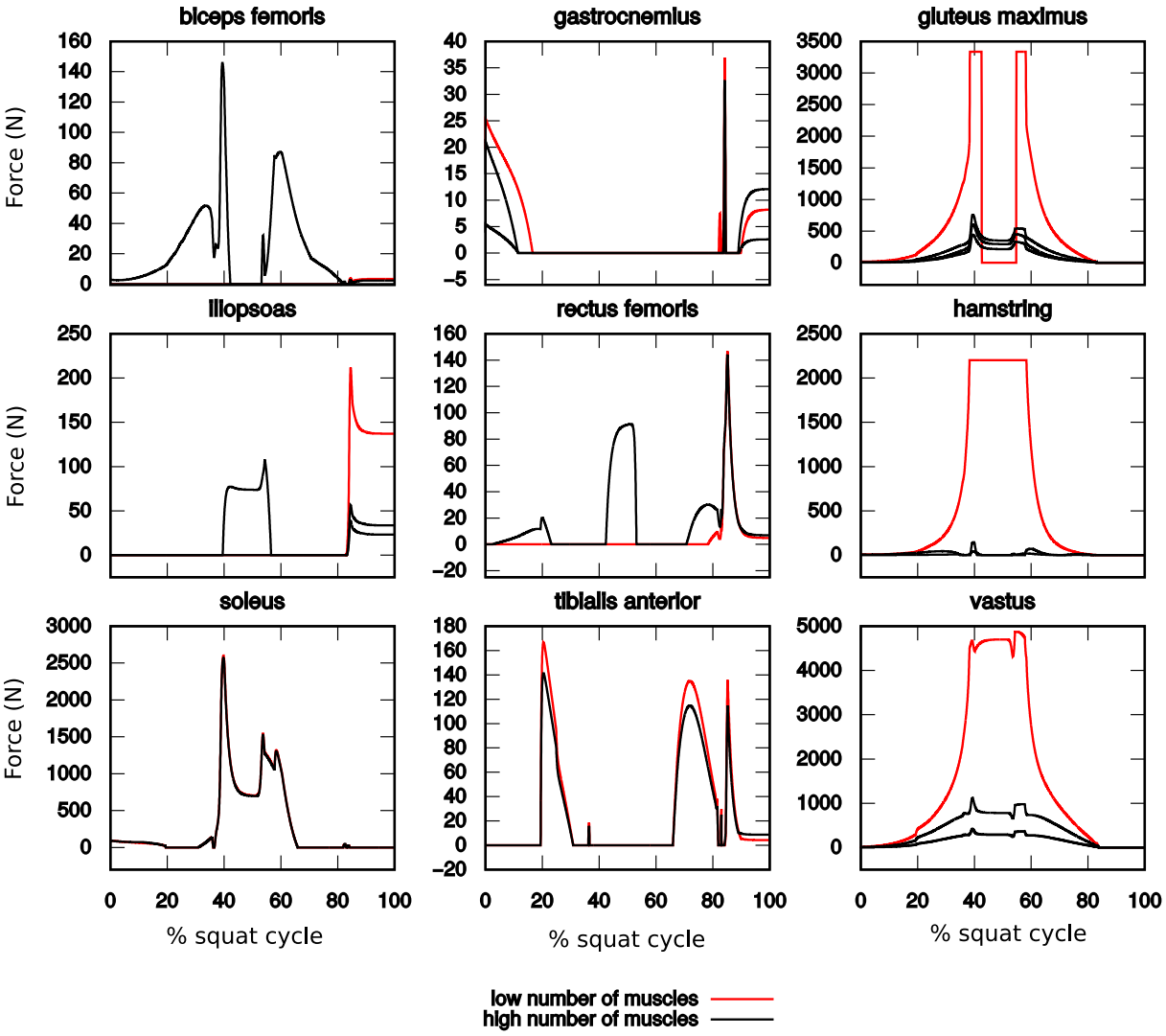

Figure 3.24: Differences in synthesized muscle forces caused by increasing the number of implemented muscles. Except the soleus, tibialis anterior and rectus femoris, the other muscles of the simplified model are replaced by a group of muscles in the other model. Remarkable gaps are observed between the two models for the gluteus maximus, the hamstring and the vastus.

Chapter 4

Synthesis of Different Squat Strategies and Patterns With The Optimization-based Dynamic Task Controller

One of the main advantage of the application of physics-based predictive simulations in the biomechanical and medical domains is the capacity of identifying the cause-effect relationship between modifications of musculoskeletal system and the outcome in terms of joint kinematics and muscle behavior. As a consequence, they can generate novel movement pattern without relying on experimental data. In this chapter, we investigate the prediction capacity of our controller by synthesizing

1. the effect of modifying a singular element of human model on squat performance;
2. the different strategies of squat.

Regarding the first item, we choose to study the effect of ankle-dorsiflexion range of motion (ROM) on the execution of squat. Restricted ankle-dorsiflexion ROM is investigated in [Macrum et al., 2012] through squat trials on an inclined surface. In parallel, it is found by some researchers that to be able to perform squats, especially Asian squat (cf. 4.1), sufficient ankle dorsiflexion is essential [Blair, 1994, Bridger, 1991, Kasuyama et al., 2009]. Indeed, with the constraint of keeping the heels on the ground, this flexibility of the ankle joints allows adjustment of the CoM position to maintain balance. "A lack of sufficient ankle dorsiflexion is perhaps the foremost reason why a Western individual has difficulties squatting", as stated in [Bridger, 1991, Mulholland and Wyss, 2001]. Inspired from these findings, our objective regarding the first item is to synthesize Asian squats with models exhibiting different ankle ranges of motion to investigate this hypothesis.

For the second item, our goal is to study the generation of different squat strategies by altering the priorities of the physically-relevant high level tasks. As these priorities reflecting the intention of a person to perform squat in a certain way, their modifications generate new squat patterns. We propose to synthesize two squat strategies by using our proposed squat synthesis method. The distinction between the two strategies lays in the management of the inclination of the torso. We demonstrate that these strategies emerge as a result of altering the priorities of the physically-relevant high-level tasks and study their impact on the joint torque and muscle activity patterns To validate the simulation results, we carry out squat trials on two different squat strategies and collect joint kinetics data as well as electromyographic (EMG) signals.

Figure 4.1: Asian squat with feet flat on the ground. Image courtesy [Brazil and Peña,]

4.1 Synthesis of Asian Squat

4.1.1 Overview of Asian Squat

The Asian squat is the deep squat adopted by millions of people in many parts of Asia, Africa, Latin America and Oceania [Bridger, 1991]. In this posture, while being completely comfortable, they execute their daily live activities, from cooking, working, cleaning to using a toilet and even resting. Deep squat is rarely seen amongst Caucasian adults, even though their children can easily achieve the posture. One possible explanation is the availability of furniture [Mulholland and Wyss, 2001]. The most notable feature of Asian squat is the high ranges of motion of knee and ankle joints. The plantar surfaces of the feet stay flat on the ground, while the hips and knees are almost fully flexed and the calves are in contact with the thighs.

To maintain balance, the centre of gravity of the body is kept low and over the feet while the trunk is flexed and inclined anteriorly towards the thighs [Bridger, 1991]. In terms of muscle activities, the gluteals contract eccentrically while the iliopsoas concentrically. The hamstrings and quadriceps muscles are activated moderately. [Bridger, 1991]. It is reported that full hip flexion can reach 130°and the range of full knee flexion can be between 111°and 165°[Mulholland and Wyss, 2001].

To investigate the differences of kinetics and loading between Asian and Caucasian individuals, [Lu et al.,] conducted experiments and performed tracking marker data with customized OpenSim models. Significant lower squat depth, greater knee range of motion and contact forces and lower ankle contact forces were estimated in the Asian individuals while performing the deep squat compared to the Caucasian groups. With sufficient ankle dorsiflexion, one can adjust ankle rotation to move the CoM over the feet and maintain balance [Bridger, 1991]. Even though the Asian squat is much less popular among Caucasians, "the increased ability to squat is more likely to be due to lifestyle than a genetic or innate ability to squat" [Mulholland and Wyss, 2001]. To perform this type of deep squat, one can train regularly to improve flexibility of the ankle joint [Mulholland and Wyss, 2001].

4.1.2 Method

The main objective is to study the prediction capacity on the impacts of ankle dorsiflexion on the performance of deep squats, under the constraint of maintaining foot/ground contact without lifting the heel. Simulations are carried out on two models that built based the models used in the previous chapter 3. We keep the same musculoskeletal structures while modifying the range of motion of the ankle joint to obtain different level of ankle flexibility. The first model representing Asian individuals has an ankle with the lower coordinate limit of -30°. The second model representing Caucasian individuals has a reduced ankle range of motion, with the lower coordinate boundary of -20°. In terms of task priorities, the same weight values are applied during the simulations with both models, as shown in Table 4.1. Indeed, our goal is to only study the dependence of Asian squat performance on the ankle range of motion, hence

Table 4.1: Weighting coefficients for tasks and optimization variables for step I - Asian squat synthesis

Model	**Asian**		**Caucasian**	
Phase	Descent	Ascent	Descent	Ascent
Task				
Head vertical displacement	0.010	0.050	0.010	0.050
Angular momentum variation	0.050	0.060	0.060	0.060
Balance	0.100	0.100	0.100	0.100
Control				
All actuators	0.010	0.010	0.010	0.010
Generalized acceleration				
Ankle	0.003	0.003	0.003	0.003
Knee	0.003	0.003	0.003	0.003
Hip	0.003	0.003	0.003	0.003
Lumbar	0.100	0.100	0.100	0.100

the same optimization strategy applied to both models. At the end of the simulations, data related to joint kinematics and torques, muscle moment arms and forces are analyzed to assess the validity of our hypothesis.

Implementation of Task Switch for Asian Squat

Task switch for Asian squat is slightly different than the one implemented in the previous chapter for half squats. While the two Task Switches occurring during the ascent phase of half squat (Switch Option 2 and 3) are still applied to Asian squat, the one at the end of descent phase (Switch Option 1) necessitates additional condition regarding the achievement of the squat depth. In the case of half squats, Task Switch is developed based on the assumption that the subject reacts to the external instruction to stop descending at the desired squat depth. On the contrary, the execution of Asian squat does not require any instruction as there is no predefined squat depth to target. We hypothesize that a person performing Asian squat descends as low as he/she can until it is impossible to go lower the body further down. As a result, the squat depth of an Asian squat is considered as the lowest level (the greatest absolute value of knee flexion angle) that a person can achieve. This value is unknown prior to squat performance and influenced by multiple factors, including the adopted strategy and the constraints related to the body, especially the joint limits.

Assuming that the person performing Asian squat is healthy and flexible at the hip and knee joints, we consider two scenarios in which the squat depth is achieved:

1. The knee joint reaches its boundary. In this case, the Asian squat is considered successfully executed.
2. The projection of the CoM reaches the posterior boundary (at the level of the heel).

For scenario 2, due to the limit range of motion of the ankle joint, the knee and hip joints are more solicited for the head vertical displacement task (Task 3.2.1). This leads to the translation of the CoM towards the heel as the torso is lowering towards the ground. Once the projection of the CoM reaches its lower boundary, the performer stops descending further to avoid lowing balance.

As a reminder, the evolution of weight values during task switch follows the model established in Subsection 3.2.2.

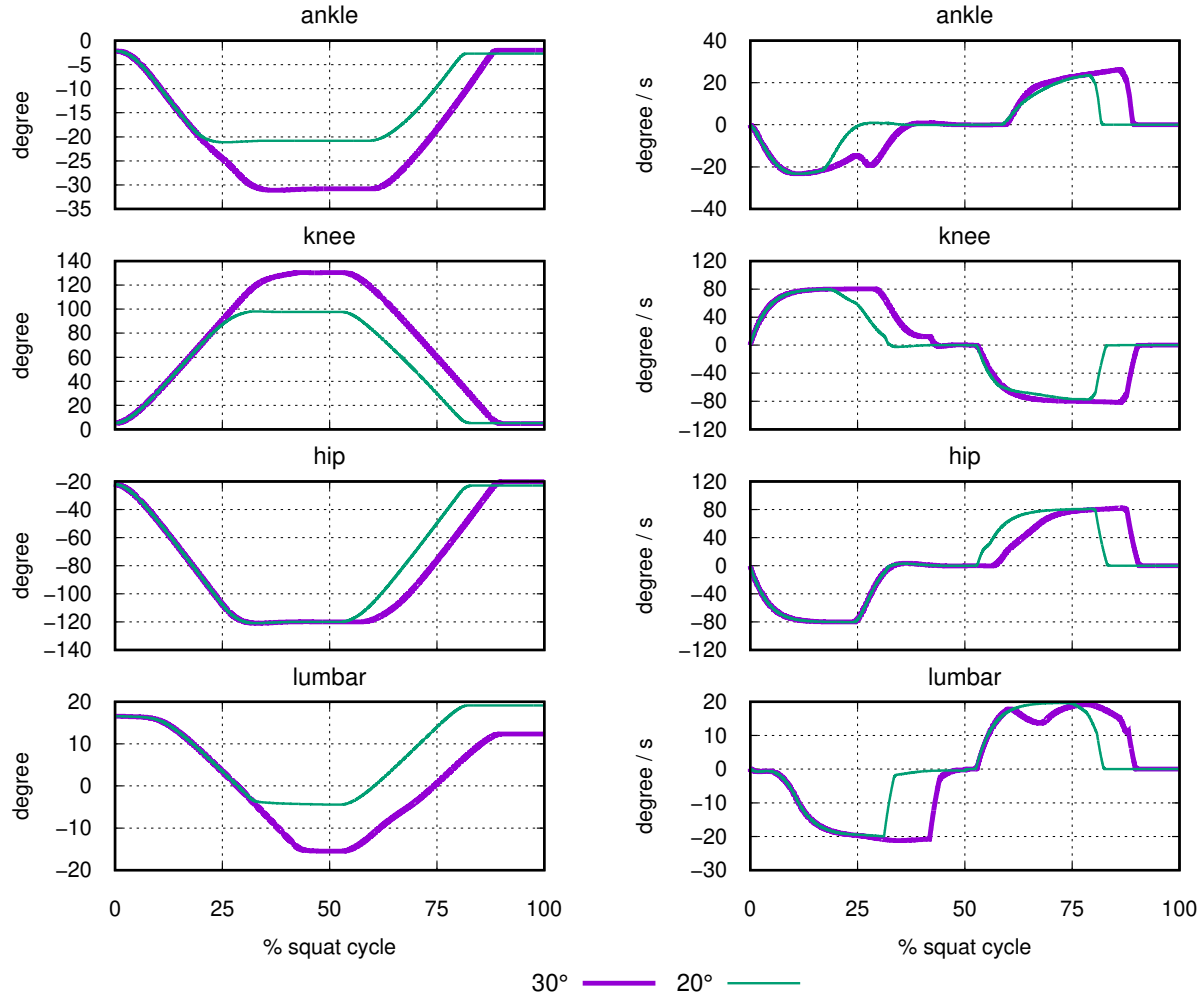

(a) Joint angles of individuals with flexible (blue) and blocked ankle (red)

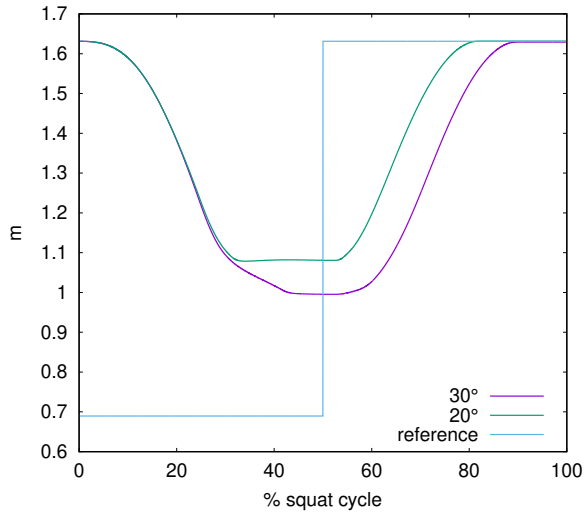

(b) The head height during the squat cycle

Figure 4.2: Comparison of squats two models with different ankle range of motion. Thanks to the ankle dorsiflexion flexibility, the Asian model (30°) reaches a lower height. Note that the reference of target forehead positions serves the main purpose of moving the body vertically and not tracked with precision.

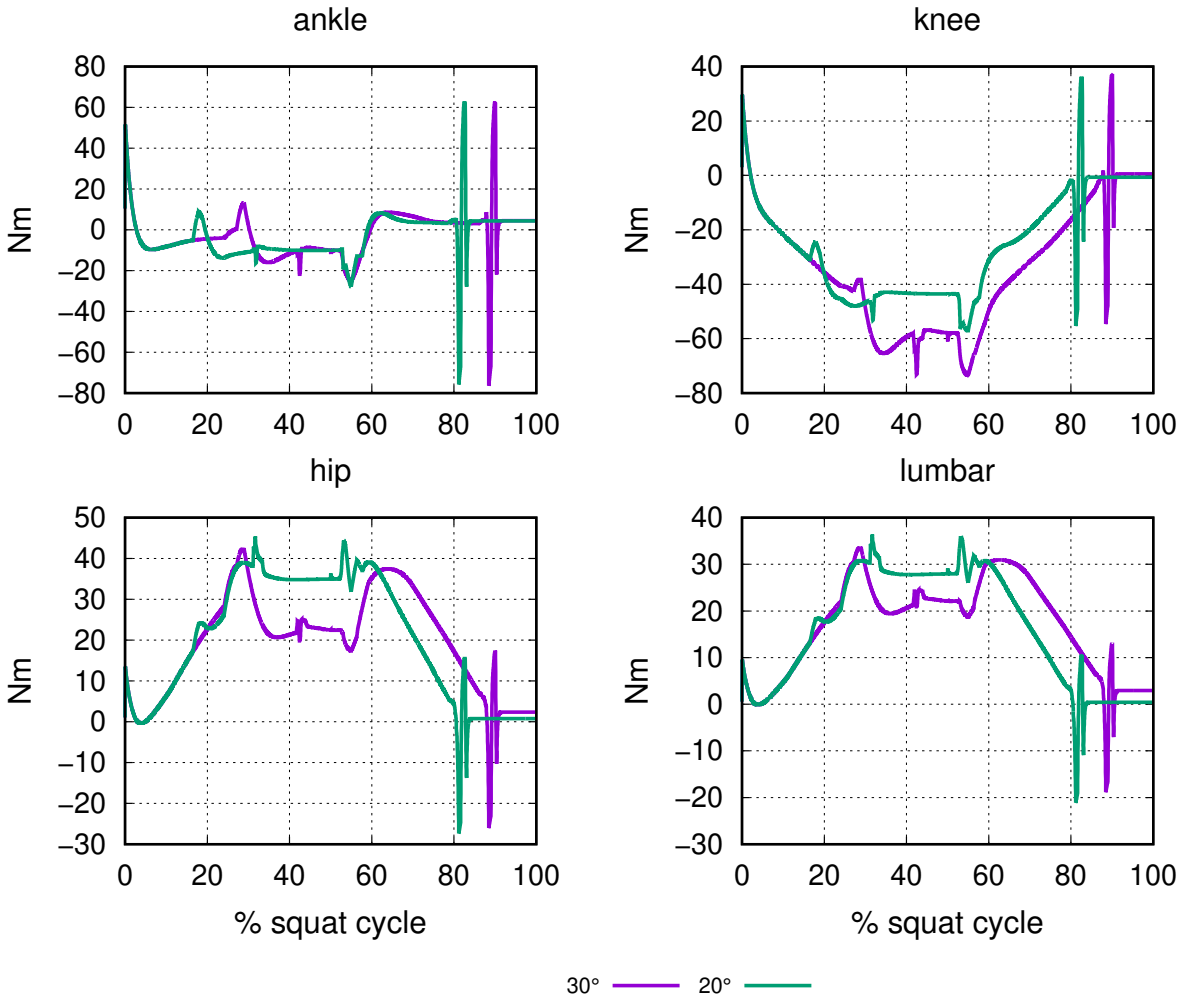

(a) Differences in joint torques due to different levels of ankle flexibility.

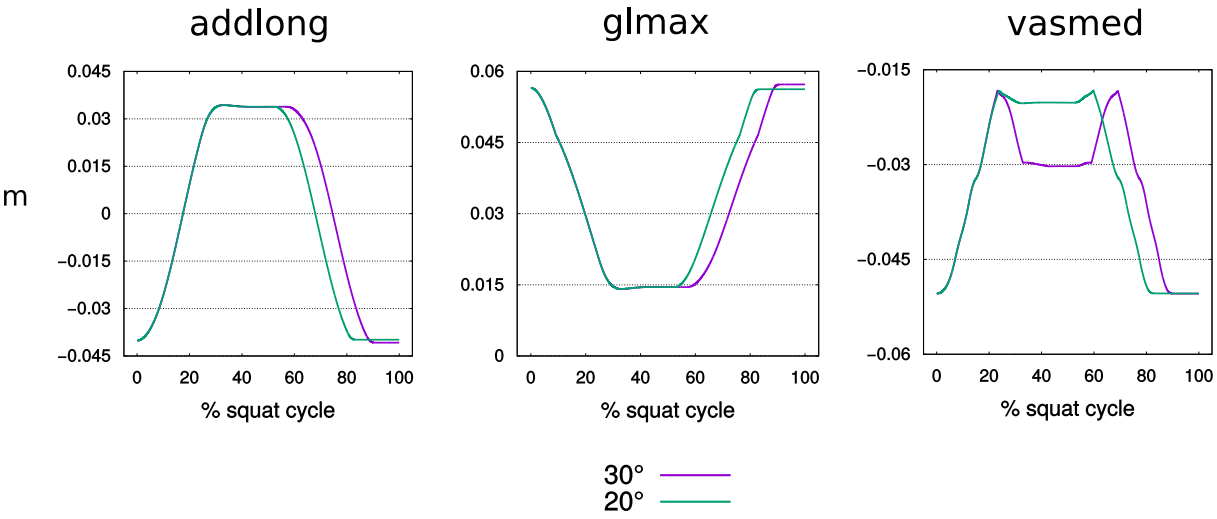

(b) Differences in moment arms between Asian and Caucasian squats.

4.1.3 Results and Discussions

Comparing joint angles and joint torques between Caucasian and Asian squats

We use the term Caucasian squat to indicate the squat produced with model having the less flexible ankle. The typical wide ranges of joint rotations of the Asian squat are noticeable in the computed kinematics. The joint ankle reaches the lowest value (around -30°) just before the end of the descent phase. The flexibility of the ankle allows the knee to rotate to great coordinate values (130°). Consequently, the head height can go further down comparing to blocked ankle model, with the boundary of -20°manifested in the ankle joint curve, as shown in Fig 4.2a. In the meantime, to maintain the balance, the lack of mobility of ankle joint induces the limited rotation of knee joint. Consequently, the act of lowering the head depends mostly on hip rotation, even though the head height is still bigger comparing to the Asian squat (Fig. 4.2b). However, in this posture, it is impossible to keep the thigh in contact with the calf, making it impossible to adopt the deep squatting posture [Kasuyama et al., 2009]. The implication of the limited ankle rotation is also visible in the joint torques curves (Fig. 4.3a). Greater knee rotation of successful Asian squat requires more torque than the Caucasian squat. On the other hand, the hip torque is higher at the maintenance phase in case of Caucasian squat, as the torso is more anterior horizontally w.r.t the hip.

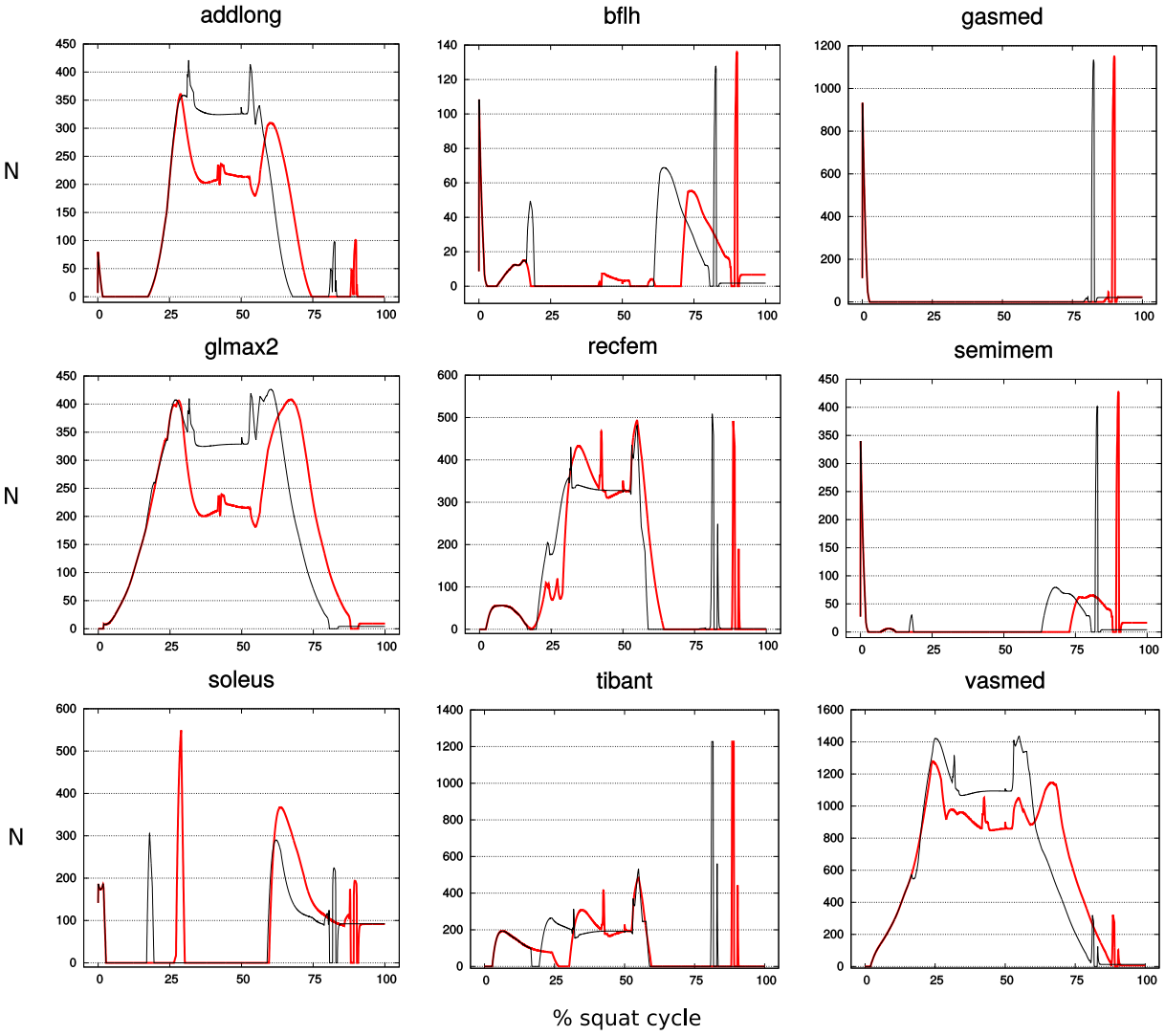

Figure 4.4: Differences in muscle activities between Asian (red curve) and Caucasian squats (black curve).

Comparing muscle forces between Caucasian and Asian squats

Fig. 4.4 shows the forces of the muscles with significant amplitudes. For the muscle groups in which the individual muscles exhibit similar activity patterns, we choose one muscle to represent the associated group. These are the cases for adductor longus (addlong) of the adductor group, middle gluteus maximus (glmax2) of the gluteus maximus group and vastus medialis of the vasti group.

Hip extensors (addlong, glmax2), knee extensors (recfem, vasmed) and ankle dorsi flexor (tibant) have their activities increased during the descent phase and decreased during the ascent phase. Soleus, as a ankle plantar flexor, is activated mainly at the beginning of the ascent phase, together with semimembranosus (semimem), a bi-articular hip extensor. Their extension functions create joint torques at the hip and knee to overcome the gravity effect. Tibialis anterior (tibant) exhibits an opposite patterns to the ones of soleus and semimembranosus (semimem). This muscle, activated mainly during the descent phase and the maintenance phase, is slightly more solicited when the ankle rotation is limited to -20°. Indeed, its function contributes in maintaining balance by keep the CoM inside the boundaries.

Between the muscle activities of the two models, significant contrasts are observed in the patterns of adductor longus (addlong), middle gluteus maximus (glmax2) and vasti medialis (vasmed) during the maintenance phase. Specifically, the muscle forces are smaller for all these three muscles during Asian squat. To explain this, we take into account two factors dictating computed muscle forces: the moment arm (Fig. 4.3b) and the joint torque. In case of hip extensors (addlong, glmax2), their moment arms remain at the same level for the maintenance phase since the hip reaches the boundary of -120°regardless of the type of squat. Meanwhile, as mentioned earlier, the hip torque is lower for Asian squat in the maintenance phase, leading to smaller muscle activities for these hip extensors. On the other hand, the uni-articular knee extensors, including vasti medialis (vasmed), exhibit smaller muscle forces while producing higher knee torque in Asian squat during the maintenance phase. The reason is that the moment arms of these knee extensors are substantially higher (in absolute value) at the extreme knee flexion of the Asian squat. The vastus medialis (vasmed) produces less important force in Asian squat than in Caucasian squat. Regarding rectus femoris, this bi-articular muscle does not exhibit dependence on the ankle range of motion in terms of activity.

4.2 Synthesis of Two Different Squat Strategies

Movement strategies can arise as the result of modifications in the intentions of the performer (corresponding to altering high-level tasks) or in the constraints related to the musculoskeletal system and the performance conditions. In the previous section, we explored how a singular modification of the skeletal system could impact the adopted strategy for Asian squat execution. In this section, we investigate how squat strategies are created from modifying task priorities and their influence on joint kinematics and torques, muscle activations and forces.

Two strategies of squat are in consideration (Fig. 4.5). Strategy I is the "straight back strategy", imposing the back to be as straight as possible throughout the movement. As a side note, "straight" indicates the verticality in the ground frame. Strategy II is the "inclined back strategy", requiring the hip to be placed as far back as possible during the whole cycle. The aim of the second strategy is to reduce the knee joint torque. As the first step towards this goal, we carry out squat trials of two different strategies and collect kinematic and electromyographic (EMG) data. Meanwhile, simulations are created to synthesize these strategies by our controller (Chapter 3) to compute joint kinematics, joint torques and muscle activations and forces.

4.2.1 Method

Experimentation

The data was collected from a healthy male subject. His height is 163 cm and his body mass is 55 kg. His participation was voluntary, and a written informed consent, as approved by the Sorbonne University, was obtained prior to the experiments. The subject was instructed to perform three repetitions of squat cycles of the two different movement strategies (Fig. 4.5). The squat depth (the knee joint angle) is fixed at 60°. A person supervises the trials and instruct the subject to stop when he reaches the squat depth.

The acquisition is performed with a Vicon system. Captured motion of the markers is then used to scale the dimensions, mass and inertial properties of the body segments of the OpenSim models. EMG data are acquired in 7 muscles (HAM, GLU, RF, VAS, GAS, SOL, TA) through 14 Delsys sensors at 2000Hz.

Figure 4.5: Squat strategy I (left) with straight back and strategy II (right) with hip pushed behind to reduce knee joint torque.

Simulation

To created the numerical model of the subject, we scale the model shown in Fig. 3.14 using the Scaling Tool of OpenSim. It is a inverse kinematics optimization process that match the virtual markers of the computational model to the experimental marker locations. For this process, the raw marker trajectories of a static trial, where the subject poses in a known static position, are used as input.

The generation of squat strategies in this study is based entirely on the modifications in the task priorities. These priorities are represented by a coefficient, or weight, and are manually tuned and then fixed for a simulation. As a result, the strategy is decided before the squat movement commences. This is contrary to the study in the previous section, in which the strategy emerges during the squat movement when the ankle boundary is reached.

To create the two movement strategies, we only consider the priorities of the physically-relevant high level tasks (Table. 4.2). The weights associated to the terms in the regularization task are kept unchanged when simulating both squat strategies. We find that the distinction between the two squat strategies is mainly related to the weight associated to the angular momentum task. Indeed, choosing a greater weight for this task keeps the back erected during the squat cycle and leads to strategy I, while allowing more angular momentum variation gives rise to strategy II. We also increase the weight of the generalized lumbar acceleration for the ascent phase of strategy II as wider range of motion is observed by using the same value as in the descent phase. On the other hand, the purpose of adopting different values for the head vertical displacement task is only to fine-tune the kinetic results more closely to the captured joint

Table 4.2: Weighting coefficients for tasks and optimization variables of the two strategies in step I

Squat strategy	**Strategy I**		**Strategy II**	
Phase	Descent	Ascent	Descent	Ascent
Task				
Head vertical displacement	0.013	0.006	0.015	0.008
Angular momentum variation	0.040	0.040	0.010	0.010
Balance	0.400	0.400	0.400	0.400
Control				
All actuators	0.010	0.010	0.010	0.010
Generalized acceleration				
Ankle	0.003	0.003	0.003	0.003
Knee	0.003	0.003	0.003	0.003
Hip	0.003	0.003	0.003	0.003
Lumbar	0.014	0.014	0.014	0.020

angle profiles. This fine-tuning adjustment is not mandatory as the synthesis scheme does not require any predefined trajectory.

4.2.2 Results and Discussions

In this section, the computed results and the experimental data are analyzed and compared to evaluate the impact of each strategy on the joint kinematics and muscle behavior, as well as the performance of our synthesis method. As a side note, some artifacts due to controller computation, such as spikes in computed joint torques, muscle activities and muscles forces, are removed to facilitate the visualization of the figures.

Influence of The Squat Strategies on Joint Kinematics and Torques

In strategy I, the ankle and knee joints have a wider range of motion whereas the hip and lumbar joints are more engaged in strategy II. The trend is also reflected in the synthesized torques where a substantially higher torque is produced at the knee joint than other joints in strategy I, whereas in strategy II, these torques have considerably closer values one to another. This can be explained partly that the straight back in strategy I increases the gravity effect on the knee. In reality, passive knee torque [Riener and Edrich, 1999] also contributes to the dynamic equation, but our modeling does not take this phenomenon, among others, into account.

On the other hand, some disparities between the simulation and the captured data are present, notably the evolution of joint speeds. In the captured data, the joint speeds reach their peak values towards the beginning of descent phase and the end of ascent phase while the synthesized peak joint speeds appear toward 50% of the cycle. Additionally, several artifacts are observed towards the end of the phases. They are related to the trigger of the posture task and the simple linear model of the actuators.

Influence of The Squat Strategies on Muscle Activities and Forces

We investigate the qualitative characteristics of muscle activities and forces between EMG data and the simulation (Fig. 4.9). Due to the simple model of path actuators, the synthesized forces are proportional to the activations (Fig. 4.8).

In the computed results, between the two strategies, no difference observed in terms of muscle recruitment.

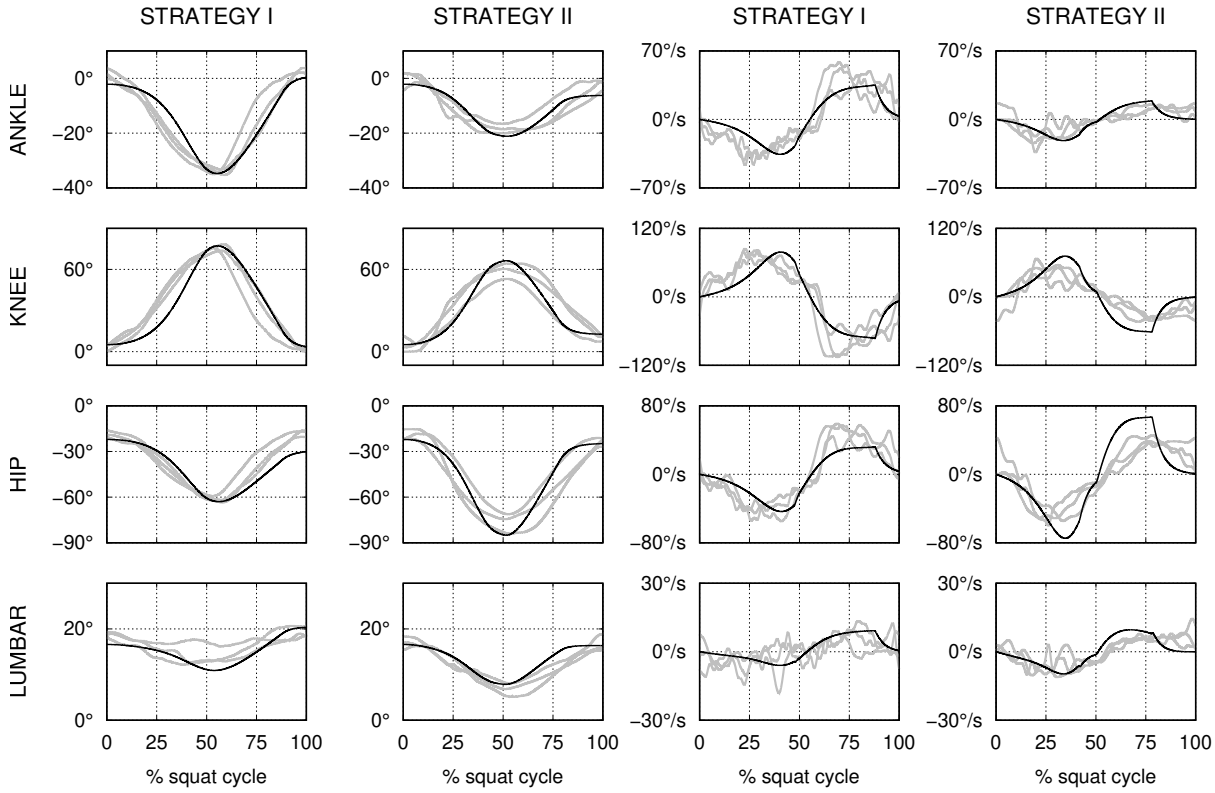

Figure 4.6: The synthesized squat cycle (black) has the joint angles (first and second columns) and the joint speeds (third and forth columns) staying in the area of movement captured data (gray).

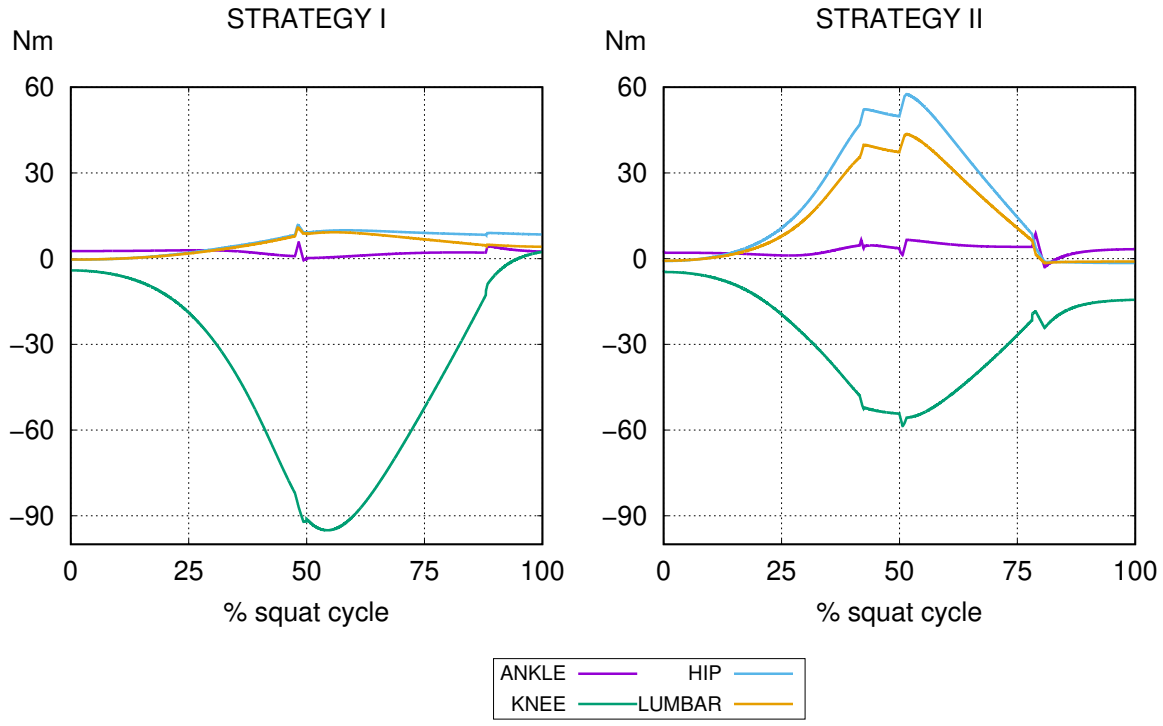

Figure 4.7: Distinct synthesized torque profiles between the two strategies.

The muscles showing highest contribution in terms of force are hip extensor gluteus maximus (GLU), knee extensor vasti (VAS) and the bi-articular muscle rectus femoris (RF). Since RF is a hip flexor, it can form a pair of agonist-antagonist muscles with GLU. The computed activations and forces of these two muscles indicate a co-contraction during the squat. As the knee joint torques required for strategy I is higher than strategy II, the forces produced by the knee extensors increase. This also lead to a more enhanced co-contraction of RF and GLU, thereby providing more stability towards the end of the descent phase and during the maintenance phase. Meanwhile, the higher demand of hip torque of strategy II induces higher activity of GLU and HAM. These hip extensors control the torso movement during descent phase and extend the hip during the ascent phase.

Both in synthesized activities and measured EMG, the knee extensor VAS exhibits the highest activity among all muscles. On the other hand, no considerable activity is obtained for the two bi-articular hamstring (HAM) and gastrocnemius (GAS) and the plantar flexor soleus (SOL), both in recorded EMG data and computed muscle activities. As a side note, GAS is a plantar flexor and knee flexor, and HAM is a knee flexor and hip extensor. In the literature, GAS and HAM have been observed, through the recorded EMG signals, to be less active than the knee extensors VAS and RF [Kongsgaard et al., 2006] [Schwanbeck et al., 2009] [ISEAR JR et al., 1997]. However, these two bi-articular muscles can co-contract with the knee extensors to improve knee stability [Draganich et al., 1989] [Escamilla, 2001]. Our synthesized forces generated for GAS and HAM are not significant enough to produce co-contraction between knee flexors and extensors. Another pair of agonist-antagonist muscle, SOL and tibialis anterior (TA) demonstrates co-contraction during squat movement. TA is a ankle dorsiflexor, responsible for the ankle rotation towards the tibia (the shin bone), while SOL as, a plantar flexor, rotates the ankle away from the tibia when activated. With the slight increase of ankle torque from strategy I to strategy II, the co-contraction of this muscle pair is augmented lightly. However, this is not the case concerning the recorded EMG activities, as disparity is observed between EMG data and computed muscle activity of then dorsiflexor tibialis anterior (TA). According to the subject, during strategy I, at the end of the descent phase, he struggles to keep balance and therefore contracts this muscle to avoid falling backward. Indeed, TA, as a dorsiflexor, rotates the tibia towards the knee and thereby adjusts the projection of CoM on the ground towards the toes and increases balance. This is reflected by important EMG signals from TA towards the end of the descent phase. On the other hand, the computed activity of TA is optimized to assure the muscle function with minimum level for both strategies.

The most noticeable disparity between EMG data and computed muscle activities regards the hip extensor GLU. The simulations of both strategies yield substantial values of GLU, for which only minor EMG signals are observed. A possible cause of this disparity is the simplicity of our muscle model which does not incorporate elastic and damping elements like Hill-type muscle models [Haeufle et al., 2014] to modelize passive forces. Indeed, thanks to the collagenous structures holding the muscle fibers together and resisting stretch even when the muscle is relaxed [RJ and Kirsch, 2004], muscles can still produce passive forces while exhibiting little EMG activity. Secondly, substantial EMG signals are observed for TA whereas the synthesized control inputs are negligible.

4.3 Conclusion

In this chapter, we study how our synthesis method can generate two different squat strategies and new movement patterns due to modifications in high-level task priorities and in skeletal system respectively. In the synthesis of Asian squat, the effect of ankle dorsiflexion flexibility on the ability of performing Asian squat is demonstrated in terms of joint kinematics and muscle forces. With our simulations, higher ankle range of motion is proven to be an essential factor, allowing the Asian squat to be successfully executed. The obtained results are coherent with the findings in [Mulholland and Wyss, 2001, Bridger, 1991, Kasuyama et al., 2009, Brazil and Peña,]. As the formulation and the parameters of the controller remain unchanged, the generation of Caucasian squat is entirely due to the limitation of ankle rotation.

Regarding the synthesis of two different squat strategies, despite the low complexity of the human models, the obtained results demonstrated a certain level of coherence with the captured data. Furthermore, with

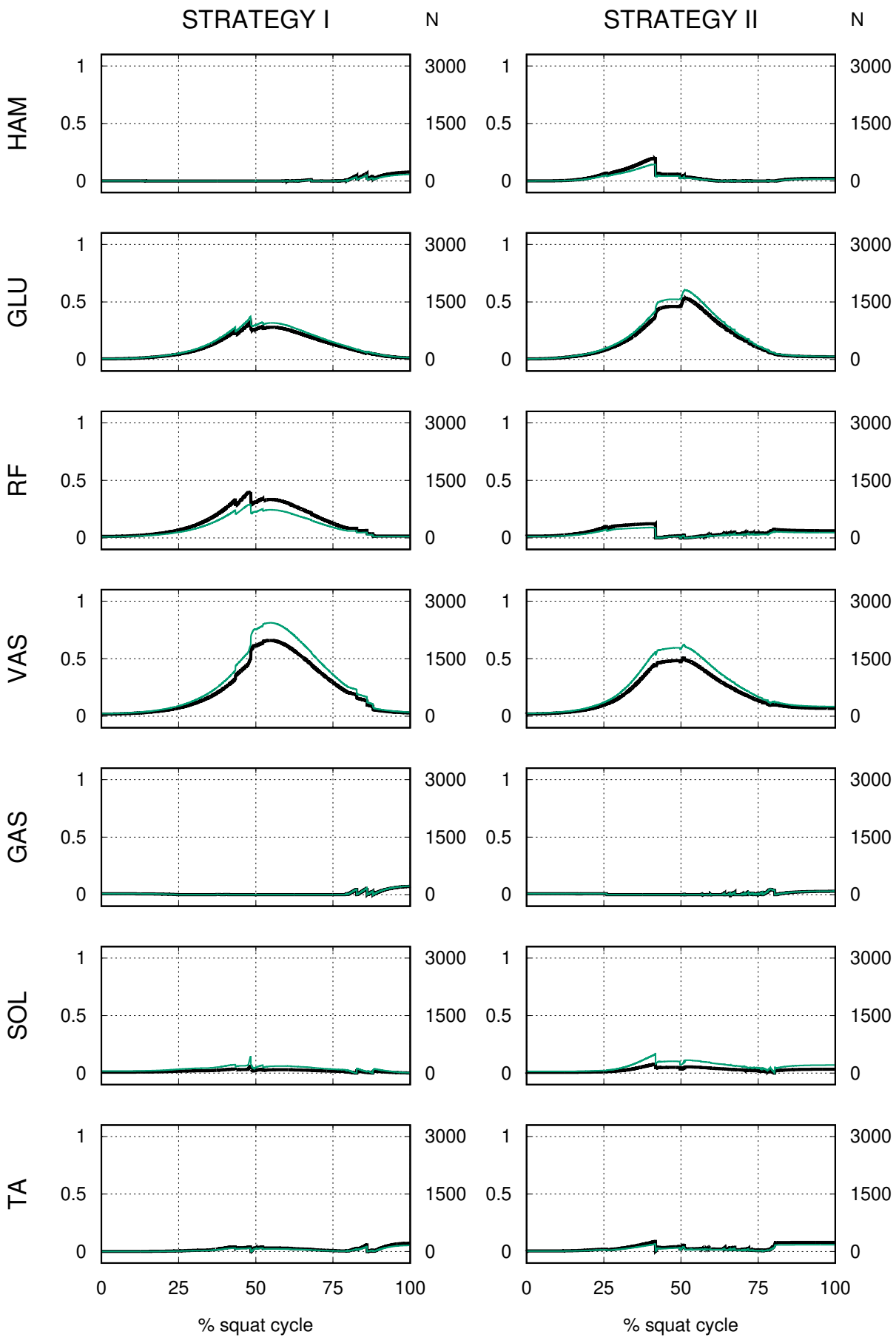

Figure 4.8: Synthesized muscle activations (black) and forces (green) during a squat cycle.

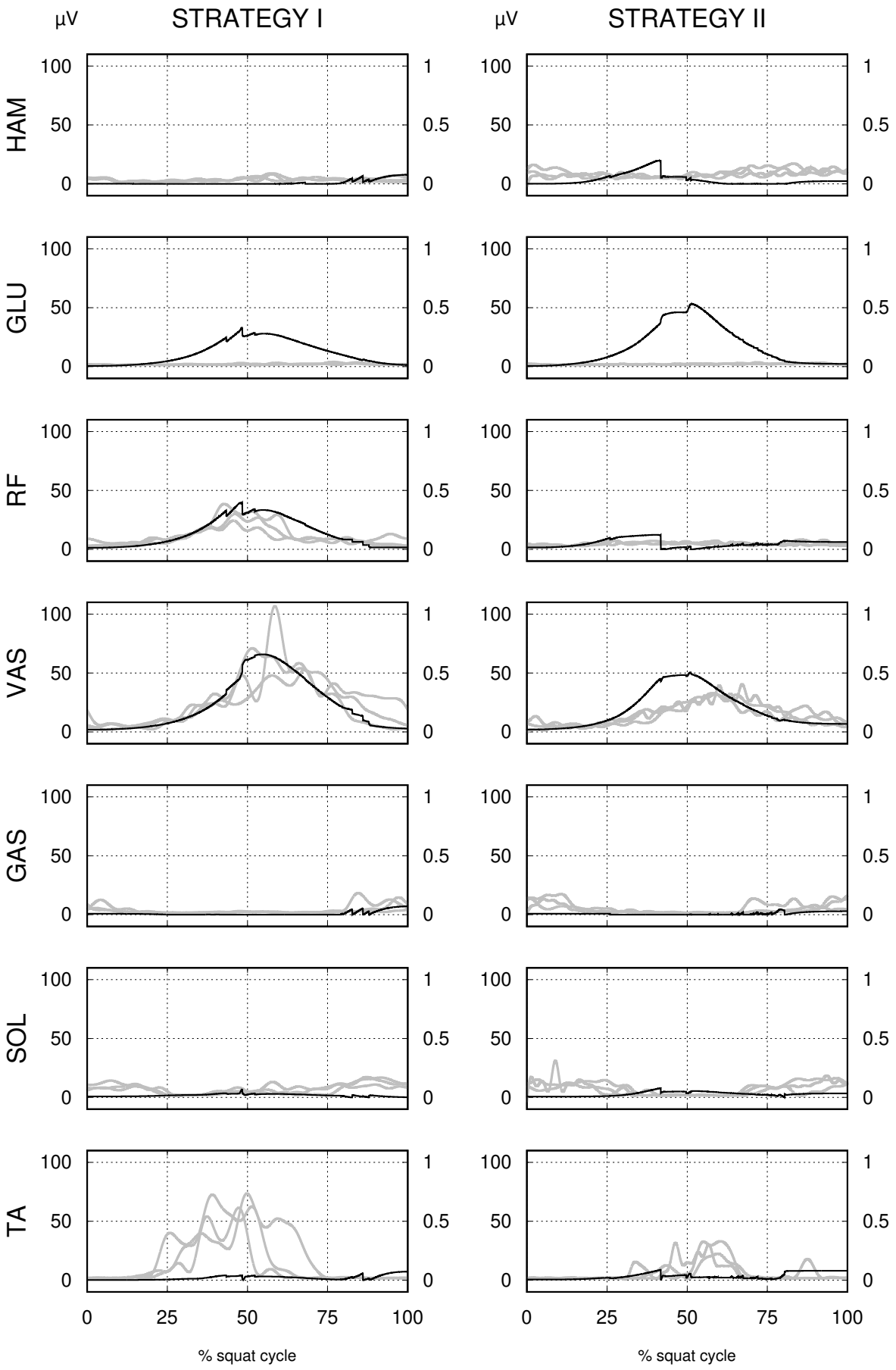

Figure 4.9: Synthesized muscle activations (black) and EMG signals (gray) in during a squat cycle.

the low number of tasks, we were able to observe the influence of the tasks on the movement and identify the variation of angular momentum as a potential factor influencing the squat movement. Therefore, we believe that the proposed synthesis scheme offers a potential framework of synthesizing motions of muscle-actuated systems. However, the manual tuning is the weak point of the method, especially in case other types of movement or altered human models are considered as each type of movement requires its own practical rules of weight tuning. Also, it's not certain that the tuned weighting factors for healthy movement of a model would predict the movement of the same model being altered.

Perspectives are open for the application of our synthesis approach. As the computational time is relatively small ($<$ 2 minutes), the synthesis can be used to provide initial guesses for a global optimization problem to facilitate the convergence of optimal solutions.

Chapter 5

Simulation of The Effect of Different Rectus Femoris Transfer Sites on Muscle Recruitment During Knee Extension

Stiff knee gait is one of the most common gait abnormalities in children with cerebral palsy [Reinbolt et al., 2009]. On of the common causes of this gait pathology is rectus femoris overactivity which reduces the knee flexion function and delays knee swing during gait. Rectus femoris (RF) transfer is a common treatment for stiff knee gait. The procedure consists in releasing the RF from the patella and transferring it to one of the four sites: sartorius, semitendinosus, gracilis and iliotibial bands (Fig. 5.1 [Delp et al., 1994]. In the literature, studies on the implication of attachment sites on the improvement of knee flexion have been conducted. Through gait analysis a [Chung et al., 1997] concludes that between gracilis and sartorius, no significant differences in terms of gait kinematics and energy consumptions. In the mean time, as the main purpose of the operation is to improve knee flexion during the swing phase in the gait cycle, semitendinosus is the preferred site as the knee flexion moment arm of RF is the greatest [Delp et al., 1994]. Similar findings are made through gait analysis by [Ounpuu et al., 1993] for all the four transfer sites, concluding no statistically significant differences in the effect on knee range of motion at initial contact and in mid stance and maintained knee flexion in swing. In practice, the choice of RF transfer site can be dictated by the surgeon's preferences or by the nature of other simultaneous procedures, such as hamstring lengthening [Ounpuu et al., 1993]. RF transfer to the gracilis is the popular choice, while transferring the RF muscle to the semitendinosus, while resulting larger peak knee flexion moment arm than other potential transfer sites, can disturb the sagittal balance of the pelvis [Khouri and Desailly, 2013]. Lateral transfer to the IT Band is much less common than other medial transfers due to lack of knee flexion moment [Khouri and Desailly, 2013].

Despite the different impacts exhibited by the attachment sites, it is no doubt that RF improves the knee flexion [Khouri and Desailly, 2013]. However, there is concerns regarding whether the knee extension is impacted negatively by the knee flexion treatment. Specifically, the transfer of RF reduces its knee extension effect [Asakawa et al., 2002], thereby limits the torque generated at the knee by the quadriceps. The weakening of quadriceps during activities requiring knee extension can lead to difficulties or even impairment of movements, such as crouch gait. For this reason, we propose to investigate the potential iatrogenic impact of RF transfer on knee extension function using our movement synthesis tool. To achieve this goal, our approach is to analyse the muscle moment arms and activities resulting from the choice of attachment sites during squat, a movement that requires quadriceps strength for knee extension during the ascent phase. We start by performing RF transfer procedure virtually on a musculoskeletal model. Next, the method developed in Chapter 3 is applied to synthesize squat on the model. Computed muscle moment arms, activities and energy expenditures during squat are studied to evaluate

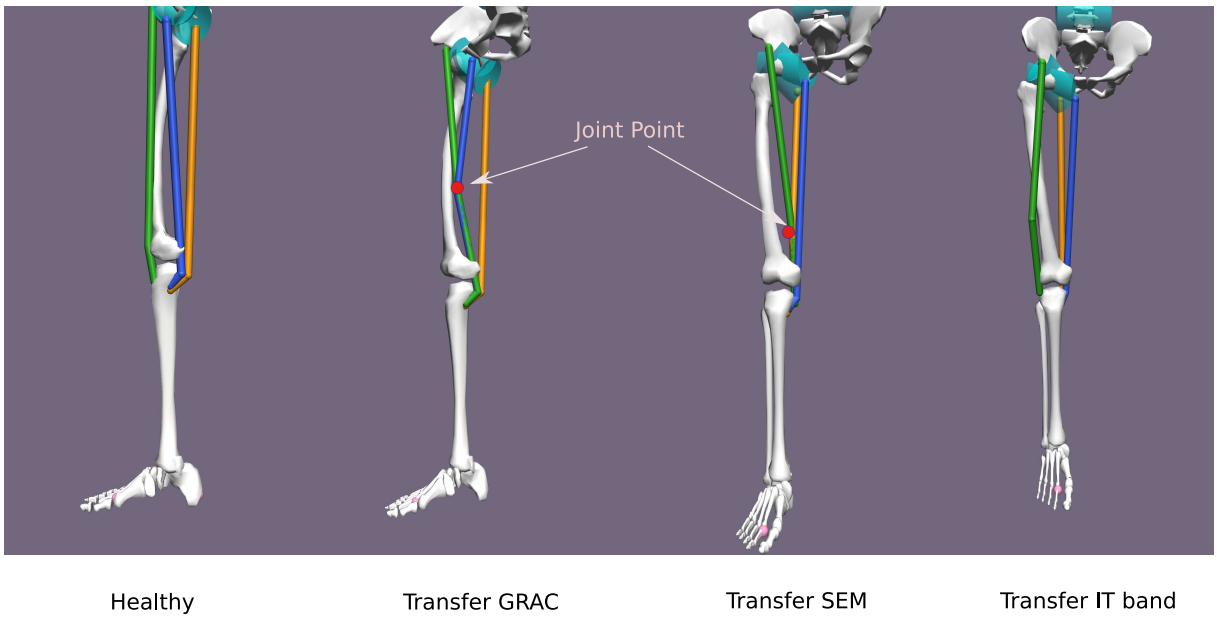

Figure 5.1: The altered models where the rectus femoris (RF) is transferred to one of three sites (target muscles): the semitendinosus (SEM), the gracilis (GRAC) or the iliotibial band (IT Band). The color of the muscle is: red for GRAC, orange for SEM and green for RF. The transfer is performed by joining the muscle paths of RF and the target muscle at the joint point. This is the point representing the actual attachment site of the anatomical insertion. From this point to the insertion point into the tibia, RF and the target muscle share the same path.

- the effect of RF overactivity on squat movement
- the effect of different attachment points of RF transfer on RF moment arms
- the effect of different attachment points of RF transfer on muscle activities

5.1 Method

Among multiple factors influencing the outcome of the procedure, there are two in which we are interested that have major contribution: the level of RF overactivity and the RF attachment point. Our goal is to study the evolution of muscle activities due to the variation of these factors through physics-based simulation. To perform virtually RF transfer, we use the model created in Section 3.4 and change the minimal activation of RF from 0 to 0.15 and 0.3 to represent the basal overactivity. Then, for each level of basal overactivity, we perform RF transfer to three different sites: gracilis, semitendinosus and iliotibial band. The muscle activities are assessed during a squat movement with the depth of 90°, synthesized by our controller introduced in Chapter 3.

5.1.1 Computational Modeling of RF Transfer

In this sections, we detail the computational modeling of the RF transfer procedure. As described in Section 3, the muscle model is a linear relationship between the control input and the output force. A "healthy" muscle has the range of input control from 0 to 1. To represent the basal activity of a muscle, the lower boundary of the control input is increased. Despite the fact that this minimal activation value does not correspond to the real physical phenomenon, it still grants us an approximate representation of the muscle overactivity.

In a RF transfer procedure, the distal end of the muscle is released from its insertion point at the patella and sutured to a new attachment site, resulting in a permanent change in the length of the muscle-tendon

unit [Lieber and Fridén, 2019]. These transfer options are performed virtually on our musculoskeletal model, as shown in Fig. 5.1. Note that we cannot attach the RF distal end to one of the aforementioned muscles as in a real surgery since there is no available function in OpenSim 4.0 offering this feature. Instead, we create a via point (cf. Chapter 2) on the target muscle at which its muscle path joins with the RF's path. The distal end of RF is then attached to same insertion point into the tibia as the target muscle.

5.1.2 Results

Effect of RF Transfer on RF's Moment Arm

The function of rectus femoris (RF) w.r.t a joint can be identified by its moment arm value w.r.t the joint axis. Before analyzing RF function, it is important to note the convention of moment arm presented in this work. As shown in Fig. 5.2a, the moment arm is positive when RF is a flexor of the considered joint, and negative when RF is a extensor. The evolution of RF moment arms in terms of hip and knee angles for each attachment point is shown in Fig. 5.2b. In general, the moment arm of RF w.r.t the knee are altered substantially after the intervention after the transfer surgery. Before the procedure, RF is a knee extensor, with negative values of moment arm. In case of the transfers to semitendinosus and gracilis, the RF's moment arm is positive throughout the squat cycle, indicating that RF becomes a knee flexor. If the attachment point is located on IT band, RF remains as a knee extensor until the squat depth reaches 80°, then acts as a knee flexor.

If RF is a knee flexor over the complete range of motion of the knee, the moment arm amplitude increases with the flexion. On the contrary, the pattern is reversed if RF is a knee extensor, with the moment arm reducing substantially at high knee flexion. IT band is a particular case, where the moment arm is zero at mid range, and increases towards knee extension and extreme flexion. Among the three attachment sites, semitendinosus gives the biggest moment arm, followed by gracilis. IT band does not offer neither high flexion or high extension moment arm.

Concerning the moment arms of RF w.r.t the hip, no alteration of function is observed; RF remains as a hip flexor. Slight variations of moment arms between the different attachments are exhibited. At terminal extension of the hip, the moment arm is greatest before transfer procedure, whereas attaching RF to semitendinosus gives the maximal moment arm at high flexion angle.

Effect of RF Overactivity and RF Transfer on Distribution of Muscle Forces

To study the impact of RF overactivity and attachment sites on muscle functions, we introduce the total forces of multiple muscles to demonstrate the variations in muscle activities induced by these factors. The total force is calculated as the total accumulation of muscle force at each step time of the simulation.

$$F_{tot} = \sum_{i=1}^{N} f_i \tag{5.1}$$

The presented muscles are the most sensitive to the introduction and variation of the level of RF basal overactivity. As a side note, in the following sections,

- we use the term "normal total force" to indicate the total force measured in the simulation with the model representing a healthy person manifesting no RF overactivity.
- to indicate the level of RF overactivity, we use the relative level to the maximal control input in percentage: 15 and 30 for the basal activity of 0.15 and 30 respectively.

In terms of total muscle forces during the squat (Fig. 5.3), knee extensors (recfem, vasint, vaslat, vasmed) exhibit highest total forces regardless of the RF overactivity level and the attachment sites. They are

followed by the total forces of semimembranosus (semimem) and biceps femoris long head (bflh). Before RF transfer, the forces produced by the quadriceps (knee extensors) decrease with the augmentation of the RF overactivity level. After RF transfer, the knee extensors increase the activity with the RF level of overactivity. The highest total forces achieved by the quadriceps occur after the RF transfer to semitendinosus, followed closely by the ones associated to the attachment sites gracilis. Attaching RF to IT band also provokes more activity in knee extensors, but less than the other two attachment sites.

The variations of total forces of other groups of muscles are better visualized through their relative variations with their normal forces, as shown in Fig. 5.4. RF basal overactivity provokes substantial increases of activity in knee flexors (bflh, bfsh, gasmed, gaslat, grac, sart, semimem, semiten). The hamstring forces skyrocket, with biceps femoris short head (bfsh) exhibiting highest relative augmentation, more than 80 times its normal total force, followed by semimembranosus (semimem) with more than 60 times the normal force and semitendinosus (semiten) with 50 times the normal force. Other groups of muscles such as ankle dorsi flexors (edl, ehl, tibant), hip extensors (bflh, semimem, semiten) and hip flexors (iliacus, psoas) also see their activities increased tremendously, from at least more than 2.4 times (iliacus). In addition, their total force variations also double with the rise of RF overactivity. Meanwhile, the activities of the quadriceps, except the rectus femoris (recfem), decrease to around 80% and 70% of their normal force in case of RF overactivity level at 15% and 30% respectively.

After transferring RF to gracilis or semitendinosus, the total forces, hence the activities, of all muscle groups drop dramatically, except the quadriceps with rising total forces. Multiple muscles are completely inhibited such as biceps femoris short head (bfsh), sartorius (sart) and psoas. Gastrocnemius muscles also exhibits little activities (less than 10% of their normal forces) with RF at 15% overactivity, and completely relaxed with RF at 30% overactivity. Gracilis produces no force if RF is attached to it, and less than 50% of its normal force in case of RF transferred to semitendinosus (semiten). Quadriceps augment their total forces around 1.5 time and 2 times with RF overactivity at 15% and 30%.

In case of choosing IT band as the transfer site, the total forces of knee extensors do not change substantially, between 1.1 to 1.3 times their normal forces, but still increase with RF overactivity level. The rest of the presented muscles see their total forces rising substantially. The hamstrings still demonstrate highest relative variation with their normal forces, with semimembranosus reaching 33 times of their total normal forces, followed by semitendinosus (24 times of the normal forces) when RF is at 30% of its capacity.

Regardless of RF overactivity level, these general trends of total forces in terms of attachment sites remain the same. The relative evolution of the total forces with respect to the normal total forces, with RF at 15% of its capacity, is shown in Fig. 5.5.

5.1.3 Discussions

The overactivity of RF influences all groups of muscles, from hip flexors and extensors, to knee flexors and extensors and finally ankle dorsi flexors and plantar flexors. Before RF transfer, RF provokes the reduction of other quadriceps' forces, as RF contribution to knee extension torque increases. Meanwhile, the antagonist muscles of RF, e.g. knee flexors, have their activities increased substantially. As some of these knee flexors are bi-articular muscles, responsible for hip extension (hamstrings) and ankle plantar flexor (gastrocnemius), they induce the augmentation of muscle forces in hip flexors (iliacus, psoas) and ankle dorsi flexor (edl, ehl, tibant). In the end, the amplitudes of co-contractions at all lower limb joints rise, hence the stiffness of the model. After the procedure, if RF is attached to semitendinosus or gracilis, it becomes knee flexor for the entire range of motion of the knee. With the same principles mentioned earlier related to co-contraction of agonist-antagonist muscles, the RF overactivity leads to diminution of force in other knee flexors, and considerable augmentation of force in knee extensors. In addition, the increase in RF overactivity accentuates these tendencies.

Besides the level of RF overactivity, the moment arm of RF also has a direct consequence on the activities of other muscles. Increases in RF's moment are accompanied with higher knee flexion, or knee extension, depending on the chose attachment site for the procedure. The alteration of RF function concurs with

the original intention of the procedure of converting the muscle from a knee extensor to a knee flexor [Perry, 1987] and the anatomical studies in [Delp et al., 1994]. In parallel, the dependence between the moment arm amplitude and the attachment point observed in our results is in in agreement with the information provided in [Khouri and Desailly, 2013], with semitendinosus providing the highest moment arm, IT band offering limited moment arm. Therefore, attaching RF to gracilis or semitendinosus leads the quadriceps' forces surge, while almost no clear distinction is noted with the normal force in case of transferring RF to IT band. It is interesting to note that the patterns of relative variations of total muscle forces with the normal ones observed between two transfer sites gracilis and semitendinosus are highly similar, as a result of the small difference of moment arms. In parallel, after being IT band, the RF remains knee extensor most of the squat cycle (until the knee angle reaches 80°). This leads to the resemblance in the variations in total muscle forces before and after RF transfer to this attachment point.

5.2 Conclusions

In this chapter, we have demonstrated the implication of RF overactivity level on the muscle patterns during a squat cycle, with the reduction of muscle forces of other knee extensors, and the increase of muscle forces in other muscle groups. The RF transfer modifies its moment arm, leading to the alterations of force amplitude in multiple muscles. The vasti muscles (the other knee extensors), while being moderately solicited before the procedure and after attaching RF to IT band, are highly loaded if semitendinosus and gracilis are chosen as transfer site. Therefore, we believe that with higher level of RF overactivity, the knee extensors would be overloaded and knee extension would be impacted negatively for these two transfer sites. On the other hand, transferring RF to IT band encourages co-contraction at all lower-limb joints and RF energy is transferred to other muscle groups. However, this can potentially generates more joint forces.

Regarding the method, we are able to extract valuable information through our results with squat synthesis that highlight improvement in knee flexion due to reduced knee extension capacity of RF. However, our method relies on the assumption that the performer can execute the simulated squat movement regardless of the treatment and the severity of the impairment. In the future, more complex muscle models can be incorporated to better representing RF overactivity, as well as other similar impairments causing stiff knee gait, such as RF contracture. A study on muscle energy expenditure can also help to evaluate the effectiveness of the treatment.

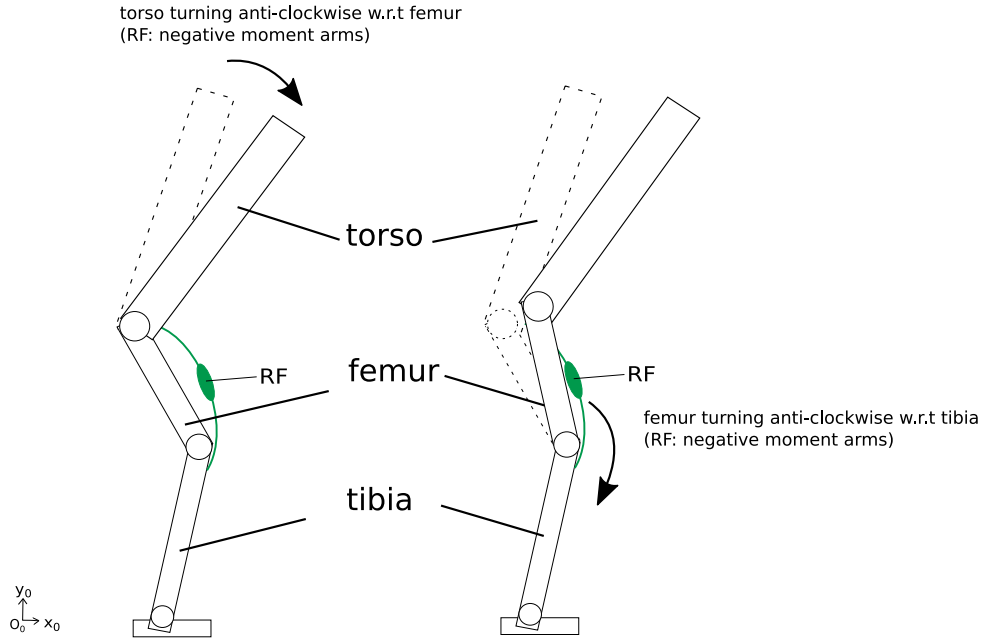

(a) The sign convention of the moment arm of rectus femoris (RF). As a hip flexor and knee extensor, RF contraction induces the rotation of the torso towards and the rotation of the femur towards the tibia. The rotations are in the anti-clockwise direction and associated with the negative sign. The joint torques generating these rotations are therefore negative. Since a joint torque is the product of a muscle force (always positive) and a muscle moment arm, the moment arm of RF is negative in these cases. If RF is converted to knee flexor, its contraction leads to the clockwise rotation of the femur and the torso. As a result, the moment w.r.t the knee is positive.

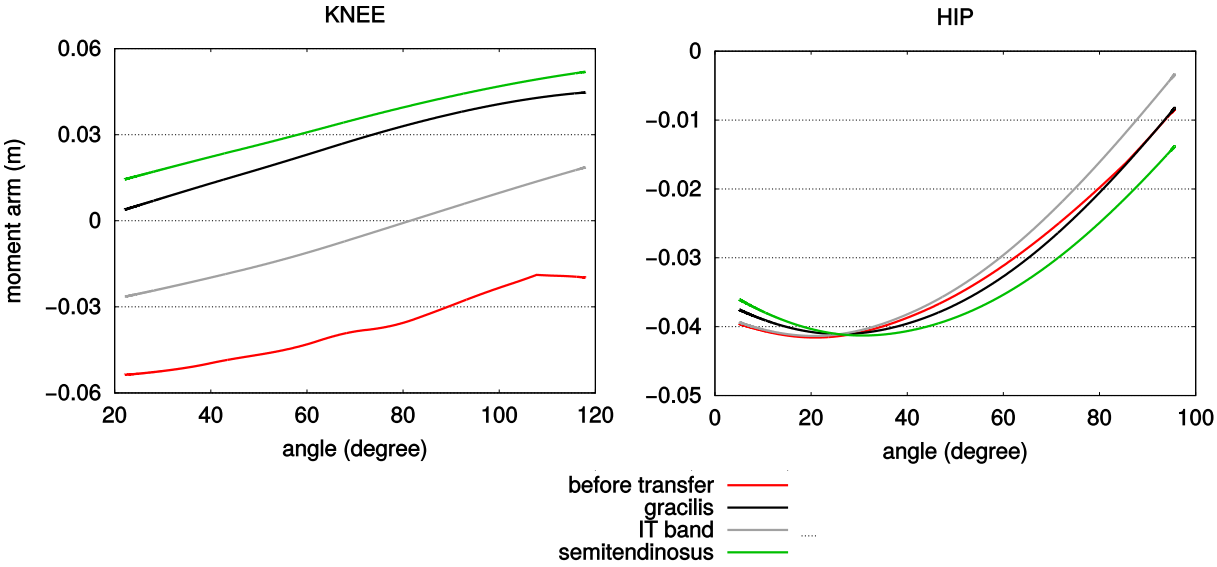

(b) The moment arm of rectus femoris (RF) depends on the attachment site.

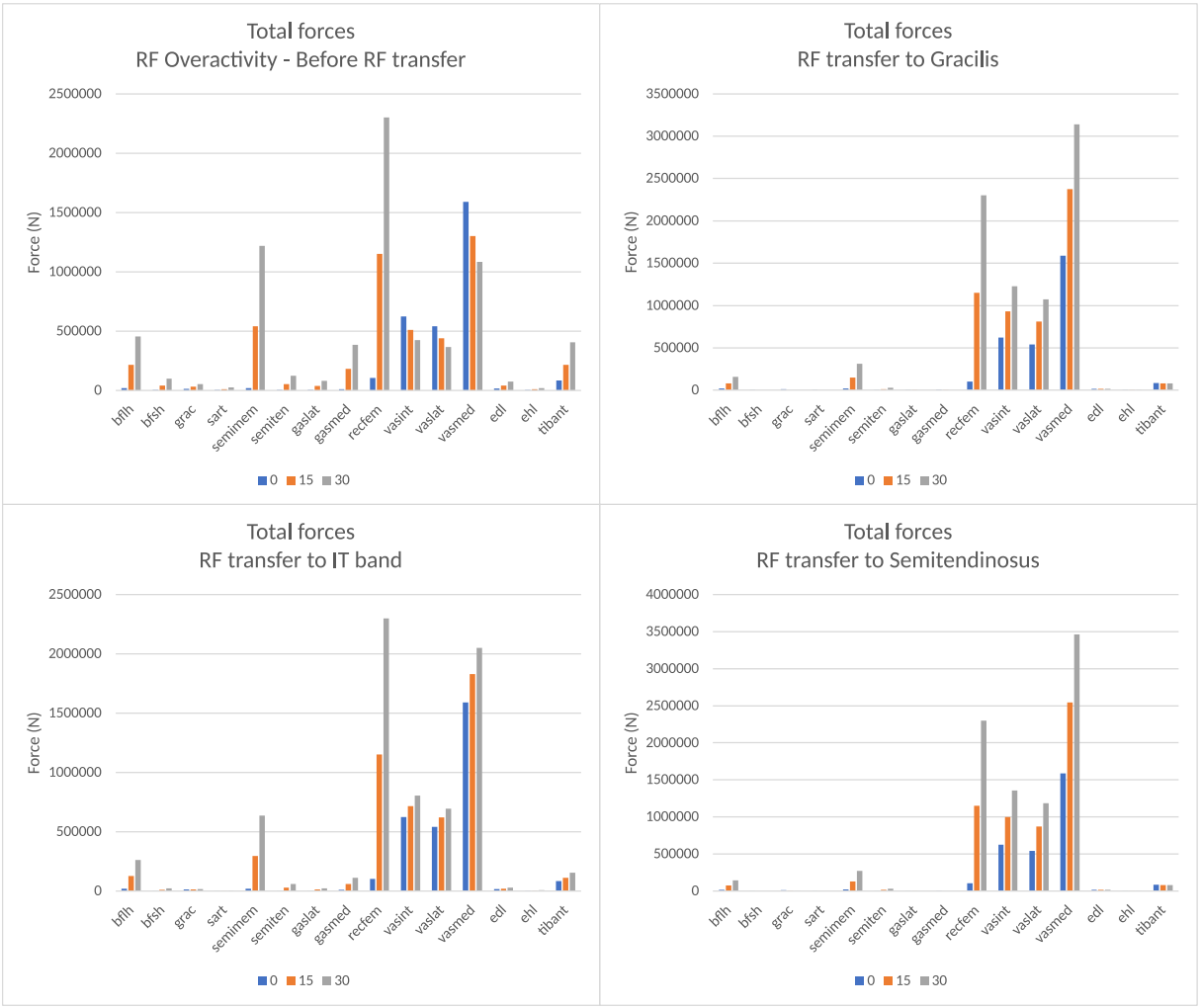

Figure 5.3: The total forces (sum of muscle forces at every simulation step time).

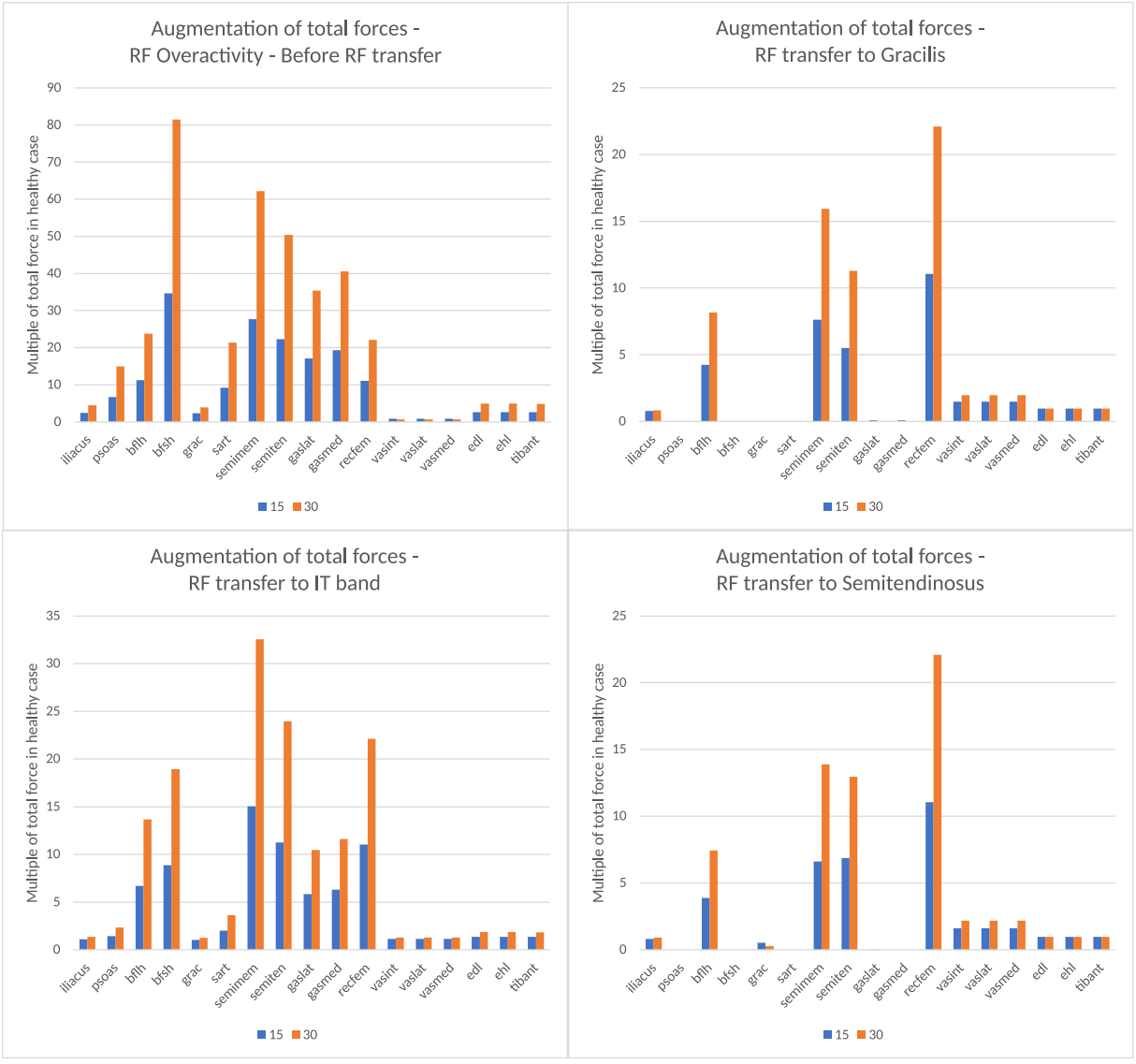

Figure 5.4: The relative variation of total muscle forces with the normal total forces.

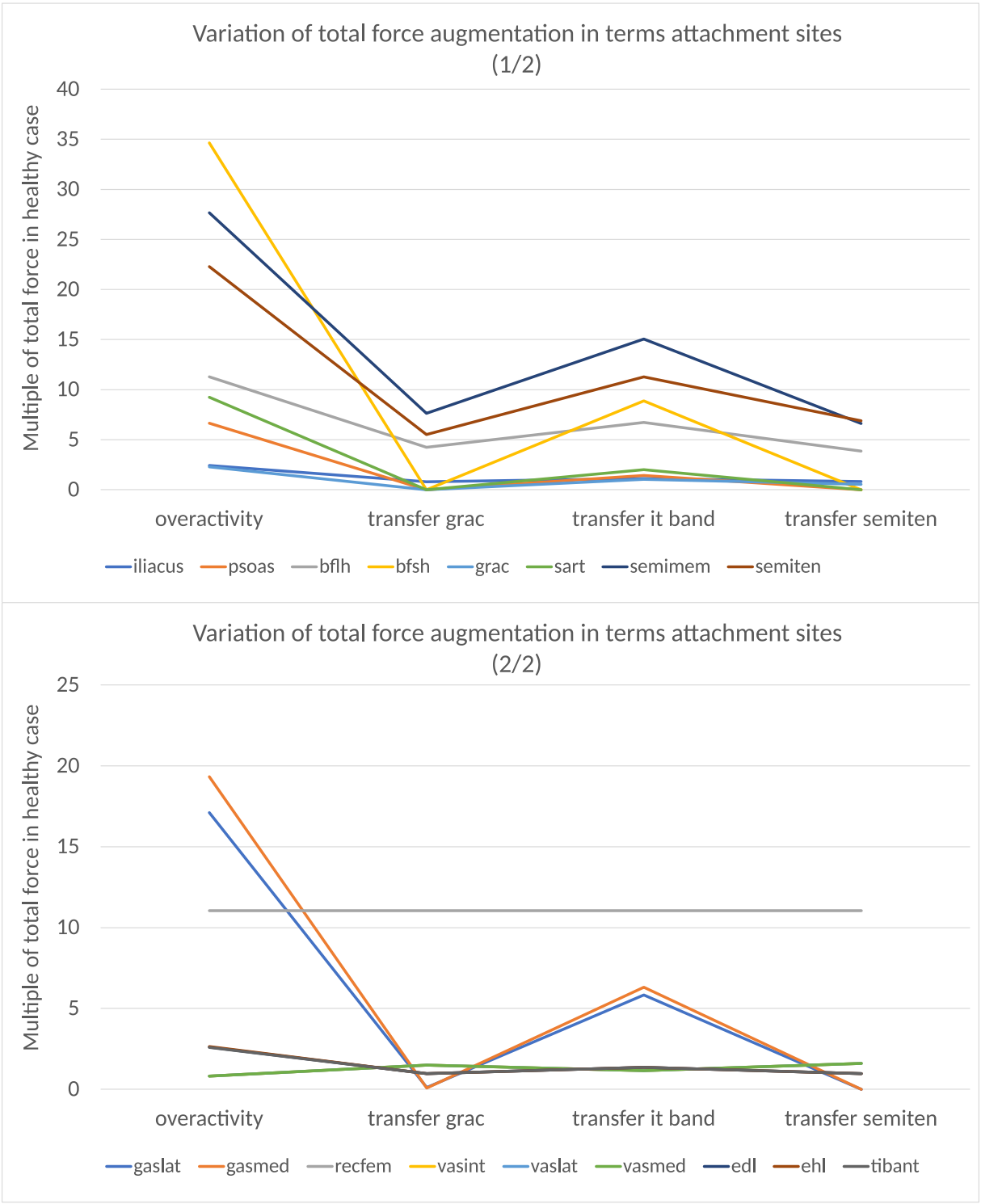

Figure 5.5: The variation of total muscle forces relatively to the normal total forces with rectus femoris overactivity at 15% of muscle capacity.

Chapter 6

Prediction of Muscle Activities After Femur Osteotomy and Patellar Tendon Advancement

Crouch gait, or excessive knee flexion during stance, phase is considered to be one of the most common pathological gait patterns among CP patients, especially children and adolescents [O'Sullivan et al., 2020, Novacheck et al., 2009]. The typical causes of crouch gait include hamstring and/or psoas tightness, insufficient quadriceps contracture or lever-arm dysfunction [Novacheck et al., 2009]. The combination of patellar tendon advancement (PTA) and distal femoral extension osteotomy (DFEO) is believed to address both fixed knee-flexion contractures and quadriceps insufficiency [Novacheck et al., 2009]. The extension osteotomy of the distal part of the femur seek to "compensate for the knee flexion contracture by creating an extension deformity of the distal part of the femur" [Novacheck et al., 2009]. The PTA has the purpose of achieving optimal patellar position in the trochlea to improve the quadriceps lever-arm, hence their function [Desailly et al., 2017]. Currently, as there is no consensus on the appropriate degree of correction, the decision is taken based on radiographic patellar height [Desailly et al., 2017].

Despite targeting multiple major causes of crouch gait, few studies exist regarding the effectiveness of the combination of PTA and distal femoral extension osteotomy. In the literature, computational musculoskeletal models have been used to study the effects of bone deformities and surgical interventions on muscle behaviour [Mehta et al., 2017]. For example, [Arnold et al., 2001] and [Arnold and Delp, 2001] demonstrate that a generic graphic-based musculoskeletal model of lower extremity can be used to determine muscle lengths and moment arms in crouch gait. The geometry of the femur of the model is automatically scaled using magnetic resonance (MR) images to represent the deformed femur of CP patients. [Lenhart et al., 2017b] uses a musculoskeletal model to perform virtually DFEO. In the model, the tibiofemoral and patellofemoral joints are represented by a 6-DoF joint incorporating the effects of contact and ligamentous constraints. The sensitivity of femur, quadriceps, and hamstring lengths to DFEO factors such as wedge location and magnitude (cf. 6.1.1) are determined. [Lenhart et al., 2017a] studies the influence of patellar position on patellar tendon and quadriceps forces during walking in normal and crouch gait patterns. [Bittmann et al., 2018] investigates the relationships between patellar position, knee flexion, and the patellar tendon moment arm in children treated with the DFEO and PTA procedures. Despite providing useful information, these previous works do not investigate the contribution of the combination of DFEO + PTA on muscle activities during a dynamic movement. In fact, the moment arms of quadriceps, thereby their produced forces, are strongly influenced by the combined parameters from both procedures. These parameters include the translation, the angle and the location of the wedge as well as the patellar position. Therefore, a detailed analysis of the muscle moment arms, which considers variations of these above-mentioned parameters, is needed to improve the planning of DFEO + PTA.

We believe that our method of squat synthesis with musculoskeletal models can be used to predict the

muscle behavior after these surgical procedures for crouch gait treatment, as knee extension function is highly implicated in this movement. To this aim, we synthesize the effects of DFEO + PAT on the muscular capacity of generating torque during a half squat. As a first step towards this goal, we build a musculoskeletal model with which DFEO and PTA are virtually performed. Then our controller developed at chapter 3 is applied to compute muscle moment arms and activities, especially those of the quadriceps during a squat cycle. We analyze the results to evaluate the impact of different patellar positions on muscle behavior and extract relevant information for decision-making and planning of DFEO + PTA.

6.1 Computational Modeling

The DFEO and PAT procedures are detailed by [Novacheck et al., 2009]. To assess the effectiveness of these procedures, we analyze the muscle activities and moment arms during a squat cycle of three models representing a healthy person and a CP patient manifesting crouch gait before and after surgery. In the following subsections, we detail the fundamental steps of these procedures. The DFEO is then virtually performed with our musculoskeletal model. The generation of patella trajectories during a squat cycle created as a result of PAT is also described.

6.1.1 Distal Femoral Extension Osteotomy (DFEO)

A DFEO consists in removing an anterior femoral wedge or trapezoid, of the same angle than the knee flexion contracture to straighten the knee, as shown in Fig. 6.1. The distal osteotomy for the wedge is perpendicular to the tibial shaft, and the proximal cut is perpendicular to the femoral shaft [Novacheck et al., 2009, Desailly et al., 2015]. If the apex (the intersection of the two cuts) is at the posterior surface of the femur location, a wedge is removed. If the apex is further behind the femur, a cuneiform wedge (trapezoid) is removed [Lenhart et al., 2017a]. After removing the wedge, the distal fragment of the femur, together with the rest of the leg, is rotated about the wedge apex and slid along the proximal cut plane to assure the alignment of the lower limb structure [Novacheck et al., 2009].

These surgical act is virtually performed on our musculoskeletal model representing a CP patient suffering crouch gait, as shown in Fig. 6.2. We used the model created in Section 3.4 to represent a healthy individual. From this model, we create a new model to represent a CP patient with knee flexion contracture. To do this, we change the knee range of motion by increasing the lower boundary of the knee joint coordinate to 30°. The DFEO procedure is performed on the new model. An anterior wedge of bone close to the distal end of the femur is removed, separating the femur into a proximal fragment (connected to the pelvis) and a distal fragment (connected to the tibia). The angle at the wedge apex is equal to the knee flexion contracture, which is 30°. Next, the distal femoral fragment is rotated about the wedge apex to close the wedge, and finally translated relatively to the proximal femoral fragment, as described above. As a result, we create a third model representing the CP patient after DFEO. The resulting length and the moment arm w.r.t the knee joint of several muscles are modified due to the osteotomy. Note that the knee joint is still affected by the knee flexion contracture, meaning the range of motion of the tibia w.r.t the distal fragment of the femur remains unchanged.

6.1.2 Patellar Tendon Advancement (PTA)

After compensating knee flexion contracture with DFEO, PTA is often performed to increase the moment arm of knee extensors, allowing greater torque generated by these muscles, especially in case of quadriceps insufficiency [Lenhart et al., 2017b]. The procedure modifies the patellar tendon insertion such that the patella is lowered towards the tibia [Novacheck et al., 2009]. The patellar tendon length is varied with the aim to optimize its moment arm w.r.t the knee in order to improve knee extension during gait.

The patellar position is characterized by the Insall-Salvati ratio (ISR) [Insall and Salvati, 1971], which is

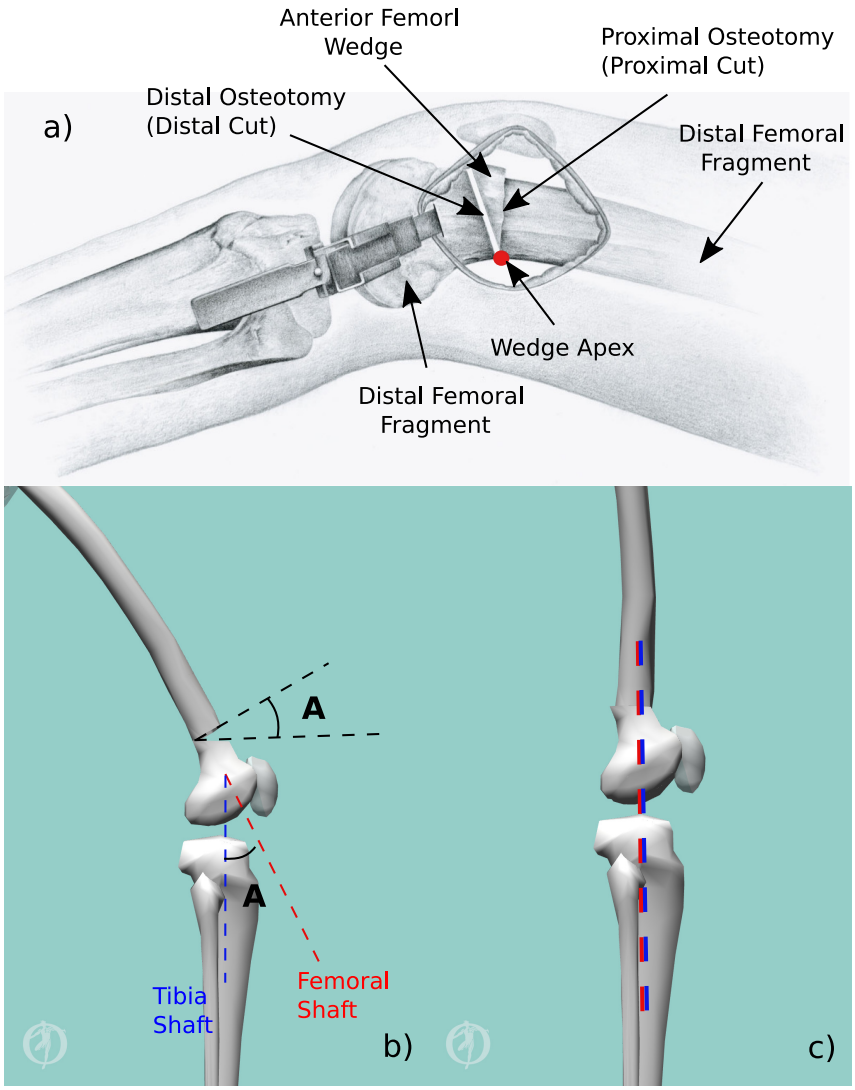

Figure 6.1: Illustration of Distal Femoral Extension Osteotomy (DFEO). a) The distal osteotomy is parallel to the chisel, and the proximal osteotomy is perpendicular to the femoral shaft. Image taken from [Novacheck et al., 2009]. b) The angle ***A*** *of the wedge to be removed is equal to the angle of the knee flexion contracture. c) After DFEO, the femur and the tibia are aligned.*

calculated as

$$ISR = LT/LP \tag{6.1}$$

where LT is the length of tendon, measured from its origin on the lower pole of the patella to its insertion into the tibia, and LP is the greatest diagonal length of the patella [Insall and Salvati, 1971]. The patellar position is considered

- alta (high) if $ISR > 1.2$
- normal if $0.8 \leq ISR \leq 1.2$
- baja (low) if $ISR < 0.8$

These positions are illustrated in Fig. 6.3.

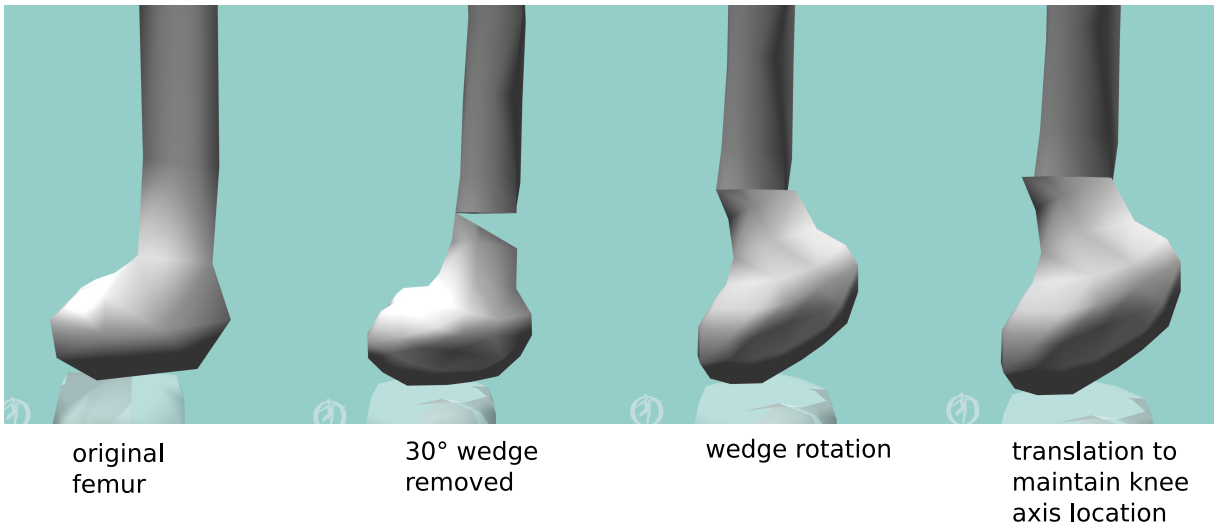

Figure 6.2: Illustration of a 30° distal femoral extension osteotomy (DFEO) procedure. A 30° wedge is removed from the femur. Then, the wedge is rotated to close the wedge. Finally the distal femoral fragment is translated, such that the knee flexion extension axis remains in the same anterior-posterior location.

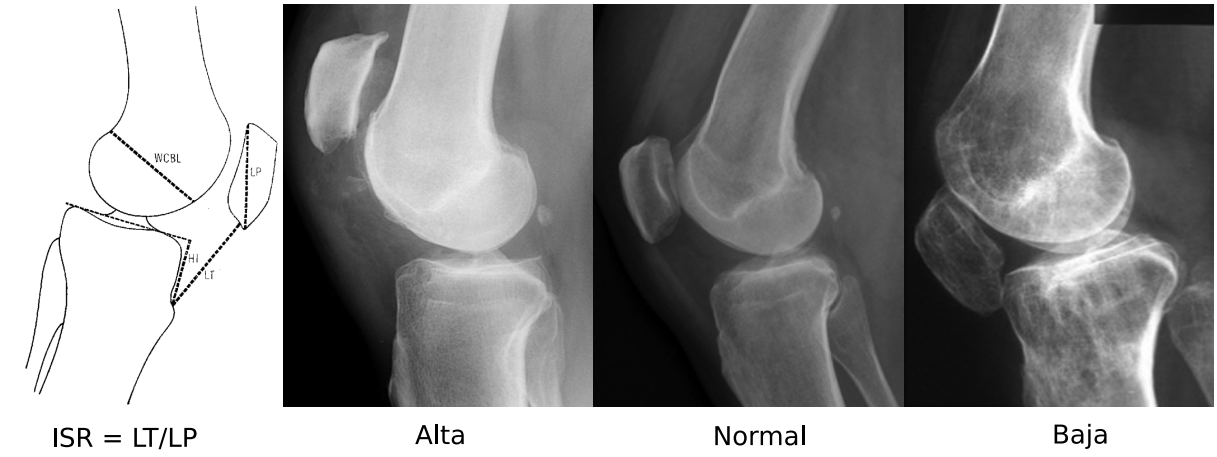

Figure 6.3: The patellar position is characterized by by the IS ratio (ISR). The diagram is taken from [Insall and Salvati, 1971] and the radiographic images from [Gaillard et al., 2019].

Modeling Patellofemoral Joint - Generation of Patella Trajectories After PTA By Optimization

Patellofemoral is a unique joint, created by the patella (kneecap bone) and the femoral condyles of the femur (two large bony prominences located at the end of the long bone of the upper thigh). These two bony prominences create a central concave 'V' shaped groove (known as the trochlea) which perfectly fits the back of the patella, which has a reciprocally convex shape. By following the articulation of the patellofemoral, we obtain a trajectory of the patella, including the its position and orientation. The surface of the trochlea and the patella are not represented in the musculoskeletal model that we use. Instead, to model the patellofemoral joint, the above mentioned trajectory of the patella is constructed in [Rajagopal et al., 2016], and the knee rotation is accompanied by the patella movement on the trajectory.

To simulate the effect of PTA on the knee extensor mechanism, we start by generating the patellar trajectories during knee flexion for different patellar tendon lengths. As stated in [Insall and Salvati, 1971], "because the ligamentum patellae is not elastic, its length determines the position of the patella, provided that the point of insertion into the tibia is constant". In our study, instead of computing the patella position from the patellar tendon directly, we compute the insertion point position of the patellar tendon into the patella (P2) first, then the patella position in terms of P2's position and the orientation of the

patella (Fig. 6.4). Note that the patellar ligament is not modeled directly. Instead, the quadriceps lines of action insert onto the patella at P1, wrap over the patella until P2 and insert onto the tibia at P3. For the rest of this chapter, we indicate the patellar tendon as the section P1-P2 of the quadriceps lines.

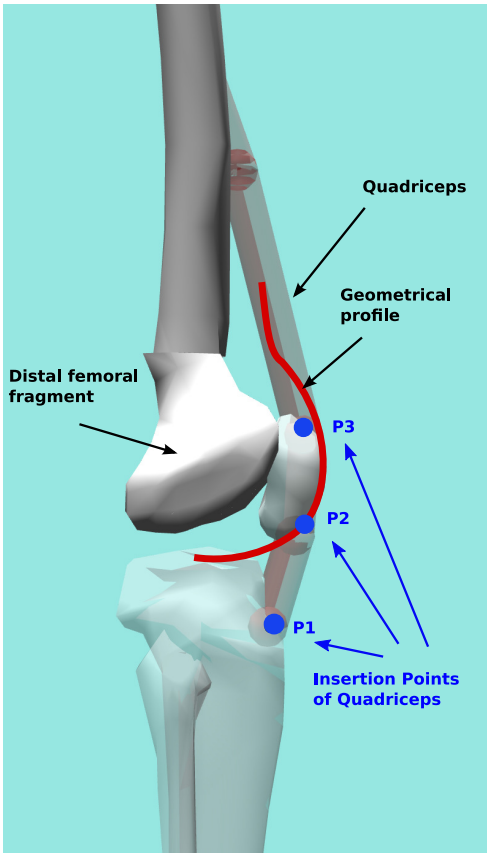

Figure 6.4: The patellar tendon is not modeled. Instead, the quadriceps wrap around the patella through P2 and P3 then insert onto the tibia at P1. The patellar tendon length (LT in Eq. 6.1)is represented by the length of the section P1-P2.

To generate the trajectories of P2 and the patella orientations in the sagittal plane, we start by creating a geometrical profile on which P2 is translated. This profile is based partially from the trajectories of patella positions and orientations created by [Rajagopal et al., 2016] for a healthy individual. It is a second order polynomial line as a function of the coordinates of P2 in the local frame of the distal femoral fragment.

The next step is to determine the position of P2 for a knee angle value. To do this, we formulate an optimization problem in which the coordinates of P2 in the local frame the distal femoral fragment (x^{P2}, y^{P2}) are the optimization variables. Assuming the function of the geometrical profile created above is $f_p(x, y)$. If P2 is on the profile, $f_p(x^{P2}, y^{P2}) = 0$. In parallel, the length of the patellar tendon can be retrieved from OpenSim for any given configuration of the model by a function $f_l(x^{P2}, y^{P2}, \phi_k)$, with ϕ_k the knee angle. Our goal is a position of P2 closest to the profile that allows the patellar tendon length to be equal to a predefined constant value. As a result, the optimization problem is expressed as following

$$\begin{aligned} \underset{\boldsymbol{x^{P*2}, y^{P2*}}}{\text{argmin}} \quad & \| f_p(x^{P2}, y^{P2}) \|_2^2 \\ \text{s.t} \quad & x^{P2}_{min} \leq x^{P2} \leq x^{P2}_{max} \\ & y^{P2}_{min} \leq y^{P2} \leq y^{P2}_{max} \\ & f_l(x^{P2}, y^{P2}, \phi_k) = cste \end{aligned} \tag{6.2}$$

Once the position of P2 is obtained by solving Problem 6.2, we can compute the patella position. As

each position of P2 on the profile is associated with an orientation of the patella w.r.t the distal femoral fragment, we can compute the position of the patella by simple transformation.

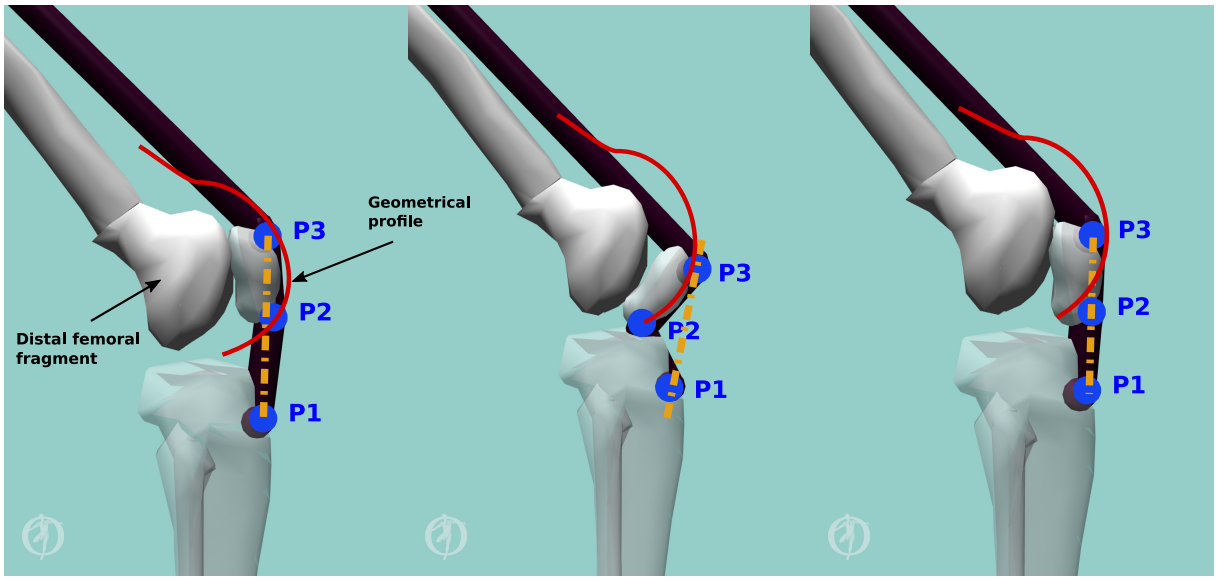

patella normal (valid)

P2 position computed by optimization (on the red profile)

patella baja (not valid)

P2 position computed by optimization (on the red profile)

patella baja (valid)

P2 position manually corrected (NOT on the red profile)

Figure 6.5: The P2 positions generated by solving the optimization problem 6.2 are not realistic for some particular configurations of patella baja or even patella normal. The manual correction modifies the position of P2 and the orientation of the patella such that P2 is aligned with P1 and P3 and the patella is as close to the distal femoral fragment as possible.

Manual Correction of Patellar Positions

In reality, as the patella translates distally towards the tibia during knee flexion, the contact between the patella and the condyles can be partially or completely lost in case of patella baja or even patella normal for the patients undergone DFEO. In these cases, the computation of P2 position described above can give unrealistic patellar positions and orientations, as the patella is no longer close to the distal femoral fragment (Fig. 6.5). We correct these invalid positions manually by following these steps

1. choose a new value for x^{P2}
2. calculate y^{P2} to assure such that the patellar tendon length is maintained.
3. choose an orientation of the patella w.r.t the distal femoral fragment.
4. calculate the position of the patella.
5. verify visually. The new patellar position is valid if
   - P2 is aligned with P3 and P1, as we assume this is the case when the quadriceps is stretched.
   - P2 is as close to the distal femoral fragment as possible.

   If one of these two criteria is not respected, we go back to the first step.

Table 6.1: Weighting coefficients for tasks and optimization variables for step I - Study of patellar position on knee mechanism

Phase	Descent	Ascent
Task		
Head vertical displacement	0.010	0.050
Angular momentum variation	0.050	0.060
Balance	0.100	0.100
Control		
All actuators	0.010	0.010
Generalized acceleration		
Ankle	0.003	0.003
Knee	0.003	0.003
Hip	0.003	0.003
Lumbar	0.100	0.100

6.2 Method

We investigate the impact of different patellar positions on knee mechanism and muscle behavior during a squat cycle. For this purpose, we synthesize squat movement on the models representing the healthy individual and the CP patient after DFEO and PTA. Multiple values of the patellar tendon length are applied on each model, covering all possible ranges of patella position (alta, normal and baja), as shown in Fig. 6.6.

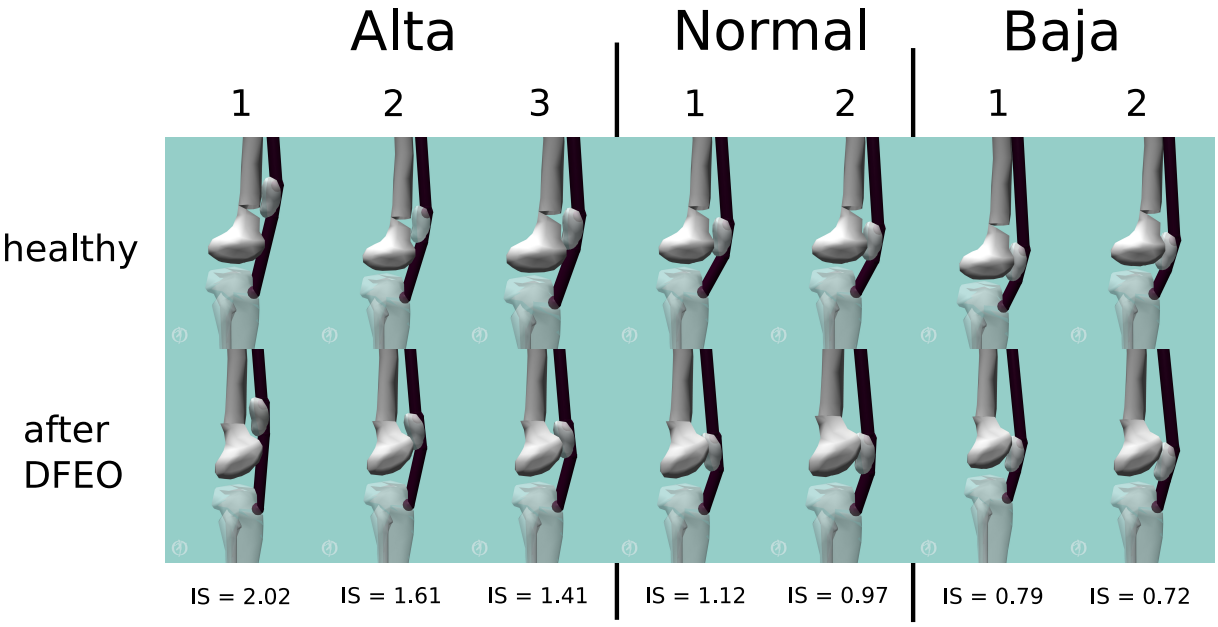

Figure 6.6: The range of patella positions for the simulations. Patella positions were classified as baja, normal, or alta based on the Insall-Salvati (IS) ratio [Insall and Salvati, 1971], (Normal: 0.8 < IS < 1.2)

6.2.1 Simulation

The depth of the squat is 40°, measured between the proximal femoral fragment and the tibia in the latter model. We choose a partial squat as our focus is on the angle range close to knee terminal extension. The

simulation starts with the synthesis of states and joint torques on both models by Step I of our two-step synthesis approach developed in Chapter 3. The weight of the tasks are detailed in Table. 6.1. Then, the muscle activities are computed by Step II of the controller, for each of the chosen patellar position. In the end, we retrieve the moment arms of the quadriceps and the muscle forces. These data are compared and analyzed to understand the influence of patellar position and DFEO on muscle behavior.

6.2.2 Results and Discussions

We start the result analysis by comparing the states and joints before and after DFEO, computed by step I of the controller. Then, we assess the influence of patellar position on the moment arm of quadriceps. Finally, the quadriceps forces are studied to understand the implication of DFEO+PTA on muscle activities.

Joint Kinematics

In general, the configuration evolves differently and is influenced by the modification of the skeletal structure. Noticeable distinctions are observed in the states before and after DFEO (Fig. 6.7). Specifically, the range of motion at the ankle during the squat is increased of approximately 3°after the osteotomy. Meanwhile, the hip rotates 10°less and the knee angle reaches the squat depth earlier after the osteotomy. Coupled with these joint angle changes are higher ankle, knee and hip joint speeds during the descent phase for the CP patient treated with DFEO.

Joint Torques

The distinctions observed in states are the consequences of the differences in the joint torque patterns (Fig. 6.8a). The torques produced are partly to counter the gravity effects (Fig. 6.8b). As indicated on the curves of the gravity terms, discrepancies are exhibited at the beginning of the descent phase at the ankle and the knee but not at the hip. This suggests that the translation to maintain the knee axis location (Fig. 6.2 is not perfectly executed during DFEO. The misalignment of the knee axis leads to the differences of computed torques between two models, thereby the ones noticed in the joint kinematics. Looking further at the beginning of the simulation, the external torques generated at the ankle and the knee are positive, meaning the distal femoral fragment is still anterior to the initial knee axis.

Moment Arms of Quadriceps w.r.t The Knee

The moment arms of the patellar tendon are shown in Fig. 6.9a. The values associated to the CP patient before surgery are in the shaded zone, as the knee angle is minimized at 30°due to contracture. In general, the absolute amplitude of moment arms increases when the knee angle approaches terminal extension. The variation range of moment arm is mainly between 5 cm and 15 cm for a knee range of motion of 40°.

It's noticeable that quadriceps moment arm achieves highest values at patellar normal during the majority of the simulations. Only when the knee of the CP patient treated with DFEO is flexed over 30°, moderate patellar alta positions demonstrate more favorable moment arm. On the other spectrum, extreme patellar alta gives the lowest moment arm, followed by moderate patellar baja. Finally, between the two models, the moment arms for all patellar positions reduce after DFEO. This result indicates the implication of DFEO on quadriceps moment arm modification. The values of quadriceps moment arm at terminal extension and at squat depth are given at Table 6.2.

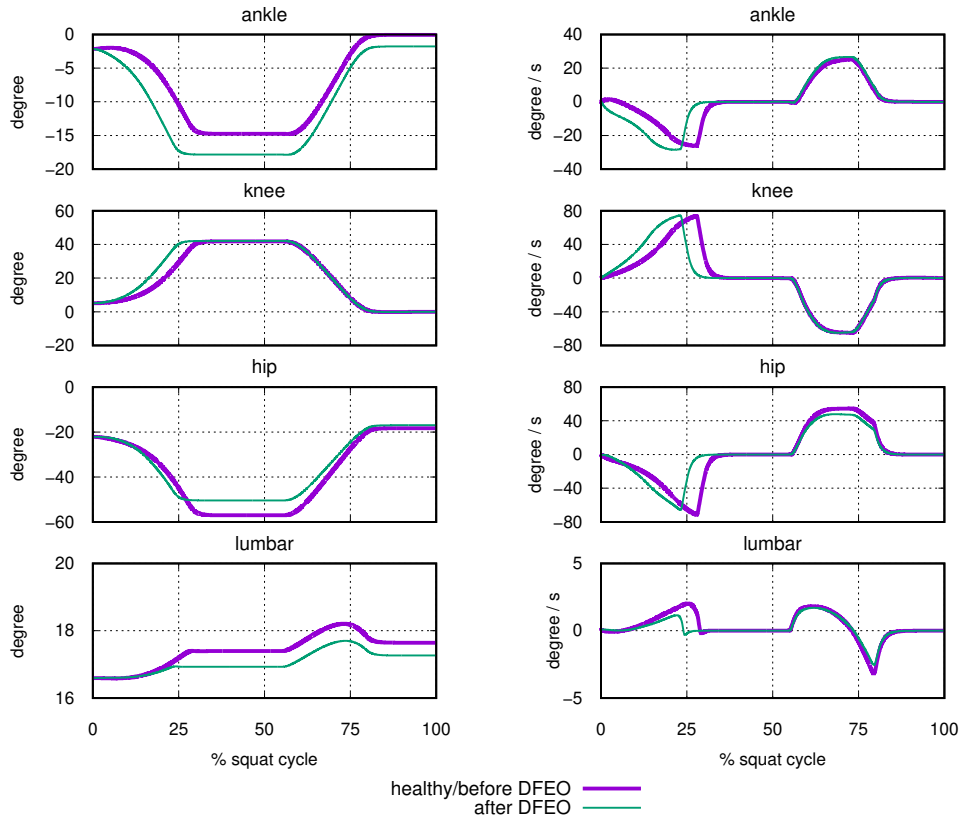

Figure 6.7: The states of the model during squat performance with squat depth of 40°. The knee angle is measured between the femoral proximal fragment and the tibia.

Table 6.2: Quadriceps moment arms in terms of patellar position

Patellar Position	**Moment Arm (m)**					
	0°		30°		40°	
	Before	After	Before	After	Before	After
alta 1	-0.053	-0.047	-0.047	-0.042	-0.046	-0.040
alta 2	-0.055	-0.052	-0.052	-0.050	-0.052	-0.049
alta 3	-0.056	-0.054	-0.055	-0.052	-0.054	-0.050
normal 1	-0.061	-0.056	-0.056	-0.052	-0.055	-0.048
normal 2	-0.061	-0.056	-0.056	-0.049	-0.054	-0.045
baja 1	-0.060	-0.054	-0.055	-0.048	-0.051	-0.046
baja 2	-0.059	-0.054	-0.053	-0.048	-0.052	-0.047

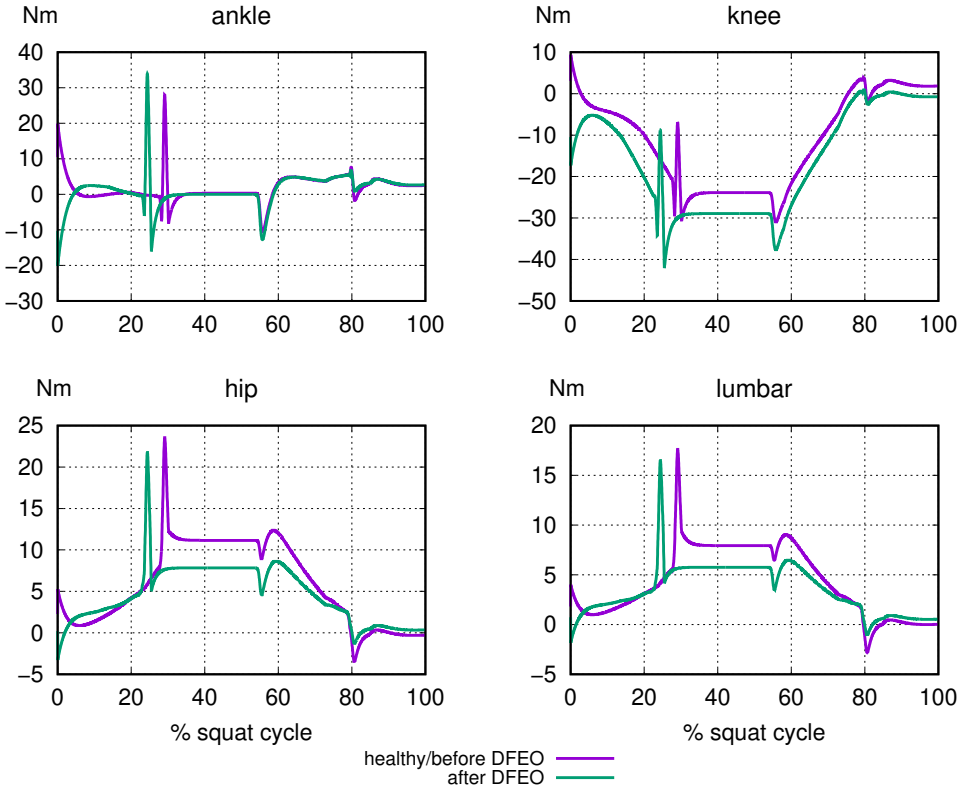

(a) The joint torques produced by step I for squat performance with squat depth of 40°. The knee angle is measured between the femoral proximal fragment and the tibia.

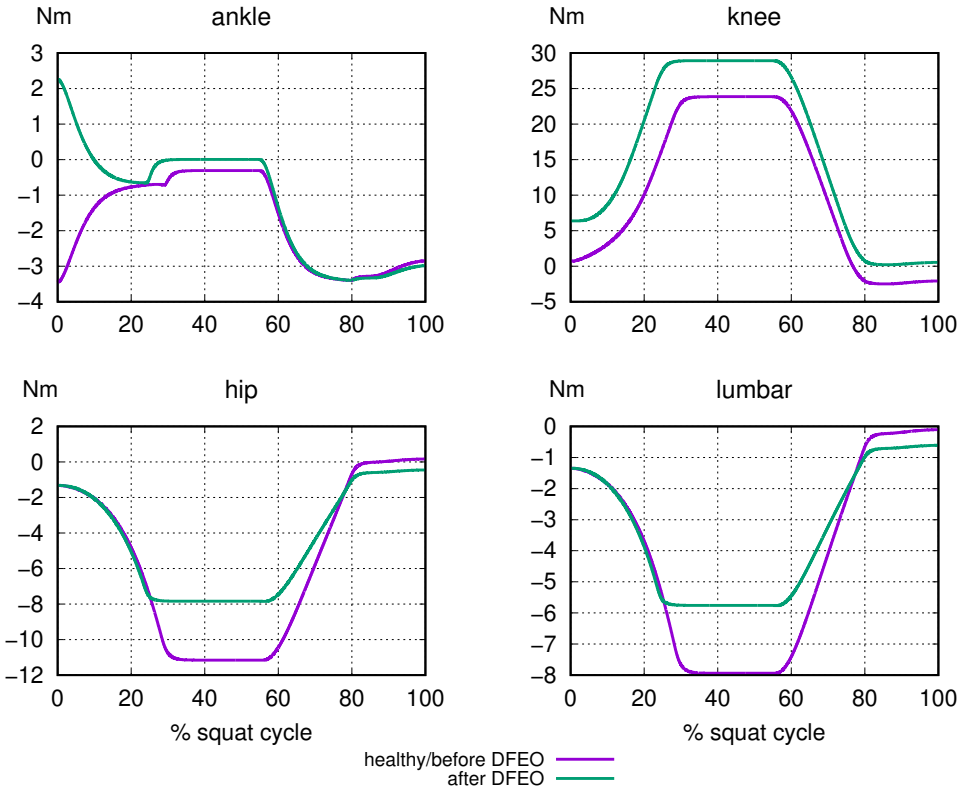

(b) The gravity effect computed at lower limb joints. Due to the modification of the skeletal structure as a result of DFEO, the torques at the joints generated by the gravity are different before and after the osteotomy. Note that at the beginning of the simulation, the same joint values are applied on both models.

Figure 6.8: The joint torques and the gravity effects at the joints.

Quadriceps Forces

The quadriceps forces (Fig. 6.9b) are influenced directly by the quadriceps moment arms. For each model, to generate the same amount of knee torque, normal patella positions allow lower quadriceps force compared to patella alta and baja. Between the two models, the quadriceps forces are greater after DFEO, as a consequence of patellar moment arm decline.

6.3 Conclusion

The aim of our study is to predict the impact of the patellar position on quadriceps activities during a squat cycle. Overall, our results indicate that the patellar position has substantial implication for extensor function. Specifically, placing the patella in a normal position assures the optimal moment arms for quadriceps at terminal extension. This is particularly advantageous for CP patients suffering patella alta, as PTA allows to reduce load on their extensors at terminal extension, thereby facilitating their movement during the gait standing phase. On the other hand, moderate patella alta and patella baja positions are also favorable after DFEO to perform other activities demanding knee flexion. After the correction of the contracture by the osteotomy, the quadriceps moment arm is reduced for all patellar positions. This results is coherent with the **literature to be added**, as the patella is moved proximally as a consequence of the rotation of the femoral distal fragment. Therefore, PTA should be required to place the patella at normal position of after DFEO if the patellar is alta or baja before DFEO. However, if the patellar is normal before DFEO, it is not necessary to perform PTA. Regarding the quadriceps activities, the computed forces rise after DFEO as the direct result of moment arm loss.

In our synthesis approach, we assume that a CP patient, after undergoing DFEO and PTA, is able to perform a squat with similar joint kinematics as a healthy individual. This assumption requires to adjust the chosen studied movement in terms of potential minimal knee flexion angle after DFEO and muscle strengths. For example, in the current study, we assume that the quadriceps are strong enough to extend the knee to terminal extension and the DFEO is accomplished. In case the knee flexion cannot extend fully after DFEO, the high level input to step I needs to be changed to reflect the new lower bound of the knee joint. Furthermore, CP patients can potentially experience pain, especially with patella baja in flexed-knee configuration, and therefore are unable to complete the movement.

In the future, our optimization-based dynamic movement synthesis tool can be developed in order to optimize both DFEO and PTA procedures. One approach is to formulate an optimization problem of finding the optimal parameters of DFEO and PTA. These parameters include the angle of the wedge apex, the distance between the wedge and the femur distal end, and the patellar position. The cost functions to be minimized could be related to the muscle energy expenditure during a dynamic movement, the maximum muscle stress or activation.

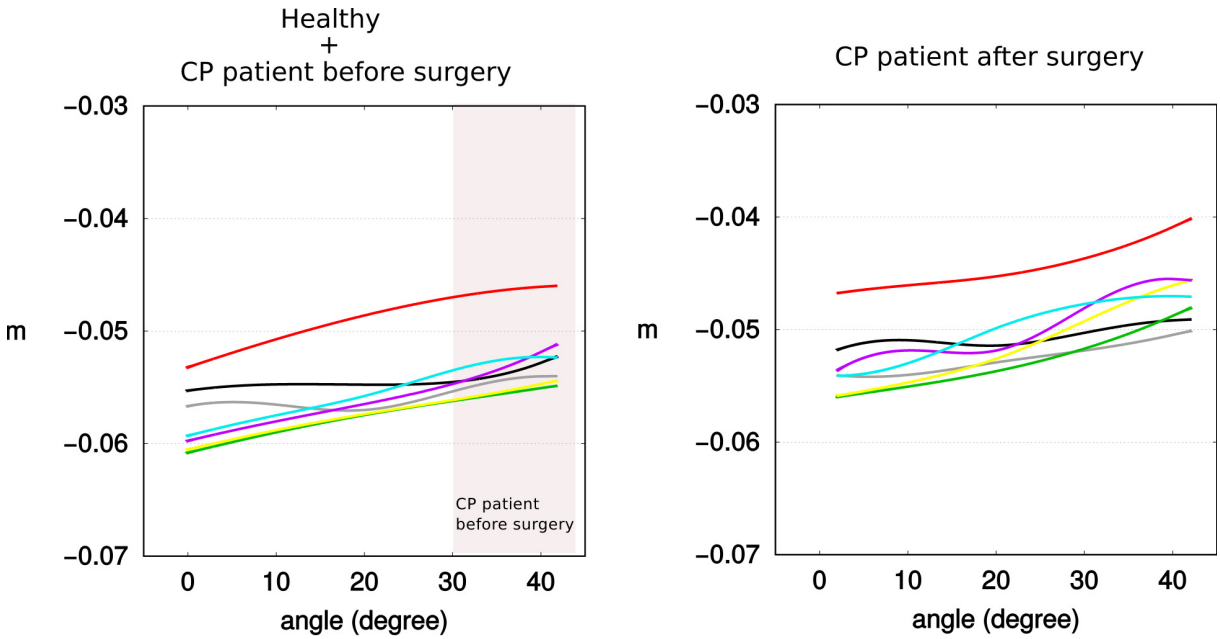

(a) Evolution of the moment arms of the quadriceps in terms of patella position and knee flexion.

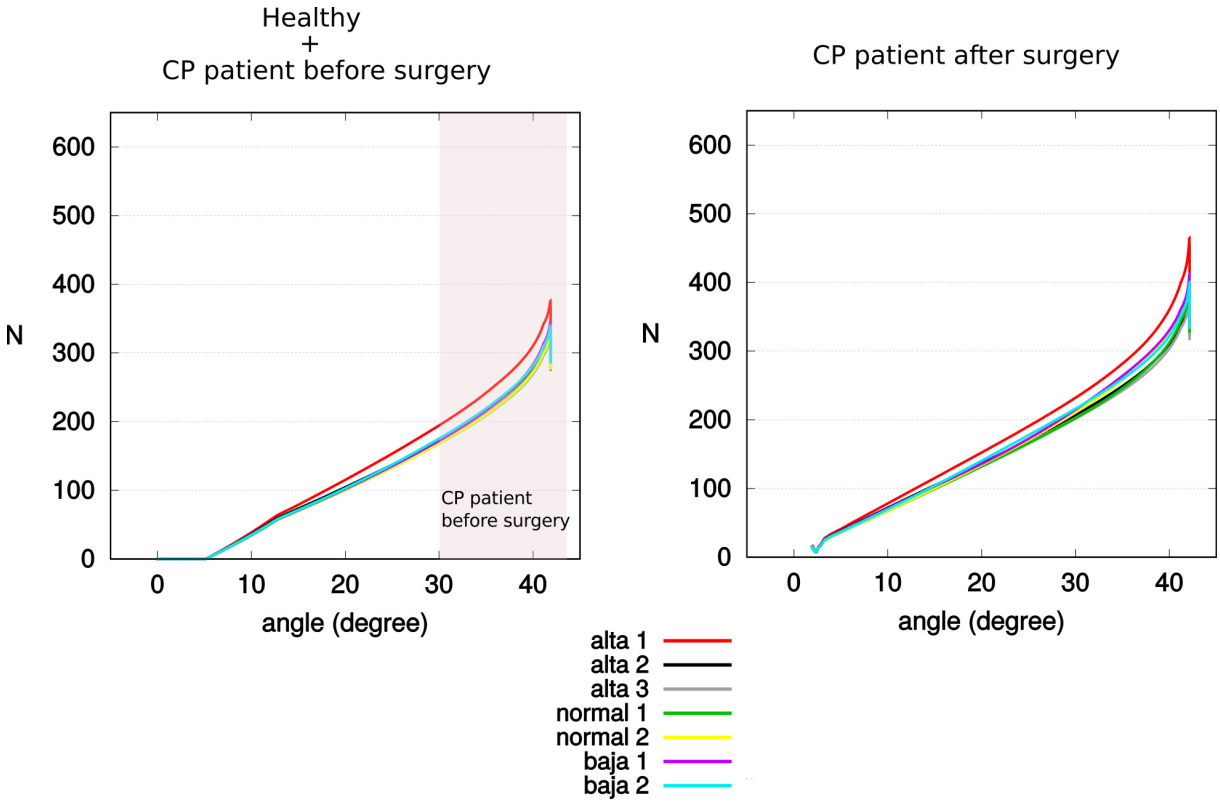

(b) Evolution of the quadriceps forces in terms of patella position and knee flexion.

Figure 6.9

Chapter 7

Conclusions and Perspectives

Single-event multilevel orthopedic surgery (SEMLS), while being the most effective method of managing musculoskeletal deformities in children with cerebral palsy (CP), is a highly complicated intervention. Despite advances in the understanding of human biomechanical mechanism and in experimental materials and protocols, clinicians are still facing great difficulties in surgical planning and predicting surgical outcomes. In this context, physics-based simulation has emerged as a promising approach, capable of taking into account the varieties of musculoskeletal impairments and surgical acts. Even more so, if a simulation is able of synthesizing human movements, without requiring prior data related to the studied movement, it presents a valuable capacity of identifying the causal relation between mechanical and physiological properties of a musculoskeletal system and its movements. Consequently, this approach can be developed to create surgical planning tools and help clinicians improve the outcome of SEMLS.

Nonetheless, synthesizing human movements is a major challenge in terms of human modeling, movement description and whole-body control. In this study, we have developed an optimization-based squat synthesis scheme inspired from the robotic whole-body control theory. Through our experiences, our method has shown to be capable of synthesizing different types of squat movement and predicting muscle behavior after surgical interventions. However, multiple obstacles and limitations are to be overcome before the method can be considered to be efficient. In this chapter, we discuss our contributions, the limitations, and perspectives as well as future work for improving on the proposed solution.

7.1 Contributions

Our study focuses on developing a physics-based simulation tool to investigate the functional implication of musculoskeletal modifications on human movements. The tool consists in a reactive optimization-based dynamic task controller, whose design is inspired from the whole-body control in robotics. We started by hypothesizing that a movement was the outcome of an optimization process in which a person executed simultaneously several tasks with different priorities to achieve physically-relevant goals. To demonstrate our method, we chose squat as the studied movement. As detailed in Chapter 3, a squat movement is considered the result of changing the head height while maintaining balance and minimizing angular momentum variation, as well as complying with the constraints related to the mechanical properties of the musculoskeletal system and the equation of motion. Next, we formulated the squat synthesis problem as a multi-objective quadratic optimization problem, in which the tasks are expressed as quadratic cost functions, and the constraints' expressions are linear. The inputs of the process are the computational musculoskeletal model and the parameters related to the high-level goals and the constraints. No motion capture data or force measurement are required for the synthesis scheme. We also implemented Task Switch to regulate the task priorities based on our observations and assumptions of different squat performances. Finally, the resolution of the quadratic optimization problems yielded the state trajectories of the squat movement, as well as the associated muscle activations. Two examples squat synthesis were given at the end of the chapter.

Our optimization-based dynamic task controller was proven, in Chapter 4 to be able of synthesizing the effect of the ankle dorsiflexion flexibility on the ability to perform the so-called Asian squat, as well as the implication of angular momentum variation of different squat strategies. To test our method in the clinical context, we applied the controller to investigate the implication of rectus femoris (RF) transfer procedure (Chapter 5). The results provided useful information related to RF attachment sites that need to be considered in the planning RF transfer. The method also exhibited potential of improving the combination of Distal Femoral Extension Osteotomy (DFEO) and Patellar Tendon Advancement (PTA) procedures (Chapter 6). Specifically, the patellar position could be computed with our controller to optimize the knee extensors moment arm w.r.t the knee. As a result, knee flexion during swing phase in the gait of cerebral palsy (CP) patients exhibiting crouch gait could be enhanced.

Through these studies of proofs of concept, we demonstrated that our simulation can offer clinicians to optimize the outcomes of interventions. These features include:

- synthesizing the effects of modifying a singular element of the musculoskeletal system on muscle activity.
- synthesizing the emergence of different movement strategies by adapting task priorities
- optimizing the outcome of orthopaedic surgical interventions

7.2 Limitations and Perspectives

In parallel with the achieved results, we face multiple difficulties that could not be resolved in time. In this section, we discuss the limitations of our method, and the perspectives on potential solutions.

7.2.1 Muscle Modeling

The actuator model adopted in this study is a linear relation between the control input and the produced force/torque. Thanks to the linearity, we were able to formulate the synthesis problem as linear quadratic optimization problems. As a result, the computational time was relatively small compared to other methods solving non-linear optimization problems. However, this model does not take into account the elasticity of muscles. This is an important property, allowing muscles to produce force passively without receiving activation. Other more advanced models, such as Hill-type models, model the elasticity with a passive element. By considering this property in the modeling of torque generators and muscles, we believe that we could achieve more realistic synthesized muscle activations.

Another advantages of increasing the complexity of muscle models is the possibility of modeling more realistically muscle impairments. For example, modeling spasticity, a common phenomenon in CP patients, requires the relation between muscle activation and muscle lengthening velocity due to its dependence upon the speed of the muscle stretch [Sheean, 2002].

Last but not least, a more complex model offers more possibilities in formulating the cost function the regularization task (cf. 3.2.1), especially those expressing physiological criteria such as minimum muscle fatigue, minimum muscle stress, and minimum metabolic energy expenditure. For instance, the metabolic cost, as formulated in [Prilutsky and Zatsiorsky, 2002] and [Alexander, 2000], requires the muscle lengthening velocity. The fatigue criterion, established in [Crowninshield and Brand, 1981], necessitates the average cross-sectional area of muscles.

On the other hand, muscle elasticity depends on muscle length and length variation in a nonlinear manner. Therefore, incorporating this property into the dynamics equation leads to the nonlinear formulation of the optimization problem. The resolution, consequently, is influenced by the initial guess values of the optimization variables and the computational time is increased.

7.2.2 Reactive Control Strategy

There are visible spikes throughout the achieved related to joint torques and muscle activities. They are caused by several factors:

- the formulation of the head vertical displacement task (cf. 3.2.1);
- the constraint boundaries;
- the evolution of the task weights;
- the muscle model.

As we do not track any reference kinematic trajectory, the inputs of the task consist of only the two positions of the control point at the end of ascent and descent phases. As a result, the desired acceleration is relatively great at the beginning of these phases, when the difference between the current position and the reference one is big. Depending on the task weight and the gains chosen for the PD controller, the impact of the sudden changes in the desired acceleration value can be more or less modulated, but not in an ideal manner.

The constraint boundaries, such as those imposed on the optimization variables, can provoke discontinuity in the computed joint torques and muscle activities when they are reached. To deal with this problem, we increase the prediction period h in the constraint formulations, such as in Eq. 2.25. This solution allows smoother joint torques with a more conservative controller.

Regarding the evolution of task weights, we implemented Task Switch, using the exponential decay function with the aim of achieving smooth transition of different weights' values. Nevertheless, this solution cannot eliminate the spikes in the obtained joint torques trajectories. Finally, as our actuation models does not incorporate a dynamic model, sharp variations of joint torques and muscle activations are hard to avoid in case of reference changes. To cope with this limitation, one solution is to design a smooth time-varying trajectory. While this solution ensures the continuity of the computed joint torques and muscles activities, it can requires extensive servo-gain tuning. Another solution which is less laborious is proposed in [De Lasa et al., 2010]. The desire acceleration is expressed an affine function of time, with the coefficients being determined by solving a simple boundary value problem at each instant of the simulation.

7.2.3 Experimental data

Experimental data is important in the creation of patient-specific musculoskeletal models and the validation of simulation results. In our work, we used the model created by [Catelli et al., 2019] to perform all the studies. Despite obtaining valuable information, it was not possible to prove the results statistically significant. Also, variations in morphology and in movement strategies are important to understand the movement generation, and create variances in the obtained results. In terms of validation, we were only able to compare our synthesized results with the measured data in the study of squat strategies synthesis (cf. 4.2 To evaluate more thoroughly our method, more comparisons with experiment data need to be performed, especially in case of prediction of surgical outcomes. Indeed, the simulation results can be conflicted or not fully cover the real outcomes of surgeries, as many complications can occur during procedures. One example taken from our work is the behavior of rectus femoris after its transfer to a new attachment site. According to our simulations as well other studies, the muscle is converted from knee extensor to knee flexor. However, in reality, the muscle can remain as a knee extensor as it remained attached to the underlying vasti through scar tissue.

7.2.4 Towards Gait Synthesis

Gait analysis is an the essential tool, allowing critical assessment of pathologies preoperatively, and assessment of outcome postoperatively [Gage, 1993]. However, this method does not have the capacity of predicting surgical outcomes. In this context, physics-based simulation can be used as a complementary tool to improve diagnosis and surgical planning. Our method can be adjusted for gait synthesis. Several improvements need to be carried out, notably:

- building floating-based musculoskeletal models
- identifying the physically-relevant tasks contributing to the generation of human gait

The floating-based models should have a sufficient level of complexity regarding contact modeling. Since floating-based models are underactuated system, the contact with the environment has major implication in the development of the control for locomotion. While the implication of muscle modeling has been developed above, the contact modeling also has a crucial role as the model is underactuated [Padois, 2016]. In parallel, apart from minimizing angular momentum variation and regularization, additional tasks must be created notably to propel the body forward and manage the foot/ground contact forces at different phases of the gait. Additionally, the management of gait phases is a challenge due to the implications of discreet states of the foot/ground contact.

In the literature, optimization-based methods have been developed human by assuming that the central nervous system (CNS) optimizes performance,e.g. minimizes the metabolic cost of transport [De Groote and Falisse, 2021]. While possessing the predictive capability, natural movement is difficult to achieve since the cost functions can only represent partially how the central nervous system commands human body [Xiang et al., 2010]. Furthermore, computational time can be substantial, especially using global optimization to to synthesize gait as demonstrated in [Pandy, 2001]. Using direct collocation methods, instead of shooting methods, has proven to reduce computational time. Shooting methods integrate the dynamic equation over a time horizon using the initial guesses of the controls. On the other hand, in direct collocation methods, the discretized states and controls are optimization variables and the integration scheme is expressed by a set of constraints that is solved simultaneously with minimizing the cost function [De Groote and Falisse, 2021]. Besides optimization-based approach, solving for gait control policy is another solution providing more robustness, as shown in [Geyer and Herr, 2010] with the reflex-driven control model of gait. However, the methods based on this approach is less computationally efficient, thereby they are usually applied on simpler neuro-musculoskeletal models than optimization-based methods [De Groote and Falisse, 2021].

Appendices

Appendix A

Muscle Parameters

Table A.1: Muscle Parameters for the models used in surgery prediction

Muscle	**Abbreviation**	**Maximal Force**
Adductor brevis	addbrev	0.006
Adductor longus	addlong	0.006
Adductor magnus		
Adductor magnus (distal)	addmagDist	
Adductor magnus (ischial)	addmagIsch	
Adductor magnus (middle)	addmagMid	
Adductor magnus (proximal)	addmagProx	
Biceps femoris short head	bfsh	0.006
Biceps femoris long head	bflh	0.006
Extensor digitorum longus	edl	0.006
Extensor hallucis longus	ehl	0.006
Flexor digitorum longus	fdl	0.006
Flexor hallucis longus	fhl	0.006
Gastrocnemius lateralis	gaslat	0.040
Gastrocnemius medialis	gasmed	0.400
Gluteus maximus		
Gluteus maximus (superior)	glmax1	0.400
Gluteus maximus (middle)	glmax2	0.400
Gluteus maximus (inferior)	glmax3	0.400
Gluteus medius		
Gluteus medius (anterior)	glmed1	0.400
Gluteus medius (middle)	glmed2	0.400
Gluteus medius (posterior)	glmed3	0.400
Gluteus minimus		
Gluteus minimus (anterior)	glmin1	0.400
Gluteus minimus (posterior)	glmin3	0.400
Gracilis	grac	0.400
Iliacus	iliacus	0.400
Peroneus brevis	perbrev	0.400
Peroneus longus	perlong	0.400
Psoas	psoas	0.400
Rectus femoris	recfem	0.400
Sartorius	sart	0.400
Semimembranosus	semimem	0.400
Semitendinosus	semiten	0.400
Soleus	soleus	0.400
Tensor fascia latae	tfl	0.400
Tibialis anterior	tib_ant	0.400
Tibialis posterior	tibpost	0.400
Vastus intermedius	vasint	0.400
Vastus lateralis	vaslat	0.400
Vastus medialis	vasmed	0.400

Appendix B

Parameters of the feedback control loops in Step I

Table B.1: Parameters of the feedback control loops in Step I and their values

Task	**Input**	**Output**	**Proportiona Term**	**Derivative Term**
Head vertical displacement	h_{ref}	$\ddot{h}_{des}$	100	20
Maintaining balance	$x_{m,ref}$	$\ddot{x}_{m,des}$	9	6
Minimizing angular momentum variation	$\boldsymbol{L}_r$	$\dot{\boldsymbol{L}}_d$	0.1	
Posture	$\boldsymbol{\nu}_{ref}$	$\dot{\boldsymbol{\nu}}_{p,des}$	1	

Bibliography

[Al Borno et al., 2012] Al Borno, M., De Lasa, M., and Hertzmann, A. (2012). Trajectory optimization for full-body movements with complex contacts. *IEEE transactions on visualization and computer graphics*, 19(8):1405–1414.

[Alexander, 2000] Alexander, R. M. (2000). Energy-minimizing choices of muscles and patterns of movement. *Motor control*, 4(1):45–47.

[Allen and Neptune, 2012] Allen, J. L. and Neptune, R. R. (2012). Three-dimensional modular control of human walking. *Journal of biomechanics*, 45(12):2157–2163.

[Anderson and Pandy, 2001a] Anderson, F. C. and Pandy, M. G. (2001a). Dynamic optimization of human walking. *Journal of biomechanical engineering*, 123(5):381–390.

[Anderson and Pandy, 2001b] Anderson, F. C. and Pandy, M. G. (2001b). Static and dynamic optimization solutions for gait are practically equivalent. *Journal of biomechanics*, 34(2):153–161.

[Arnold* and Delp, 2005] Arnold*, A. and Delp, S. (2005). Computer modeling of gait abnormalities in cerebral palsy: application to treatment planning. *Theoretical Issues in Ergonomics Science*, 6(3-4):305–312.

[Arnold et al., 2001] Arnold, A. S., Blemker, S. S., and Delp, S. L. (2001). Evaluation of a deformable musculoskeletal model for estimating muscle–tendon lengths during crouch gait. *Annals of biomedical engineering*, 29(3):263–274.

[Arnold and Delp, 2001] Arnold, A. S. and Delp, S. L. (2001). Rotational moment arms of the medial hamstrings and adductors vary with femoral geometry and limb position: implications for the treatment of internally rotated gait. *Journal of biomechanics*, 34(4):437–447.

[Asakawa et al., 2002] Asakawa, D. S., Blemker, S. S., Gold, G. E., and Delp, S. L. (2002). In vivo motion of the rectus femoris muscle after tendon transfer surgery. *Journal of biomechanics*, 35(8):1029–1037.

[Azevedo et al., 2004] Azevedo, C., Poignet, P., and Espiau, B. (2004). Artificial locomotion control: from human to robots. *Robotics and Autonomous Systems*, 47(4):203–223.

[Bar-On et al., 2015] Bar-On, L., Molenaers, G., Aertbeliën, E., Van Campenhout, A., Feys, H., Nuttin, B., and Desloovere, K. (2015). Spasticity and its contribution to hypertonia in cerebral palsy. *BioMed research international*, 2015.

[Bessonnet et al., 2010] Bessonnet, G., Marot, J., Seguin, P., and Sardain, P. (2010). Parametric-based dynamic synthesis of 3d-gait. *Robotica*, 28(4):563–581.

[Bessonnet et al., 2002] Bessonnet, G., Sardain, P., and Chessé, S. (2002). Optimal motion synthesis–dynamic modelling and numerical solving aspects. *Multibody System Dynamics*, 8(3):257–278.

[Bittmann et al., 2018] Bittmann, M. F., Lenhart, R. L., Schwartz, M. H., Novacheck, T. F., Hetzel, S., and Thelen, D. G. (2018). How does patellar tendon advancement alter the knee extensor mechanism in children treated for crouch gait? *Gait & posture*, 64:248–254.

[Blair, 1994] Blair, B. M. (1994). *Factors relating to the ability to squat.* PhD thesis, University of Nottingham.

[Brazil and Peña,] Brazil, C. and Peña, M. D. The biomechanics of the knee during high flexion posture: Asian kinetically different from caucasians.

[Bridger, 1991] Bridger, R. (1991). Some fundamental aspects of posture related to ergonomics. *International Journal of Industrial Ergonomics*, 8(1):3–15.

[Catelli et al., 2019] Catelli, D. S., Wesseling, M., Jonkers, I., and Lamontagne, M. (2019). A musculoskeletal model customized for squatting task. *Computer methods in biomechanics and biomedical engineering*, 22(1):21–24.

[Caterisano et al., 2002] Caterisano, A., Moss, R. E., Pellinger, T. K., Woodruff, K., Lewis, V. C., Booth, W., and Khadra, T. (2002). The effect of back squat depth on the emg activity of 4 superficial hip and thigh muscles. *The Journal of Strength & Conditioning Research*, 16(3):428–432.

[Chevallereau and Aoustin, 2001] Chevallereau, C. and Aoustin, Y. (2001). Optimal reference trajectories for walking and running of a biped robot. *Robotica*, 19(5):557–569.

[Chung et al., 1997] Chung, C. Y., Stout, J., and Gage, J. R. (1997). Rectus femoris transfer—gracilis versus sartorius. *Gait & Posture*, 6(2):137–146.

[Chung et al., 2015] Chung, H.-J., Xiang, Y., Arora, J. S., and Abdel-Malek, K. (2015). Optimization-based dynamic 3d human running prediction: effects of foot location and orientation. *Robotica*, 33(2):413–435.

[Clarkson, 2000] Clarkson, H. M. (2000). *Musculoskeletal assessment: joint range of motion and manual muscle strength*. Lippincott Williams & Wilkins.

[Crowninshield and Brand, 1981] Crowninshield, R. D. and Brand, R. A. (1981). A physiologically based criterion of muscle force prediction in locomotion. *Journal of biomechanics*, 14(11):793–801.

[Dahlkvist et al., 1982] Dahlkvist, N., Mayo, P., and Seedhom, B. (1982). Forces during squatting and rising from a deep squat. *Engineering in medicine*, 11(2):69–76.

[Dan et al., 1999] Dan, B., Bouillot, E., Bengoetxea, A., Nöel, P., Kahn, A., and Cheron, G. (1999). Adaptive motor strategy for squatting in spastic diplegia. *European journal of paediatric neurology*, 3(4):159–165.

[De Groote and Falisse, 2021] De Groote, F. and Falisse, A. (2021). Perspective on musculoskeletal modelling and predictive simulations of human movement to assess the neuromechanics of gait. *Proceedings of the Royal Society B*, 288(1946):20202432.

[De Lasa et al., 2010] De Lasa, M., Mordatch, I., and Hertzmann, A. (2010). Feature-based locomotion controllers. *ACM Transactions on Graphics (TOG)*, 29(4):1–10.

[Delp et al., 2007] Delp, S. L., Anderson, F. C., Arnold, A. S., Loan, P., Habib, A., John, C. T., Guendelman, E., and Thelen, D. G. (2007). Opensim: open-source software to create and analyze dynamic simulations of movement. *IEEE transactions on biomedical engineering*, 54(11):1940–1950.

[Delp et al., 1994] Delp, S. L., Ringwelski, D. A., and Carroll, N. C. (1994). Transfer of the rectus femoris: effects of transfer site on moment arms about the knee and hip. *Journal of Biomechanics*, 27(10):1201–1211.

[Desailly, 2008] Desailly, E. (2008). *Analyse biomécanique 3D de la marche de l'enfant déficient moteur: modélisation segmentaire et modélisation musculo-squelettique*. PhD thesis, Poitiers.

[Desailly et al., 2015] Desailly, E., Thévenin-Lemoine, C., and Khouri, N. (2015). Patella lowering is effective in the treatment of crouch gait in cerebral palsy: A clinical and biomechanical retrospective comparative study. *Gait & Posture*, 1(42):S55.

[Desailly et al., 2017] Desailly, E., Thévenin-Lemoine, C., and Khouri, N. (2017). Does patella lowering improve crouch gait in cerebral palsy? comparative retrospective study. *Orthopaedics & Traumatology: Surgery & Research*, 103(5):741–746.

[Dionisio et al., 2008] Dionisio, V. C., Almeida, G. L., Duarte, M., and Hirata, R. P. (2008). Kinematic, kinetic and emg patterns during downward squatting. *Journal of Electromyography and Kinesiology*, 18(1):134–143.

[Draganich et al., 1989] Draganich, L., Jaeger, R., and Kralj, A. (1989). Coactivation of the hamstrings and quadriceps during extension of the knee. *The Journal of bone and joint surgery. American volume*, 71(7):1075–1081.

[Escamilla, 2001] Escamilla, R. F. (2001). Knee biomechanics of the dynamic squat exercise. *Medicine & science in sports & exercise*, 33(1):127–141.

[Escamilla et al., 2001a] Escamilla, R. F., Fleisig, G. S., Lowry, T. M., Barrentine, S. W., and Andrews, J. R. (2001a). A three-dimensional biomechanical analysis of the squat during varying stance widths. *Medicine and science in sports and exercise*, 33(6):984–998.

[Escamilla et al., 2001b] Escamilla, R. F., FLEISIG, G. S., Zheng, N., LANDER, J. E., BARRENTINE, S. W., ANDREWS, J. R., BERGEMANN, B. W., and MOORMAN III, C. T. (2001b). Effects of technique variations on knee biomechanics during the squat and leg press. *Medicine & Science in Sports & Exercise*, 33(9):1552–1566.

[Ezati et al., 2019] Ezati, M., Ghannadi, B., and McPhee, J. (2019). A review of simulation methods for human movement dynamics with emphasis on gait. *Multibody System Dynamics*, 47(3):265–292.

[Falisse et al., 2019] Falisse, A., Serrancolí, G., Dembia, C. L., Gillis, J., Jonkers, I., and De Groote, F. (2019). Rapid predictive simulations with complex musculoskeletal models suggest that diverse healthy and pathological human gaits can emerge from similar control strategies. *Journal of The Royal Society Interface*, 16(157):20190402.

[Fregly, 2021] Fregly, B. J. (2021). A conceptual blueprint for making neuromusculoskeletal models clinically useful. *Applied Sciences*, 11(5):2037.

[Fry et al., 2003] Fry, A. C., Smith, J. C., and Schilling, B. K. (2003). Effect of knee position on hip and knee torques during the barbell squat. *The Journal of Strength & Conditioning Research*, 17(4):629–633.

[Gage, 1993] Gage, J. R. (1993). Gait analysis. an essential tool in the treatment of cerebral palsy. *Clinical orthopaedics and related research*, (288):126–134.

[Gaillard et al., 2019] Gaillard, R., Bankhead, C., Budhiparama, N., Batailler, C., Servien, E., and Lustig, S. (2019). Influence of patella height on total knee arthroplasty: outcomes and survival. *The Journal of arthroplasty*, 34(3):469–477.

[Galarraga et al., 2016] Galarraga, O. A., Vigneron, V., Dorizzi, B., Khouri, N., and Desailly, É. (2016). Predicting postoperative knee flexion and pelvic tilt at initial contact of cerebral palsy children. *Movement Sport Sciences*, (3):87–92.

[Geyer and Herr, 2010] Geyer, H. and Herr, H. (2010). A muscle-reflex model that encodes principles of legged mechanics produces human walking dynamics and muscle activities. *IEEE Transactions on neural systems and rehabilitation engineering*, 18(3):263–273.

[Gilardi and Sharf, 2002] Gilardi, G. and Sharf, I. (2002). Literature survey of contact dynamics modelling. *Mechanism and machine theory*, 37(10):1213–1239.

[Goffe et al., 1994] Goffe, W. L., Ferrier, G. D., and Rogers, J. (1994). Global optimization of statistical functions with simulated annealing. *Journal of econometrics*, 60(1-2):65–99.

[Goswami and Kallem, 2004] Goswami, A. and Kallem, V. (2004). Rate of change of angular momentum and balance maintenance of biped robots. In *IEEE International Conference on Robotics and Automation, 2004. Proceedings. ICRA'04. 2004*, volume 4, pages 3785–3790. IEEE.

[Haeufle et al., 2014] Haeufle, D., Günther, M., Bayer, A., and Schmitt, S. (2014). Hill-type muscle model with serial damping and eccentric force–velocity relation. *Journal of biomechanics*, 47(6):1531–1536.

[Halilaj et al., 2018] Halilaj, E., Rajagopal, A., Fiterau, M., Hicks, J. L., Hastie, T. J., and Delp, S. L. (2018). Machine learning in human movement biomechanics: Best practices, common pitfalls, and new opportunities. *Journal of biomechanics*, 81:1–11.

[Hamner et al., 2010] Hamner, S. R., Seth, A., and Delp, S. L. (2010). Muscle contributions to propulsion and support during running. *Journal of biomechanics*, 43(14):2709–2716.

[Hartmann et al., 2013] Hartmann, H., Wirth, K., and Klusemann, M. (2013). Analysis of the load on the knee joint and vertebral column with changes in squatting depth and weight load. *Sports medicine*, 43(10):993–1008.

[Hemmerich et al., 2006] Hemmerich, A., Brown, H., Smith, S., Marthandam, S., and Wyss, U. (2006). Hip, knee, and ankle kinematics of high range of motion activities of daily living. *Journal of orthopaedic research*, 24(4):770–781.

[Herr and Popovic, 2008] Herr, H. and Popovic, M. (2008). Angular momentum in human walking. *Journal of experimental biology*, 211(4):467–481.

[Hersh et al., 1997] Hersh, L., Sun, J., Richards, J., and Miller, F. (1997). The prediction of post-operative gait patterns using neural networks. *Gait & Posture*, 2(5):151.

[Hicks et al., 2011] Hicks, J. L., Delp, S. L., and Schwartz, M. H. (2011). Can biomechanical variables predict improvement in crouch gait? *Gait & posture*, 34(2):197–201.

[Hung and Gross, 1999] Hung, Y.-j. and Gross, M. T. (1999). Effect of foot position on electromyographic activity of the vastus medialis oblique and vastus lateralis during lower-extremity weight-bearing activities. *Journal of Orthopaedic & Sports Physical Therapy*, 29(2):93–105.

[Hunt and Crossley, 1975] Hunt, K. H. and Crossley, F. R. E. (1975). Coefficient of restitution interpreted as damping in vibroimpact.

[Huxley, 1974] Huxley, A. (1974). Muscular contraction. *The Journal of physiology*, 243(1):1–43.

[Huxley, 2004] Huxley, H. E. (2004). Fifty years of muscle and the sliding filament hypothesis. *European journal of biochemistry*, 271(8):1403–1415.

[Insall and Salvati, 1971] Insall, J. and Salvati, E. (1971). Patella position in the normal knee joint. *Radiology*, 101(1):101–104.

[ISEAR JR et al., 1997] ISEAR JR, J. A., Erickson, J. C., and Worrell, T. W. (1997). Emg analysis of lower extremity muscle recruitment patterns during an unloaded squat. *Medicine & Science in Sports & Exercise*, 29(4):532–539.

[Jensen and Davy, 1975] Jensen, R. H. and Davy, D. T. (1975). An investigation of muscle lines of action about the hip: a centroid line approach vs the straight line approach. *Journal of biomechanics*, 8(2):103–110.

[Kajita et al., 2003] Kajita, S., Kanehiro, F., Kaneko, K., Fujiwara, K., Harada, K., Yokoi, K., and Hirukawa, H. (2003). Biped walking pattern generation by using preview control of zero-moment point. In *2003 IEEE International Conference on Robotics and Automation (Cat. No. 03CH37422)*, volume 2, pages 1620–1626. IEEE.

[Kaplan and Heegaard, 2001] Kaplan, M. L. and Heegaard, J. H. (2001). Predictive algorithms for neuromuscular control of human locomotion. *Journal of Biomechanics*, 34(8):1077–1083.

[Kasuyama et al., 2009] Kasuyama, T., Sakamoto, M., and Nakazawa, R. (2009). Ankle joint dorsiflexion measurement using the deep squatting posture. *Journal of Physical Therapy Science*, 21(2):195–199.

[Khatib et al., 2009] Khatib, O., Demircan, E., De Sapio, V., Sentis, L., Besier, T., and Delp, S. (2009). Robotics-based synthesis of human motion. *Journal of Physiology-Paris*, 103(3-5):211–219.

[Khouri and Desailly, 2013] Khouri, N. and Desailly, E. (2013). Rectus femoris transfer in multilevel surgery: technical details and gait outcome assessment in cerebral palsy patients. *Orthopaedics & Traumatology: Surgery & Research*, 99(3):333–340.

[Killen et al., 2020] Killen, B. A., Falisse, A., De Groote, F., and Jonkers, I. (2020). In silico-enhanced treatment and rehabilitation planning for patients with musculoskeletal disorders: Can musculoskeletal modelling and dynamic simulations really impact current clinical practice? *Applied Sciences*, 10(20):7255.

[Kim et al., 2008] Kim, H. J., Wang, Q., Rahmatalla, S., Swan, C. C., Arora, J. S., Abdel-Malek, K., and Assouline, J. G. (2008). Dynamic motion planning of 3d human locomotion using gradient-based optimization. *Journal of biomechanical engineering*, 130(3):031002.

[Kongsgaard et al., 2006] Kongsgaard, M., Aagaard, P., Roikjaer, S., Olsen, D., Jensen, M., Langberg, H., and Magnusson, S. (2006). Decline eccentric squats increases patellar tendon loading compared to standard eccentric squats. *Clinical Biomechanics*, 21(7):748–754.

[Krigger, 2006] Krigger, K. W. (2006). Cerebral palsy: an overview. *American family physician*, 73(1):91–100.

[Kulić et al., 2016] Kulić, D., Venture, G., Yamane, K., Demircan, E., Mizuuchi, I., and Mombaur, K. (2016). Anthropomorphic movement analysis and synthesis: A survey of methods and applications. *IEEE Transactions on Robotics*, 32(4):776–795.

[Lamberts et al., 2016] Lamberts, R. P., Burger, M., Du Toit, J., and Langerak, N. G. (2016). A systematic review of the effects of single-event multilevel surgery on gait parameters in children with spastic cerebral palsy. *PloS one*, 11(10):e0164686.

[Lenhart et al., 2017a] Lenhart, R., Smith, C., Schwartz, M., Novacheck, T., and Thelen, D. (2017a). The effect of distal femoral extension osteotomy on muscle lengths after surgery. *Journal of children's orthopaedics*, 11(6):472–478.

[Lenhart et al., 2017b] Lenhart, R. L., Brandon, S. C., Smith, C. R., Novacheck, T. F., Schwartz, M. H., and Thelen, D. G. (2017b). Influence of patellar position on the knee extensor mechanism in normal and crouched walking. *Journal of biomechanics*, 51:1–7.

[Lieber and Fridén, 2019] Lieber, R. L. and Fridén, J. (2019). Muscle contracture and passive mechanics in cerebral palsy. *Journal of applied physiology*, 126(5):1492–1501.

[Liu et al., 2016] Liu, M., Tan, Y., and Padois, V. (2016). Generalized hierarchical control. *Autonomous Robots*, 40(1):17–31.

[Lloyd and Besier, 2003] Lloyd, D. G. and Besier, T. F. (2003). An emg-driven musculoskeletal model to estimate muscle forces and knee joint moments in vivo. *Journal of biomechanics*, 36(6):765–776.

[Lober, 2017] Lober, R. (2017). *Task Compatibility and Feasibility Maximization for Whole-Body Control*. Theses, UPMC.

[Lu et al.,] Lu, Y., Mei, Q., Peng, H.-T., Li, J., Wei, C., and Gu, Y. A comparative study on loadings of the lower extremity during deep squat in asian and caucasian individuals via opensim musculoskeletal modelling. *BioMed Research International*, 2020.

[Lynn et al., 2009] Lynn, A. K., Turner, M., and Chambers, H. G. (2009). Surgical management of spasticity in persons with cerebral palsy. *PM&R*, 1(9):834–838.

[Macchietto et al., 2009] Macchietto, A., Zordan, V., and Shelton, C. R. (2009). Momentum control for balance. In *ACM SIGGRAPH 2009 papers*, pages 1–8.

[Macrum et al., 2012] Macrum, E., Bell, D. R., Boling, M., Lewek, M., and Padua, D. (2012). Effect of limiting ankle-dorsiflexion range of motion on lower extremity kinematics and muscle-activation patterns during a squat. *Journal of sport rehabilitation*, 21(2):144–150.

[Magiera and Heathcock, 2020] Magiera, L. A. and Heathcock, J. C. (2020). Commentary on "intraobserver reliability and construct validity of the squat test in children with cerebral palsy". *Pediatric Physical Therapy*, 32(4):404.

[Markolf et al., 1990] Markolf, K. L., Gorek, J. F., Kabo, J. M., and Shapiro, M. S. (1990). Direct measurement of resultant forces in the anterior cruciate ligament. an in vitro study performed with a new experimental technique. *JBJS*, 72(4):557–567.

[McGinley et al., 2012] McGinley, J. L., Dobson, F., Ganeshalingam, R., Shore, B. J., Rutz, E., and Graham, H. K. (2012). Single-event multilevel surgery for children with cerebral palsy: a systematic review. *Developmental Medicine & Child Neurology*, 54(2):117–128.

[Mehta et al., 2017] Mehta, S., Tyler, A., and Hast, M. (2017). Understanding the basics of computational models in orthopaedics: a nonnumeric review for surgeons. *JAAOS-Journal of the American Academy of Orthopaedic Surgeons*, 25(10):684–692.

[Millard et al., 2013] Millard, M., Uchida, T., Seth, A., and Delp, S. L. (2013). Flexing computational muscle: modeling and simulation of musculotendon dynamics. *Journal of biomechanical engineering*, 135(2).

[Mistry et al., 2010] Mistry, M., Buchli, J., and Schaal, S. (2010). Inverse dynamics control of floating base systems using orthogonal decomposition. In *2010 IEEE international conference on robotics and automation*, pages 3406–3412. IEEE.

[Mombaur, 2009] Mombaur, K. (2009). Using optimization to create self-stable human-like running. *Robotica*, 27(3):321–330.

[Moro and Sentis, 2019] Moro, F. L. and Sentis, L. (2019). Whole-body control of humanoid robots. *Humanoid Robotics: A Reference (A. Goswami, and P. Vadakkepat, eds.), Springer, to appear.*

[Morrison et al., 2018] Morrison, T. M., Pathmanathan, P., Adwan, M., and Margerrison, E. (2018). Advancing regulatory science with computational modeling for medical devices at the fda's office of science and engineering laboratories. *Frontiers in medicine*, 5:241.

[Mulholland and Wyss, 2001] Mulholland, S. J. and Wyss, U. P. (2001). Activities of daily living in non-western cultures: range of motion requirements for hip and knee joint implants. *International Journal of Rehabilitation Research*, 24(3):191–198.

[Neptune and Hull, 1998] Neptune, R. and Hull, M. (1998). Evaluation of performance criteria for simulation of submaximal steady-state cycling using a forward dynamic model.

[Nisell, 1986] Nisell, R. (1986). Joint load during the parallel squat in power lifting and forces analysis of in vivo bilateral quadriceps tendon rupture. *Scand J. Sports Sci*, 8:63–70.

[Novacheck et al., 2009] Novacheck, T. F., Stout, J. L., Gage, J. R., and Schwartz, M. H. (2009). Distal femoral extension osteotomy and patellar tendon advancement to treat persistent crouch gait in cerebral palsy: surgical technique. *JBJS*, 91(Supplement_2):271–286.

[Oskoui et al., 2013] Oskoui, M., Coutinho, F., Dykeman, J., Jetté, N., and Pringsheim, T. (2013). An update on the prevalence of cerebral palsy: a systematic review and meta-analysis. *Developmental Medicine & Child Neurology*, 55(6):509–519.

[OSMIFW, 2021] OSMIFW (2021). Knee anatomy. [Online; accessed 12-September-2021].

[Ounpuu et al., 1993] Ounpuu, S., Muik, E., Davis 3rd, R., Gage, J., and DeLuca, P. (1993). Rectus femoris surgery in children with cerebral palsy. part i: The effect of rectus femoris transfer location on knee motion. *Journal of pediatric orthopedics*, 13(3):325–330.

[Ozsoy, 2014] Ozsoy, B. (2014). *Three-dimensional sit-to-stand motion prediction*. PhD thesis.

[O'Sullivan et al., 2020] O'Sullivan, R., Marron, A., and Brady, K. (2020). Crouch gait or flexed-knee gait in cerebral palsy; is there a difference? a systematic review. *Gait & Posture*.

[Padois, 2016] Padois, V. (2016). *Control and design of robots with tasks and constraints in mind*. PhD thesis, Université Pierre et Marie Curie (Paris 6).

[Pandy et al., 1995] Pandy, M., Garner, B., and Anderson, F. (1995). Optimal control of non-ballistic muscular movements: a constraint-based performance criterion for rising from a chair.

[Pandy, 2001] Pandy, M. G. (2001). Computer modeling and simulation of human movement. *Annual review of biomedical engineering*, 3(1):245–273.

[Perry, 1987] Perry, J. (1987). Distal rectus femoris transfer. *Developmental Medicine & Child Neurology*, 29(2):153–158.

[Physiopedia, 2021] Physiopedia (2021). Patellofemoral joint — physiopedia,. [Online; accessed 6-September-2021].

[Pitto et al., 2019] Pitto, L., Kainz, H., Falisse, A., Wesseling, M., Van Rossom, S., Hoang, H., Papageorgiou, E., Hallemans, A., Desloovere, K., Molenaers, G., et al. (2019). Simcp: A simulation platform to predict gait performance following orthopedic intervention in children with cerebral palsy. *Frontiers in neurorobotics*, 13:54.

[Pizzolato et al., 2015] Pizzolato, C., Lloyd, D. G., Sartori, M., Ceseracciu, E., Besier, T. F., Fregly, B. J., and Reggiani, M. (2015). Ceinms: A toolbox to investigate the influence of different neural control solutions on the prediction of muscle excitation and joint moments during dynamic motor tasks. *Journal of biomechanics*, 48(14):3929–3936.

[Prilutsky and Zatsiorsky, 2002] Prilutsky, B. I. and Zatsiorsky, V. M. (2002). Optimization-based models of muscle coordination. *Exercise and sport sciences reviews*, 30(1):32.

[Rajagopal et al., 2016] Rajagopal, A., Dembia, C. L., DeMers, M. S., Delp, D. D., Hicks, J. L., and Delp, S. L. (2016). Full-body musculoskeletal model for muscle-driven simulation of human gait. *IEEE transactions on biomedical engineering*, 63(10):2068–2079.

[Reinbolt et al., 2009] Reinbolt, J. A., Fox, M. D., Schwartz, M. H., and Delp, S. L. (2009). Predicting outcomes of rectus femoris transfer surgery. *Gait & posture*, 30(1):100–105.

[Ren et al., 2007] Ren, L., Jones, R. K., and Howard, D. (2007). Predictive modelling of human walking over a complete gait cycle. *Journal of biomechanics*, 40(7):1567–1574.

[Riener and Edrich, 1999] Riener, R. and Edrich, T. (1999). Identification of passive elastic joint moments in the lower extremities. *Journal of biomechanics*, 32(5):539–544.

[RJ and Kirsch, 2004] RJ, A. K. T. and Kirsch, R. (2004). Effects of spinal cord injury on lower-limb passive joint moments revealed through a nonlinear viscoelastic model. *Biomedical Engineering Department, Case Western Reserve University, Cleveland, OH*.

[Robertson et al., 2008] Robertson, D., Wilson, J.-M. J., and Pierre, T. A. S. (2008). Lower extremity muscle functions during full squats. *Journal of Applied Biomechanics*, 24(4):333–339.

[Rosenbaum, 2003] Rosenbaum, P. (2003). Cerebral palsy: what parents and doctors want to know. *Bmj*, 326(7396):970–974.

[Rosenbaum et al., 2007] Rosenbaum, P., Paneth, N., Leviton, A., Goldstein, M., Bax, M., Damiano, D., Dan, B., and Jacobsson, B. (2007). A report: the definition and classification of cerebral palsy april 2006. *Developmental medicine and child neurology. Supplement*, 109:8–14.

[Rosenberg and Steele, 2017] Rosenberg, M. and Steele, K. M. (2017). Simulated impacts of ankle foot orthoses on muscle demand and recruitment in typically-developing children and children with cerebral palsy and crouch gait. *PloS one*, 12(7):e0180219.

[Salini et al., 2011] Salini, J., Padois, V., and Bidaud, P. (2011). Synthesis of complex humanoid whole-body behavior: A focus on sequencing and tasks transitions. In *2011 IEEE International Conference on Robotics and Automation*, pages 1283–1290. IEEE.

[Schoenfeld, 2010] Schoenfeld, B. J. (2010). Squatting kinematics and kinetics and their application to exercise performance. *The Journal of Strength & Conditioning Research*, 24(12):3497–3506.

[Schultz and Mombaur, 2009] Schultz, G. and Mombaur, K. (2009). Modeling and optimal control of human-like running. *IEEE/ASME Transactions on mechatronics*, 15(5):783–792.

[Schwanbeck et al., 2009] Schwanbeck, S., Chilibeck, P. D., and Binsted, G. (2009). A comparison of free weight squat to smith machine squat using electromyography. *The Journal of Strength & Conditioning Research*, 23(9):2588–2591.

[Schwartz et al., 2013] Schwartz, M. H., Rozumalski, A., Truong, W., and Novacheck, T. F. (2013). Predicting the outcome of intramuscular psoas lengthening in children with cerebral palsy using preoperative gait data and the random forest algorithm. *Gait & posture*, 37(4):473–479.

[Seth et al., 2018] Seth, A., Hicks, J. L., Uchida, T. K., Habib, A., Dembia, C. L., Dunne, J. J., Ong, C. F., DeMers, M. S., Rajagopal, A., Millard, M., et al. (2018). Opensim: Simulating musculoskeletal dynamics and neuromuscular control to study human and animal movement. *PLoS computational biology*, 14(7):e1006223.

[Seth et al., 2011] Seth, A., Sherman, M., Reinbolt, J. A., and Delp, S. L. (2011). Opensim: a musculoskeletal modeling and simulation framework for in silico investigations and exchange. *Procedia Iutam*, 2:212–232.

[Sheean, 2002] Sheean, G. (2002). The pathophysiology of spasticity. *European journal of neurology*, 9:3–9.

[Sherman et al., 2011] Sherman, M. A., Seth, A., and Delp, S. L. (2011). Simbody: multibody dynamics for biomedical research. *Procedia Iutam*, 2:241–261.

[Sherman et al., 2013] Sherman, M. A., Seth, A., and Delp, S. L. (2013). What is a moment arm? calculating muscle effectiveness in biomechanical models using generalized coordinates. In *ASME 2013 International Design Engineering Technical Conferences and Computers and Information in Engineering Conference*. American Society of Mechanical Engineers Digital Collection.

[Signorile et al., 1995] Signorile, J. F., Kwiatkowski, K., Caruso, J. F., and Robertson, B. (1995). Effect of foot position on the electromyographical activity of the superficial quadriceps muscles during the parallel squat and knee extension. *The Journal of Strength & Conditioning Research*, 9(3):182–187.

[Solomonow et al., 1987] Solomonow, M., Baratta, R., Zhou, B., Shoji, H., Bose, W., Beck, C., and D'ambrosia, R. (1987). The synergistic action of the anterior cruciate ligament and thigh muscles in maintaining joint stability. *The American journal of sports medicine*, 15(3):207–213.

[Stanev, 2018] Stanev, D. (2018). *Biomechanical simulation of virtual physiological humans: modeling of musculoskeletal kinematic and dynamic redundancy using coordinate projection methods*. PhD thesis.

[Steele et al., 2012] Steele, K. M., DeMers, M. S., Schwartz, M. H., and Delp, S. L. (2012). Compressive tibiofemoral force during crouch gait. *Gait & posture*, 35(4):556–560.

[Sutherland, 1978] Sutherland, D. H. (1978). Gait analysis in cerebral palsy. *Developmental Medicine & Child Neurology*, 20(6):807–813.

[Thelen and Anderson, 2006] Thelen, D. G. and Anderson, F. C. (2006). Using computed muscle control to generate forward dynamic simulations of human walking from experimental data. *Journal of biomechanics*, 39(6):1107–1115.

[Thelen et al., 2003] Thelen, D. G., Anderson, F. C., and Delp, S. L. (2003). Generating dynamic simulations of movement using computed muscle control. *Journal of biomechanics*, 36(3):321–328.

[Tosi et al., 2009] Tosi, L. L., Maher, N., Moore, D. W., Goldstein, M., and Aisen, M. L. (2009). Adults with cerebral palsy: a workshop to define the challenges of treating and preventing secondary musculoskeletal and neuromuscular complications in this rapidly growing population. *Developmental Medicine & Child Neurology*, 51:2–11.

[Toutoungi et al., 2000] Toutoungi, D., Lu, T., Leardini, A., Catani, F., and O'connor, J. (2000). Cruciate ligament forces in the human knee during rehabilitation exercises. *Clinical biomechanics*, 15(3):176–187.

[Vandekerckhove et al., 2021] Vandekerckhove, I., Wesseling, M., Kainz, H., Desloovere, K., and Jonkers, I. (2021). The effect of hip muscle weakness and femoral bony deformities on gait performance. *Gait & Posture*, 83:280–286.

[Verdini et al., 2017] Verdini, F., Zara, C., Leo, T., Mengarelli, A., Cardarelli, S., and Innocenti, B. (2017). Assessment of patient functional performance in different knee arthroplasty designs during unconstrained squat. *Muscles, ligaments and tendons journal*, 7(3):514.

[Vigneron et al., 2017] Vigneron, V., Dorizzi, B., Khouri, N., Desailly, E., et al. (2017). Predicting postoperative gait in cerebral palsy. *Gait & posture*, 52:45–51.

[Wang et al., 2012] Wang, J. M., Hamner, S. R., Delp, S. L., and Koltun, V. (2012). Optimizing locomotion controllers using biologically-based actuators and objectives. *ACM Transactions on Graphics (TOG)*, 31(4):1–11.

[Xia and Law, 2008] Xia, T. and Law, L. A. F. (2008). A theoretical approach for modeling peripheral muscle fatigue and recovery. *Journal of biomechanics*, 41(14):3046–3052.

[Xiang et al., 2010] Xiang, Y., Arora, J. S., and Abdel-Malek, K. (2010). Physics-based modeling and simulation of human walking: a review of optimization-based and other approaches. *Structural and Multidisciplinary Optimization*, 42(1):1–23.

[Xu et al., 2015] Xu, H., Bloswick, D., and Merryweather, A. (2015). An improved opensim gait model with multiple degrees of freedom knee joint and knee ligaments. *Computer methods in biomechanics and biomedical engineering*, 18(11):1217–1224.

[Yamaguchi and Zajac, 1990] Yamaguchi, G. T. and Zajac, F. E. (1990). Restoring unassisted natural gait to paraplegics via functional neuromuscular stimulation: a computer simulation study. *IEEE Transactions on biomedical engineering*, 37(9):886–902.

[Zajac, 1993] Zajac, F. E. (1993). Muscle coordination of movement: a perspective. *Journal of biomechanics*, 26:109–124.